National School on Neutron and X-ray Scattering

Argonne and Oak Ridge National laboratories

X-ray and Neutron Reflectometry

August 21, 2012

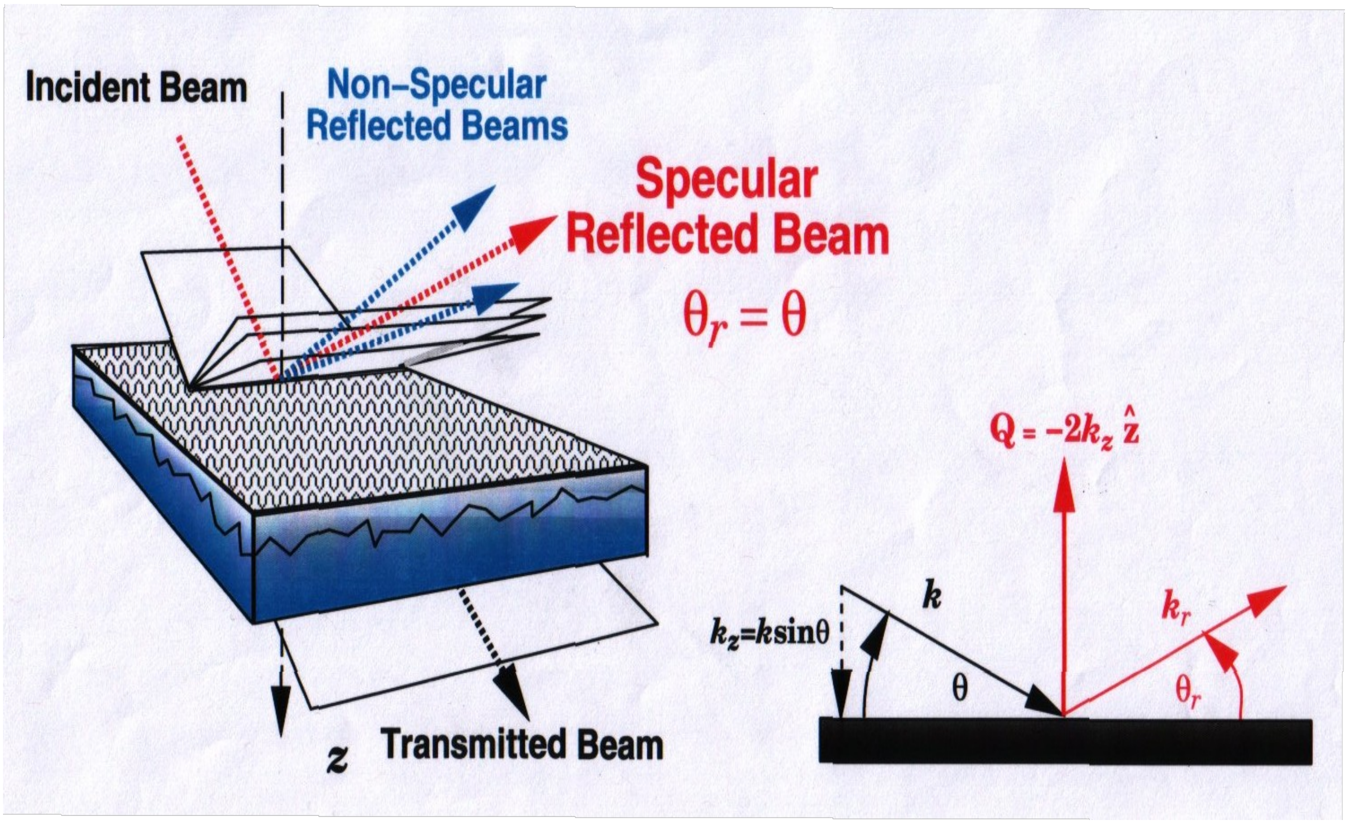

(Figure courtesy of Norm Berk)

C.F.Majkrzak, *NIST Center for Neutron Research*,
Gaithersburg, MD

Part 1: Basic Reflectometry Concepts

<> diffraction versus real space imaging

<> probing structure beneath the surface boundary

<> wave/particle behavior

<> coherence length -- plane waves and wave packets

<> specular reflection from a flat object

<> scattering length density (SLD) depth profiles

<> spatial and Q resolutions

<> non-specular scattering

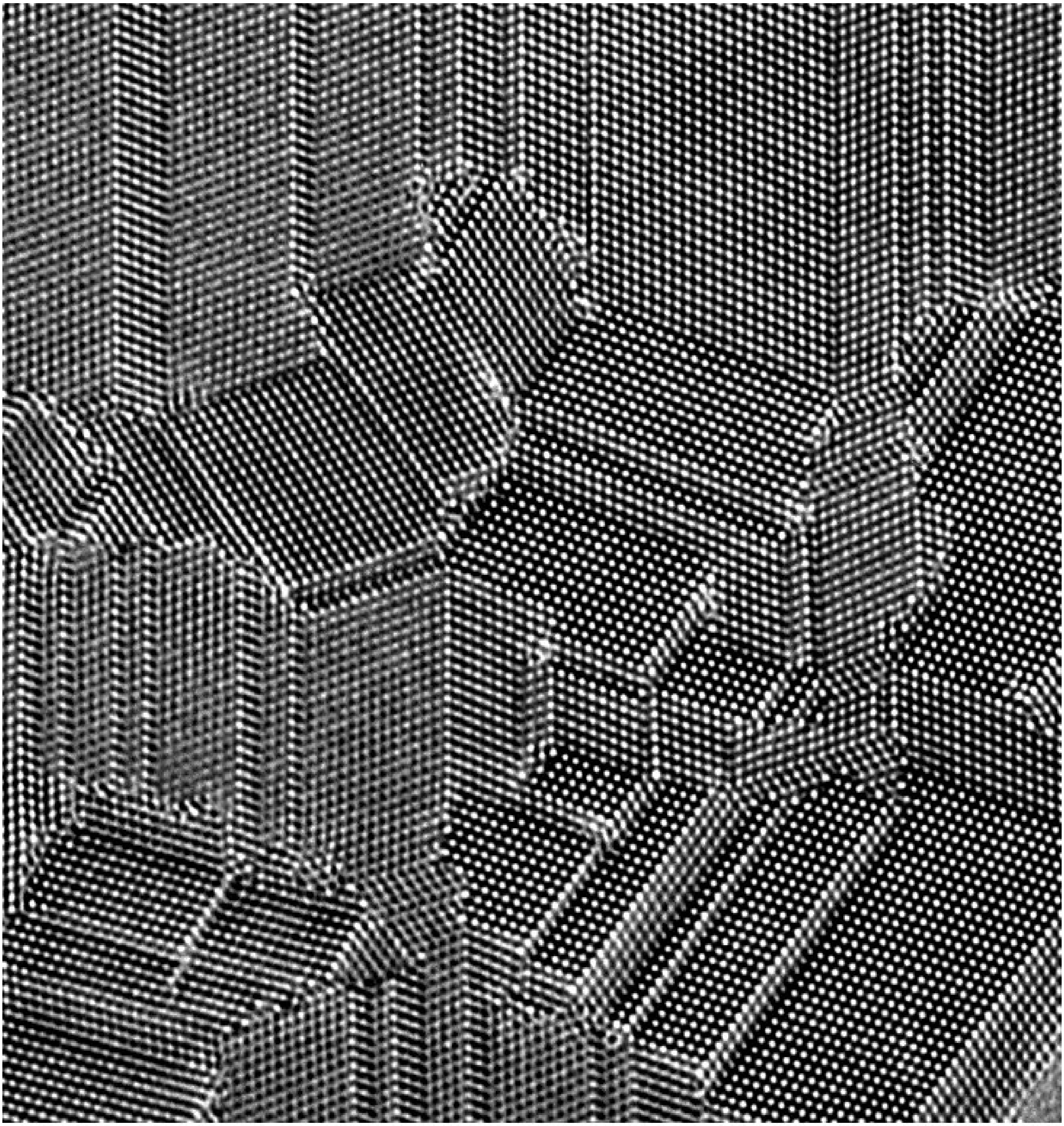

Atomic resolution micrograph of multiply-twinned nanocrystalline film of Si. (C. Song)

PROBES OF THE MICROSTRUCTURE OF SURFACES AND INTERFACES

photons, electrons, neutrons, atom and ion beams, miniature mechanical devices

* DIRECT IMAGING (REAL SPACE)

  e.g.:

  - optical microscopy (~ 1000 x magnification)
  - scanning electron microscopy (SEM) (orders of magnitude higher magnification than possible with light)
  - transmission electron microscopy (TEM)
  - atomic force microscopy (AFM)

* DIFFRACTION (RECIPROCAL SPACE)

  e.g.:

  - low energy electron diffraction (LEED)
  - spin polarized LEED (SPLEED)
  - reflection high energy electron diffraction (RHEED)
  - ellipsometry (optical polarimetry)
  - x-ray reflectometry
  - neutron reflectometry

For quantitative measurements of depth profiles along a normal to the surface, x-ray and neutron reflectometry are particularly useful because of their relatively weak interactions with condensed matter and the fact that these interactions can be described accurately by a comparatively simple theory. In the case of electron diffraction, on the other hand, the potential is non-local and the scattering is non-spherical, relatively strong and highly energy-dependent. For atom diffraction, the description of the interaction potential can be even more complicated.

Principal Uses and Advantages of Neutron Reflectometry:

* For the specular condition, provides the chemical (isotopic) scattering length density (SLD) depth profile along the surface normal with a spatial resolution approaching half a nanometer.

* With polarized neutrons, provides the *vector* magnetization depth profile of a ferromagnetic material.

* Isotopic contrast, particularly applicable to hydrogen and deuterium.

* A non-destructive probe which can penetrate macroscopic distances through single crystalline substrates, making possible reflection studies of films in contact with liquids within a closed cell.

* As a consequence of the relatively weak interaction between the neutron and material, a remarkably accurate theoretical description of the reflection process and quantitative analysis of the data is possible, although the Born approximation is often not valid and an “exact” or “dynamical” formulation is required.

> The great success in using neutron reflection/diffraction to study thin film systems of hard condensed matter, in particular the structures and fundamental interactions in magnetic materials, is largely due to the ability to tailor, with atomic-layer accuracy and precision, single-crystalline, layered sandwiches and superlattices (using vapor deposition techniques such as molecular beam epitaxy in ultra-high vacuum). Advances in film deposition techniques and lithography continue at a remarkable rate.

> Similarly, neutron reflectometry in principle can be applied as a probe to further our understanding of the structure and function of molecules in lipid membranes, of relevance in biology and bioengineering, when comparable control over the fabrication of model systems is achieved. Great progress has been made toward realizing this goal in practice. However, we are still at a relatively early stage of development in our ability to engineer soft condensed matter films on atomic and nanometer scales. Progress can be expected as efforts in creating and manipulating membrane / molecular systems accelerates.

> Employing phase-sensitive methods in reflectivity measurements ensures a unique scattering length density (SLD) depth profile. Additional application of hydrogen / deuterium substitution techniques and comparison with molecular dynamics calculations assures a correspondingly high degree of certainty of obtaining an unambiguous chemical composition depth profile.

Why is specular neutron reflectometry so special?

<> Neutron reflectometry (NR) is a valuable probe of the structure of both hard and soft condensed matter in thin film or multilayered form -- particularly for hydrogenous and magnetic materials. NR can see *beneath* the surface and provide quantitative structural information from *everywhere within* the film on a nanometer scale.

<> Both “forward” and “inverse” scattering problems for specular neutron reflection are mathematically solvable, exactly, from first-principles quantum theory. The mathematically unique solutions are thus far only possible in one dimension and for non-absorbing potentials of finite extent.

<> Phase-sensitive neutron specular reflectometry, employing references, enables direct inversion of composite reflectivity data sets to yield a unique scattering length density depth profile for an “unknown” film of interest, without fitting or any adjustable parameters.

<> The spatial resolution and accuracy of the SLD profile thereby obtained is limited only by the statistical uncertainty in the measured reflected intensities and truncation of the reflectivity data sets at the maximum value of wavevector transfer attainable.

"SPECULAR" OR "MIRROR" REFLECTION OF A WAVE

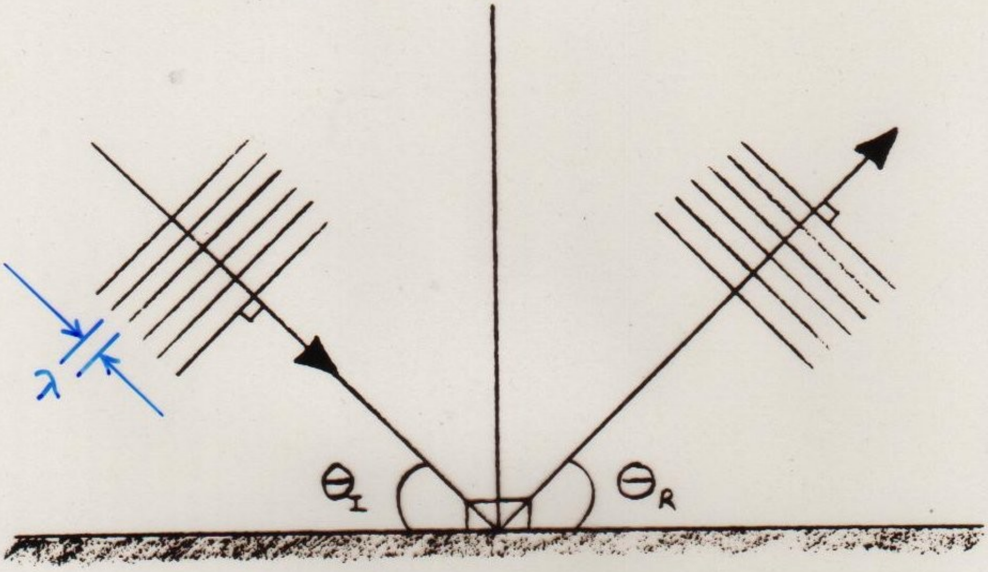

ANGLE OF INCIDENCE Θ_I
= ANGLE OF REFLECTION Θ_R

REFRACTION OF A LIGHT WAVE

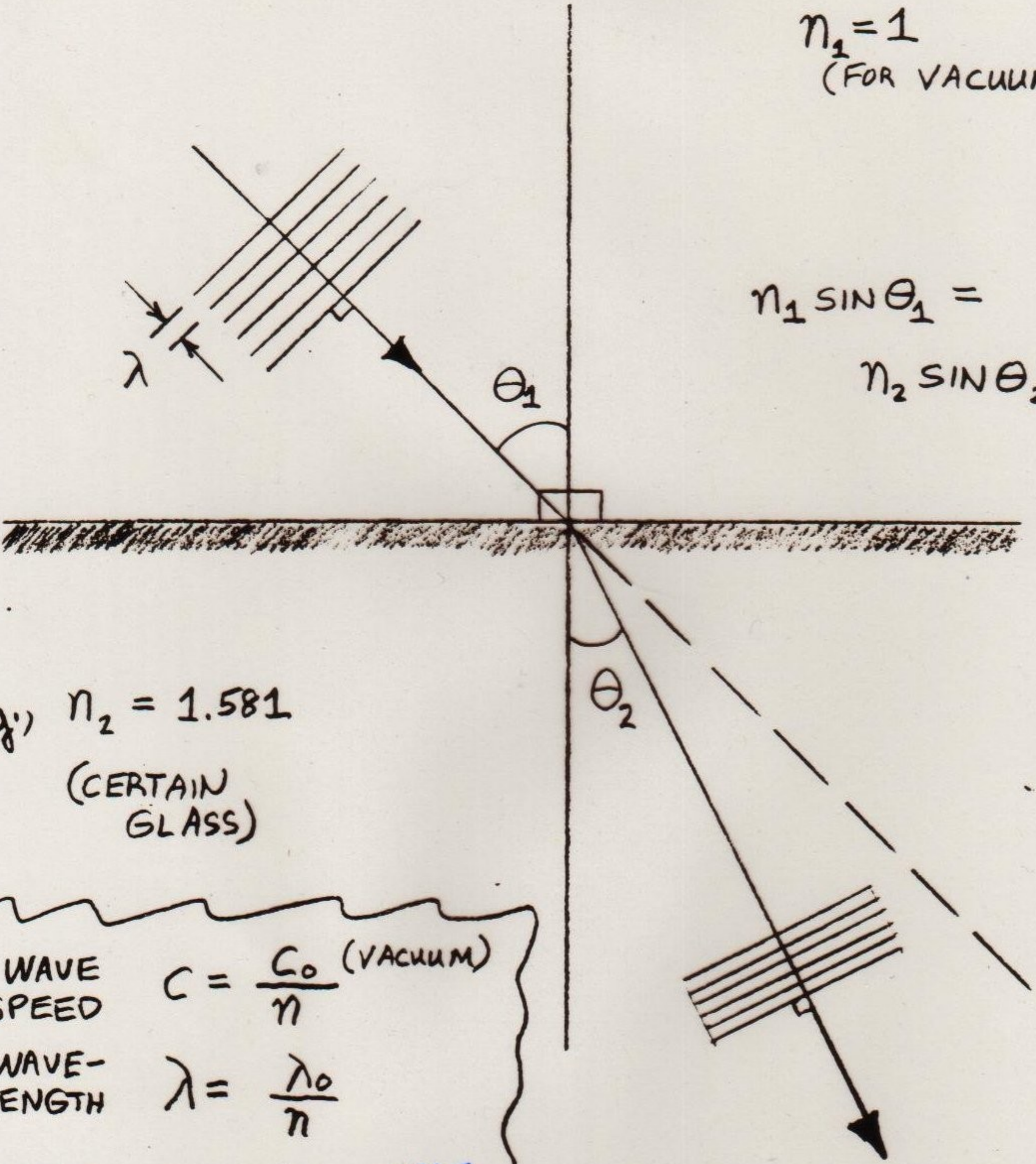

$n_1 = 1$
(FOR VACUUM)

$n_1 \sin\theta_1 =$
$n_2 \sin\theta_2$

e.g.) $n_2 = 1.581$
(CERTAIN GLASS)

WAVE SPEED $c = \frac{c_0}{n}$ (VACUUM)

WAVE-LENGTH $\lambda = \frac{\lambda_0}{n}$

WAVE-VECTOR $k = n k_0 = \frac{2\pi\nu}{c}$

FREQUENCY ν = CONSTANT

REFRACTIVE INDEX n DEPENDS ON MATERIAL <u>AND</u> WAVELENGTH OF THE LIGHT

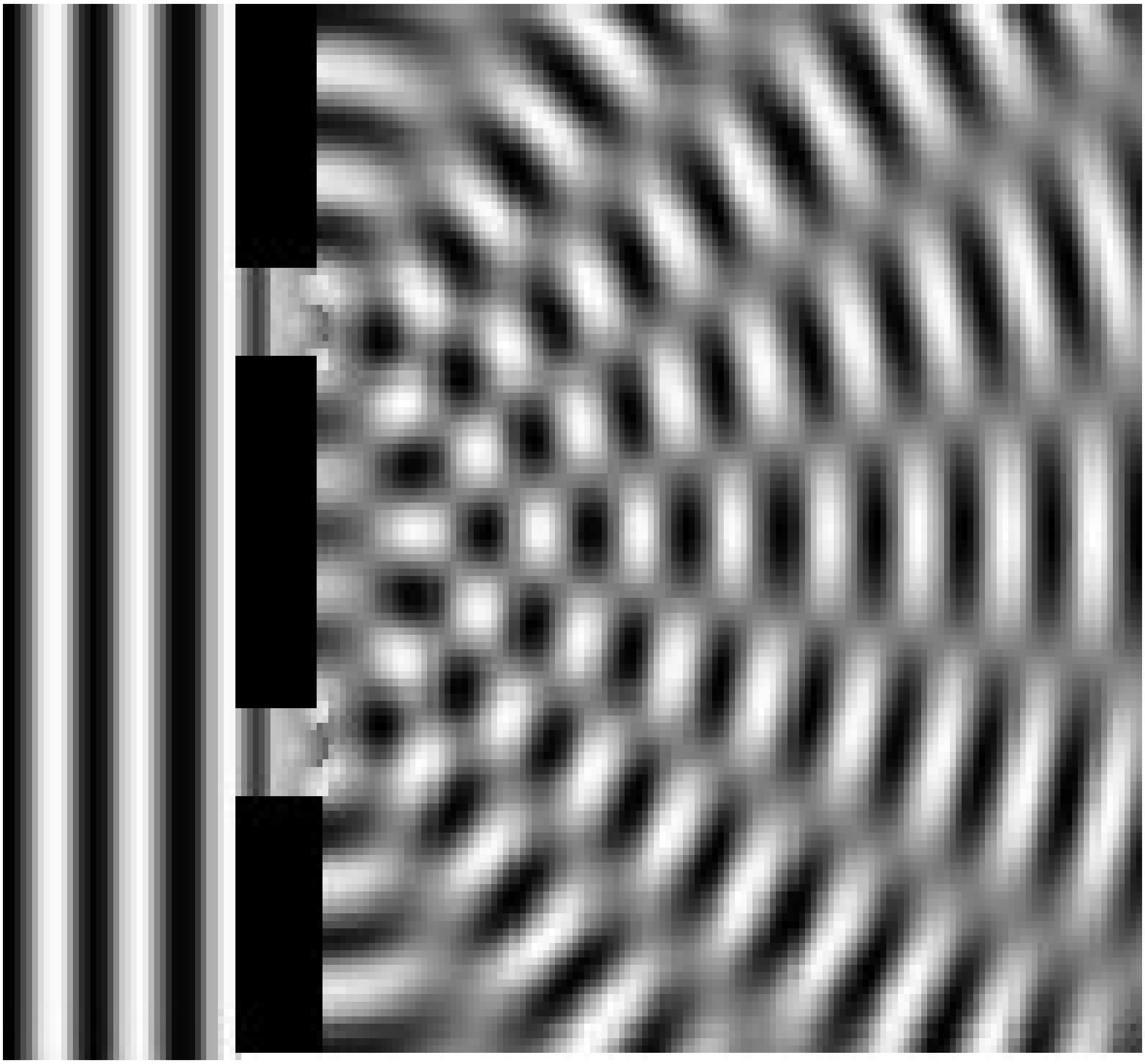

Water wave diffracting through a double aperture (from left to right) – B.Crowell, *Light and Matter*, www.vias.org/physics.

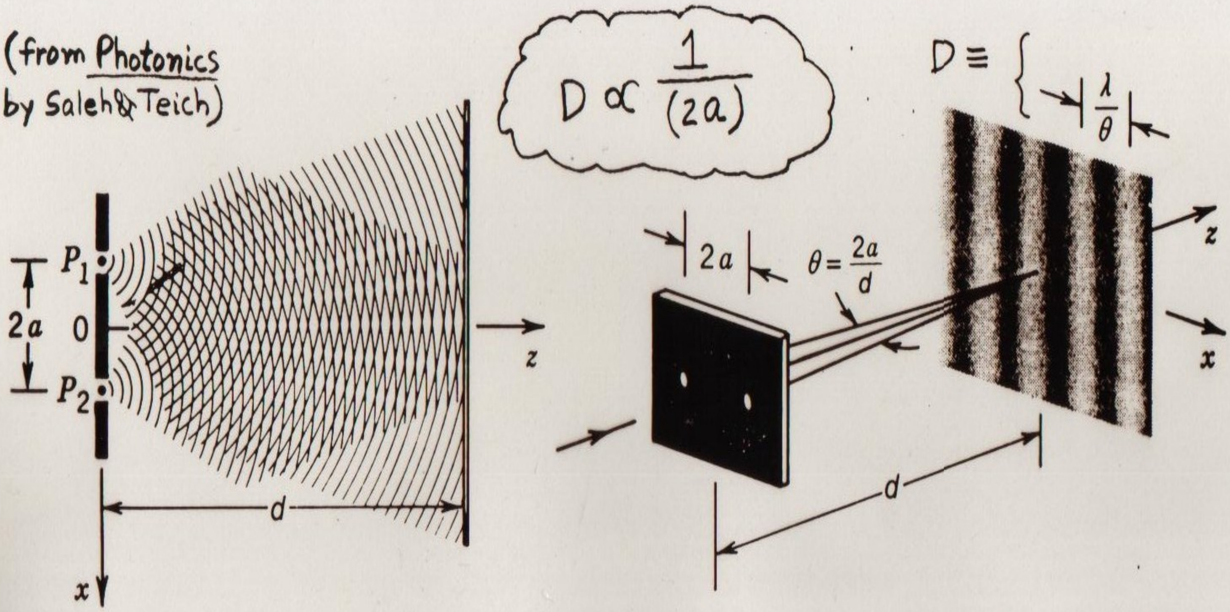
(from Photonics by Saleh & Teich)

$D \propto \frac{1}{(2a)}$

$D \equiv \left\{ \rightarrow\!\mid \frac{\lambda}{\theta} \mid\!\leftarrow \right.$

Figure 2.5-6 Interference of two spherical waves of equal intensities originating at the points P_1 and P_2. The two waves can be obtained by permitting a plane wave to impinge on two pinholes in a screen. The light intensity at an observation plane a distance d away takes the form of a sinusoidal pattern with period $\approx \lambda/\theta$.

DIFFRACTION PATTERN WHICH RESULTS FROM THE COHERENT SUPERPOSITION OF TWO WAVES (AMPLITUDES OF THE TWO WAVES ADD TOGETHER AT ANY GIVEN POINT IN SPACE)

A CHARACTERISTIC RECIPROCAL RELATIONSHIP EXISTS BETWEEN THE POSITIONS OF THE INTENSITY MAXIMA IN THE DIFFRACTION PATTERN AND THE DISTANCE SEPARATING THE OBJECTS CAUSING THE SCATTERING.

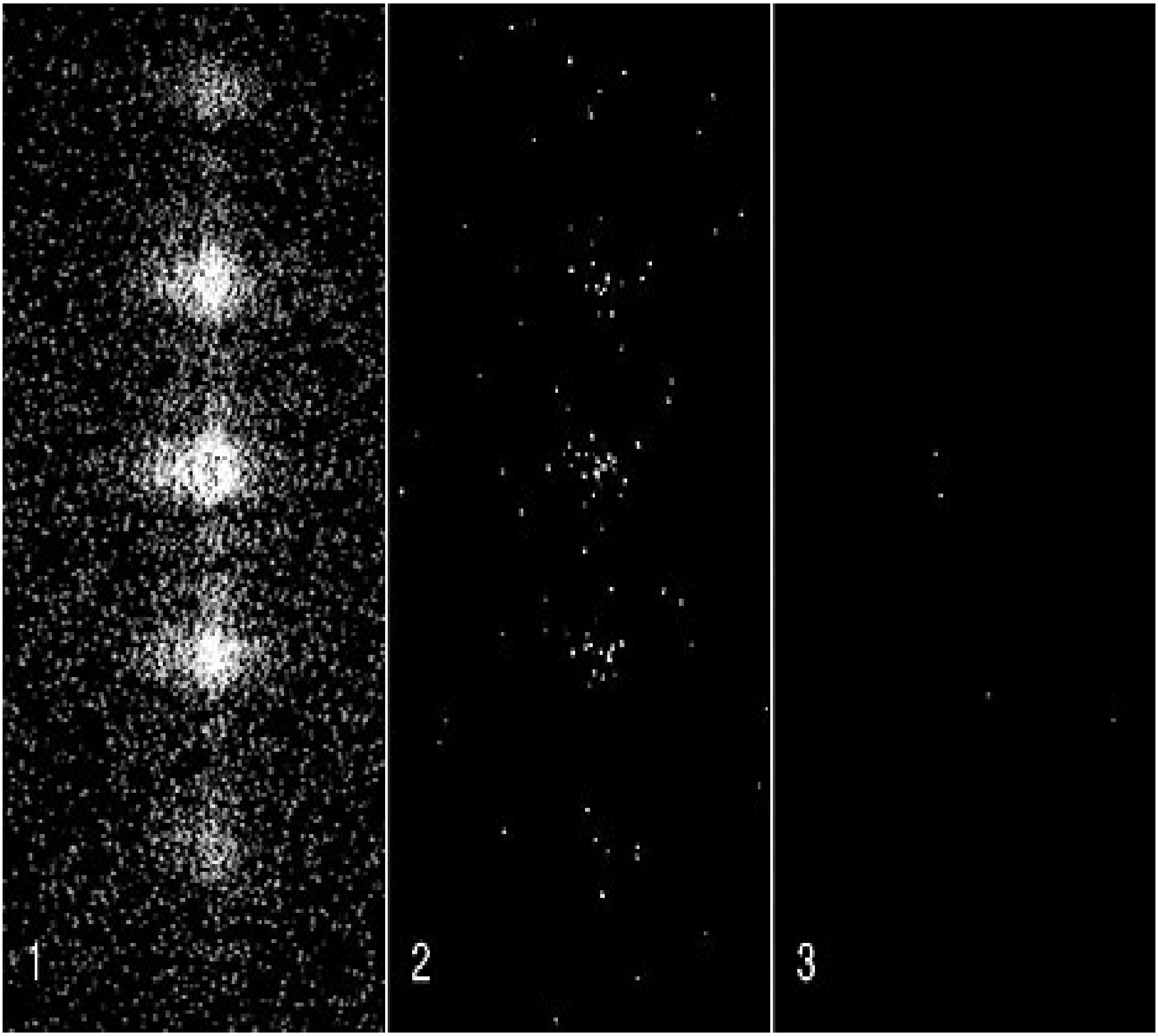

Wave interference patterns produced by monochromatic laser light diffracting through a triple slit aperture for various intensities – L.Page (www.vias.org/physics). This is a dramatic illustration of wave-particle duality.

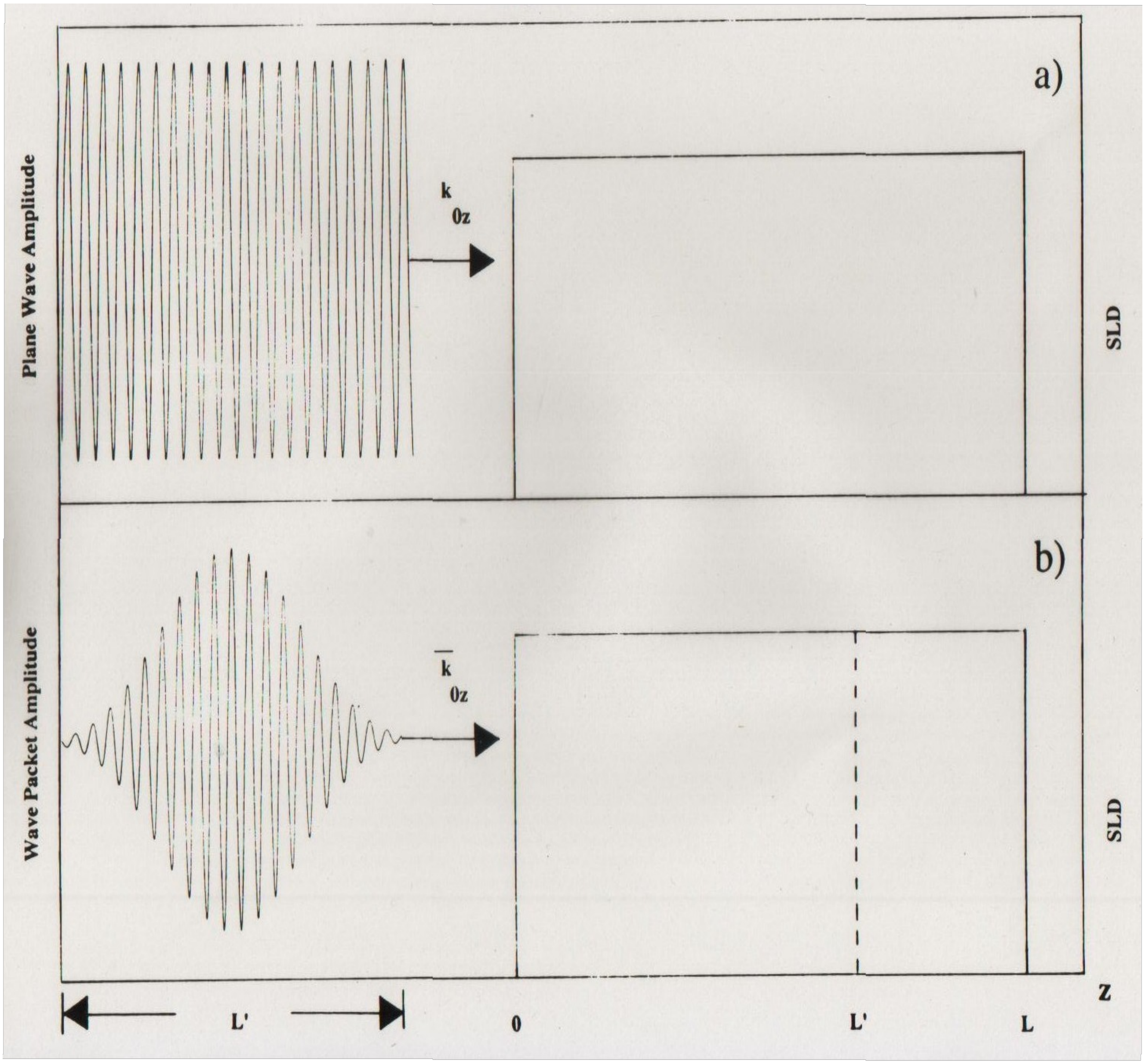
a)
Plane Wave Amplitude
k_{0z}
SLD
b)
Wave Packet Amplitude
$\bar{k}_{0z}$
SLD
Z
L'
0
L'
L

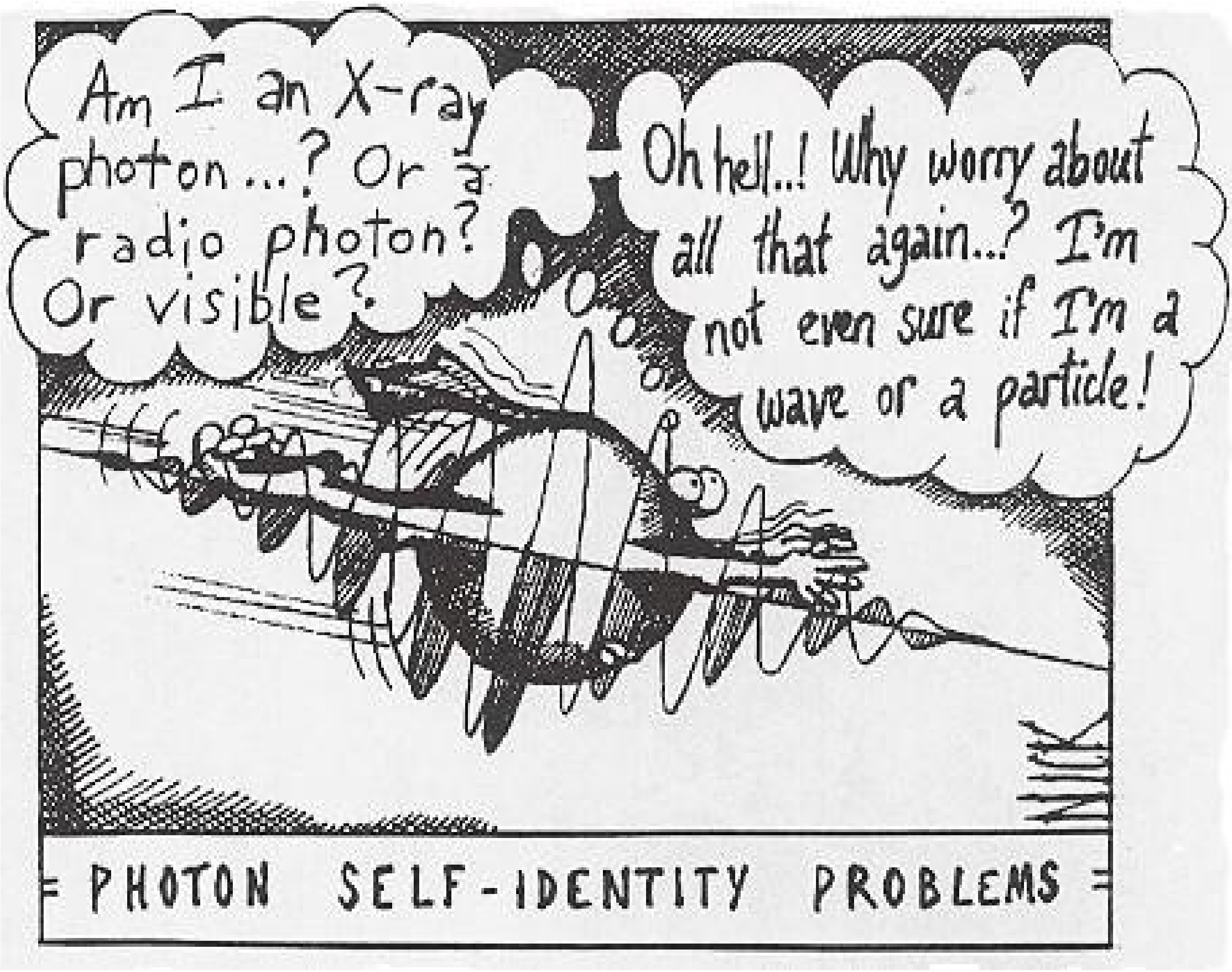

(abyss.uoregon.edu)

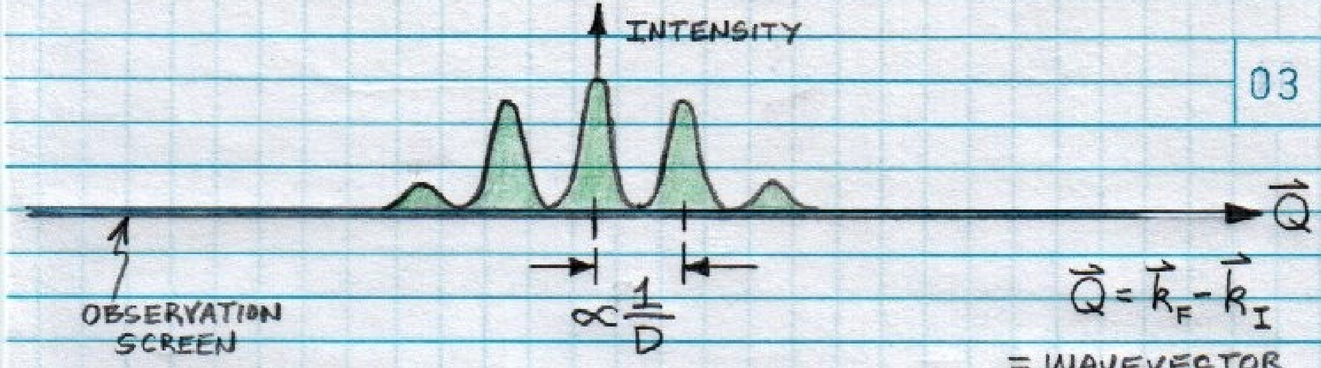

$\vec{Q} = \vec{k}_F - \vec{k}_I$

= WAVEVECTOR TRANSFER

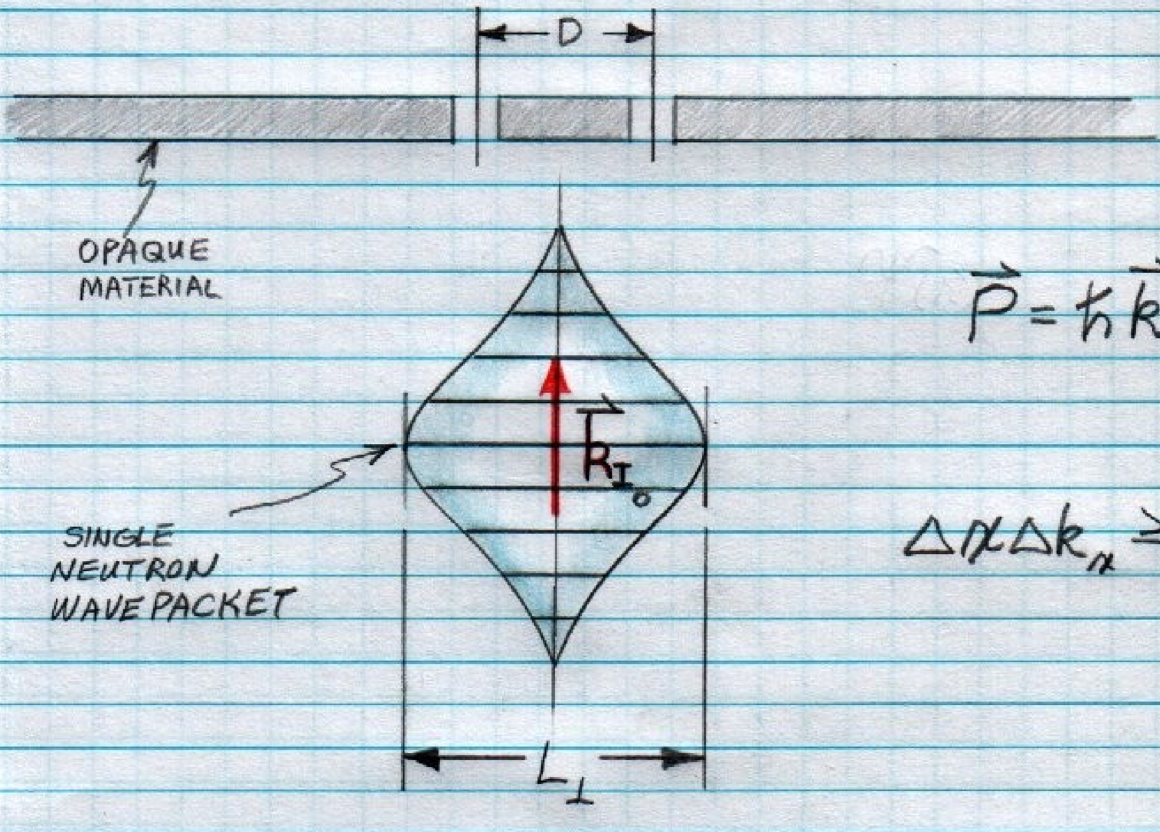

$\vec{P} = \hbar \vec{k}$

$\Delta x \Delta k_x \geq 1$

$$\Psi(\vec{r}) = \left(\frac{1}{2\pi}\right)^{3/2} \iiint_{-\infty}^{+\infty} d\vec{k}\, \phi(\vec{k})\, e^{+i\vec{k}\cdot\vec{r}}$$

$$\phi(\vec{k}) = \left(\frac{1}{2\pi}\right)^{3/2} \iiint_{-\infty}^{+\infty} d\vec{r}\, \Psi(\vec{r})\, e^{-i\vec{k}\cdot\vec{r}}$$

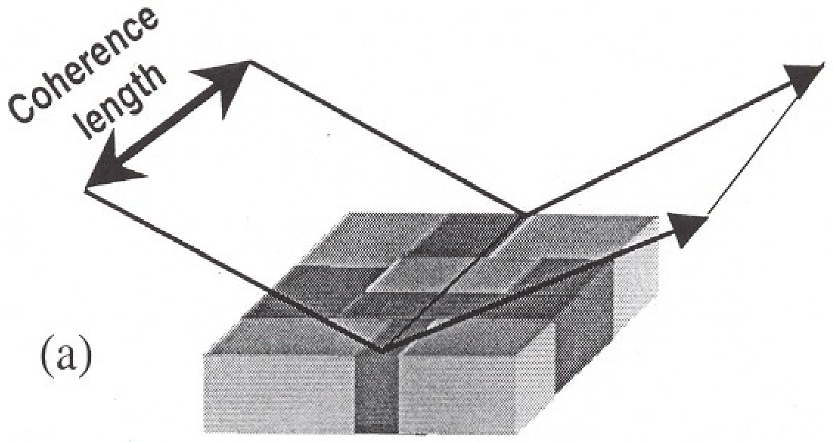

small-scale *heterogeneity* laterally averages SLD profile

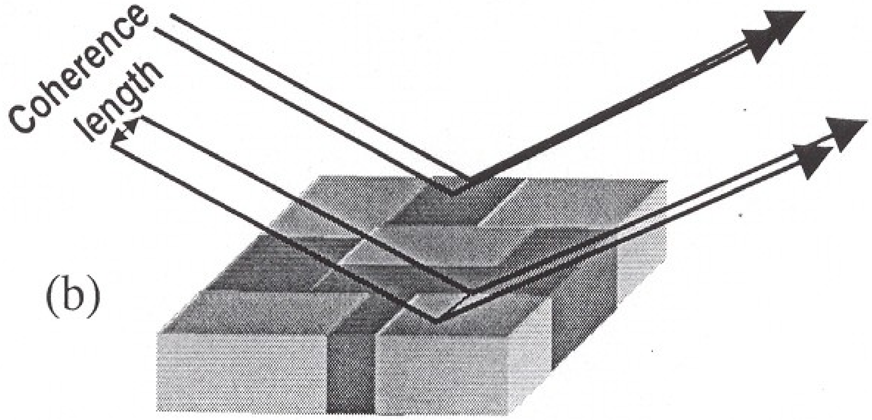

large-scale *heterogeneity* laterally averages reflectivity

Figure 12

Figure 13

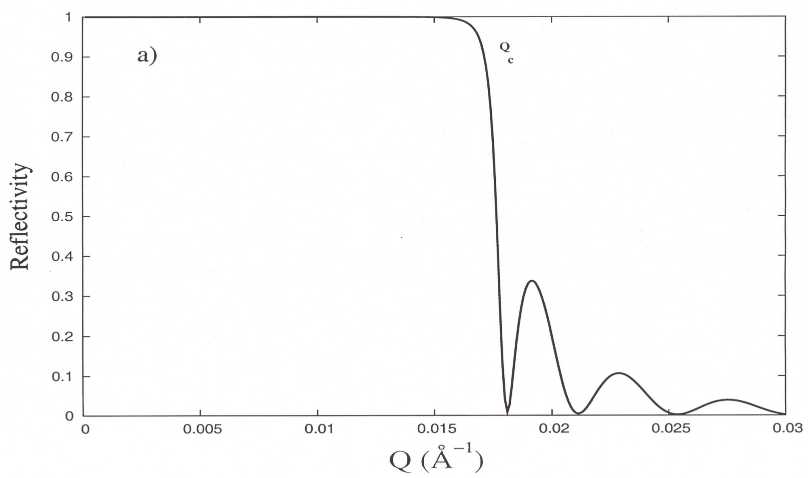

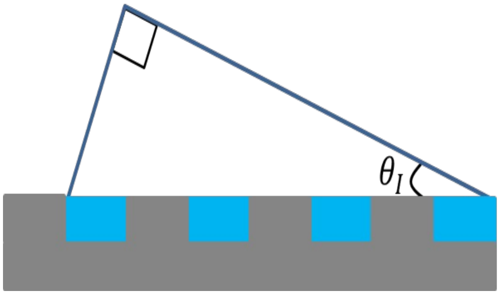

Figure 13

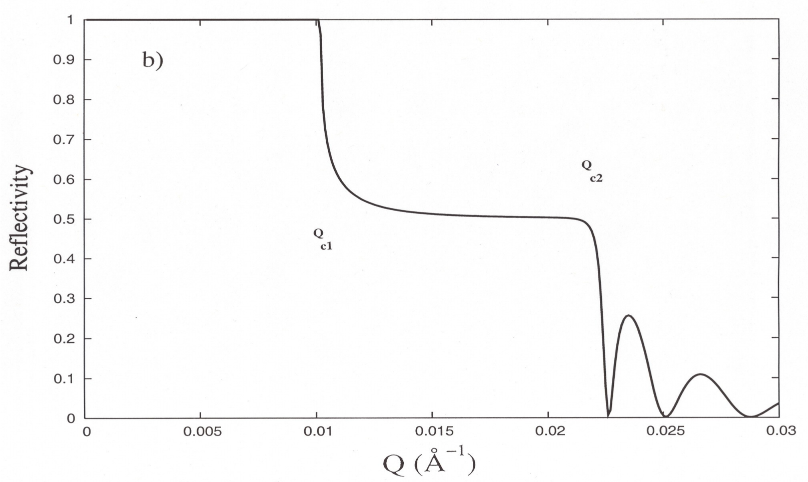

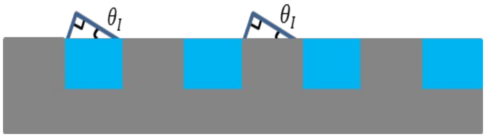

Grating Stripes Perpendicular to Scattering Plane

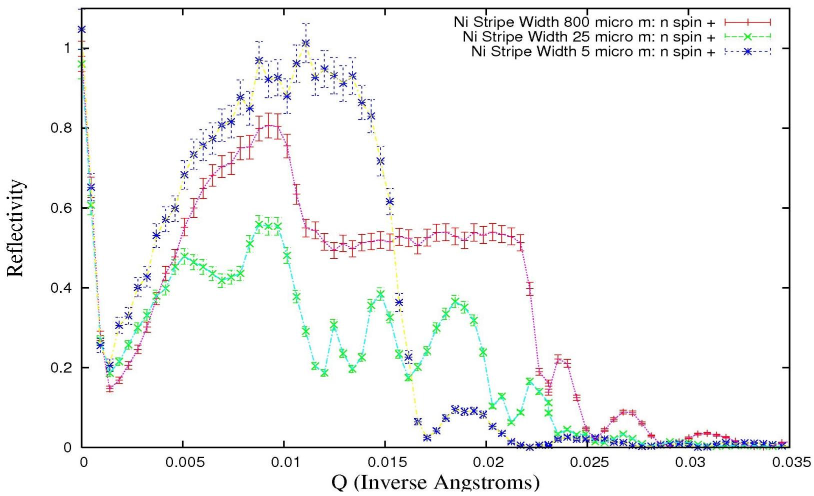

Figure 9

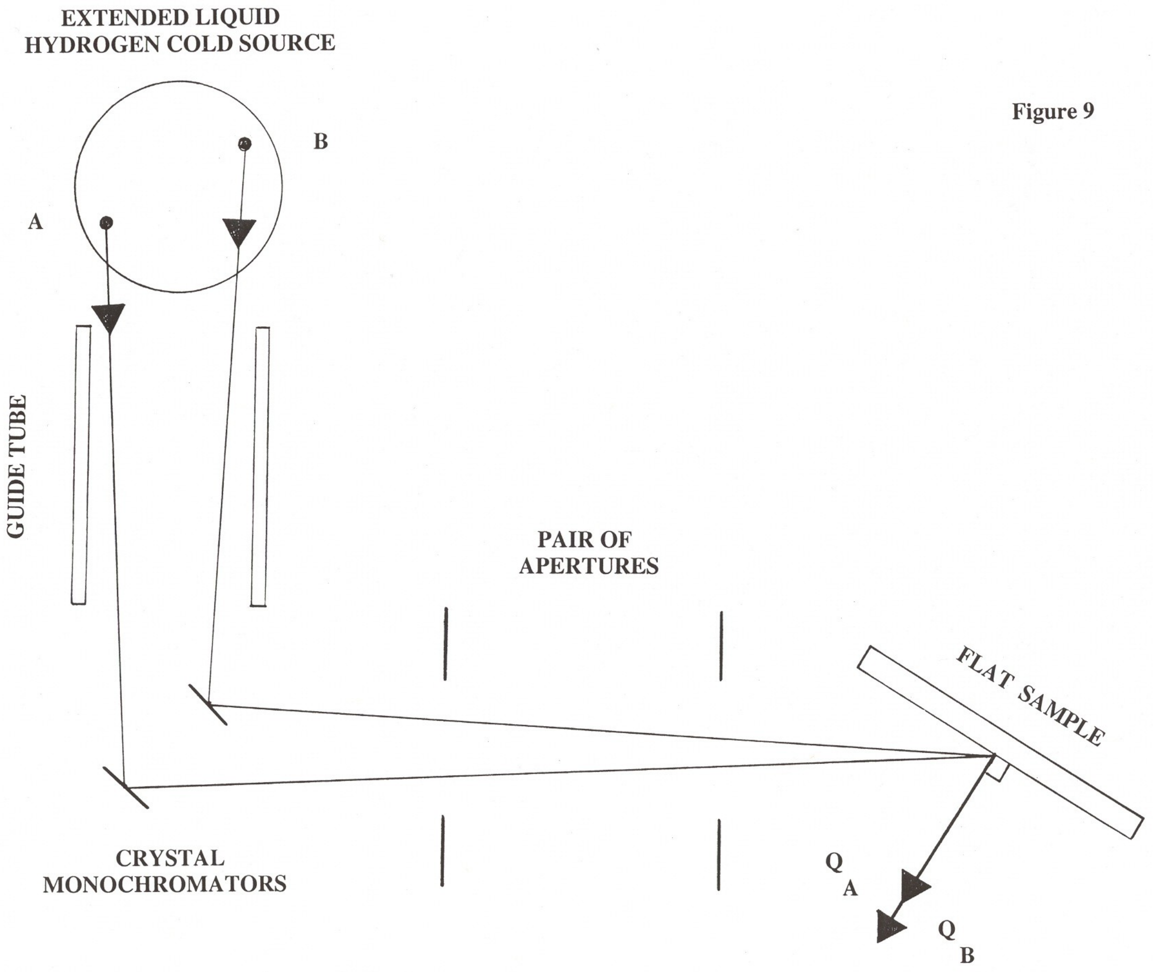

EXTENDED LIQUID
HYDROGEN COLD SOURCE
B
A
GUIDE TUBE
PAIR OF
APERTURES
FLAT SAMPLE
CRYSTAL
MONOCHROMATORS
Q_A
Q_B

$$\text{Reflectivity} = \frac{\text{Number of reflected neutrons}}{\text{Number of incident neutrons}} = |\boldsymbol{r}|^2$$

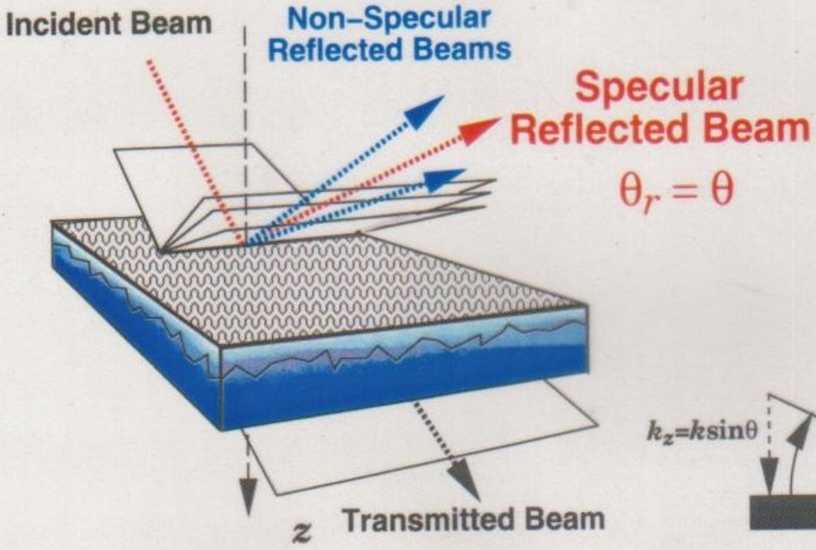

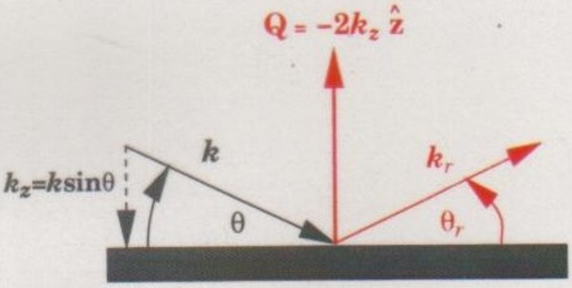

Specular reflection: $\bar{\rho}(z) = \langle \rho(x,y,z) \rangle_{xy}$

Non–Specular reflection: $\Delta\rho(x,y,z) = \rho(x,y,z) - \bar{\rho}(z)$

(AFTER N.F. BERK ET AL.)

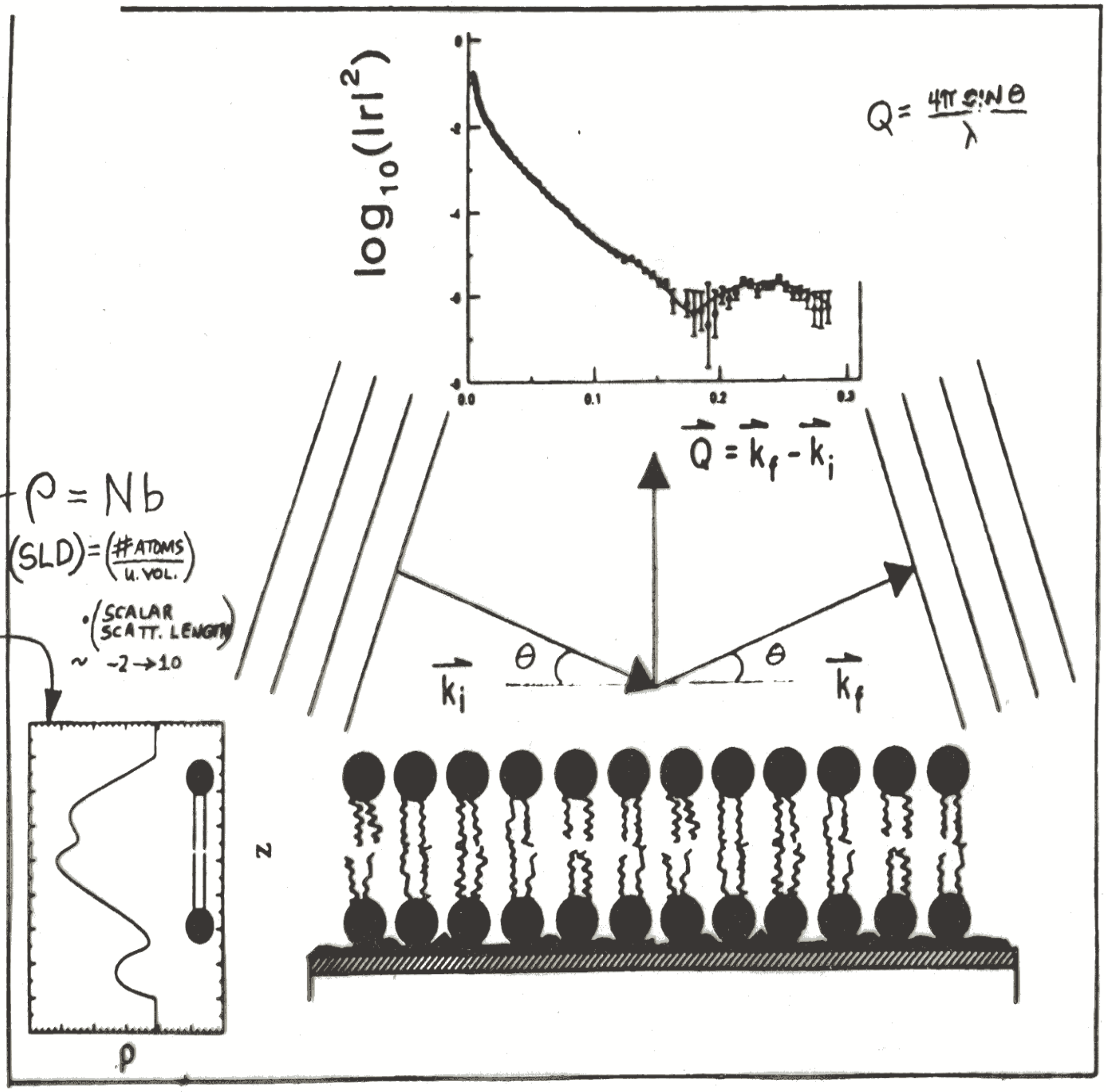
$\log_{10}(|r|^2)$
0
-2
-4
-6
-8
0.0
0.1
0.2
0.3
$Q = \frac{4\pi \sin\theta}{\lambda}$
$\vec{Q} = \vec{k_f} - \vec{k_i}$
θ
θ
$\vec{k_i}$
$\vec{k_f}$
$\rho = Nb$
$(SLD) = \left(\frac{\# ATOMS}{u. VOL.}\right) \cdot \left(\begin{array}{l}SCALAR\\SCATT. LENGTH\end{array}\right)$
$\sim -2 \rightarrow 10$
z
ρ

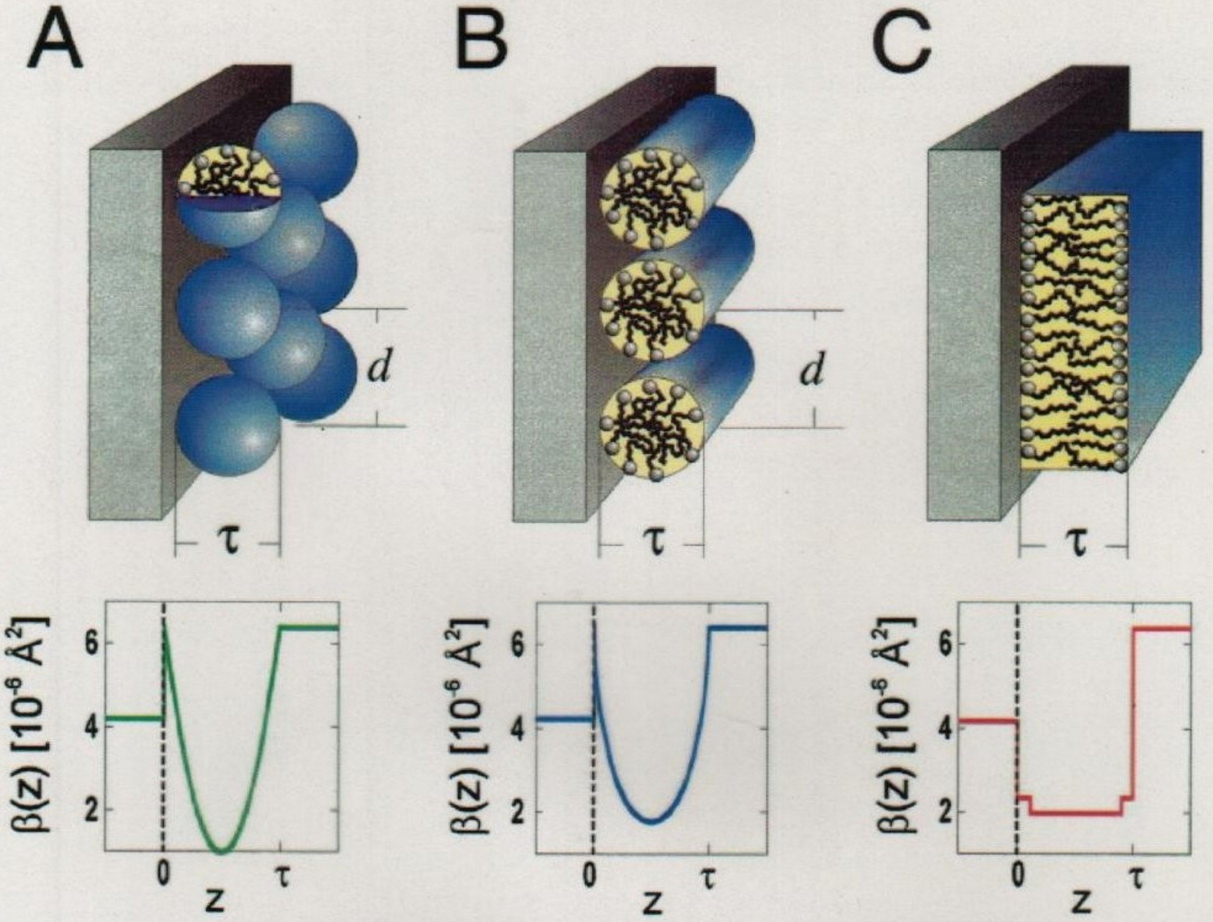

FIG. 1. (Color) Schematic diagram of adsorbed layer structures consisting of (A) spherical micelles, (B) cylindrical micelles, and (C) a bilayer, including the film thickness τ and interaggregate spacing d. Also shown are examples of neutron scattering length density profiles normal to the interface, $\beta(z)$, corresponding to each structure at the quartz/D$_2$O interface at a fractional surface coverage of 0.55. The head-group and alkyl tails of the surfactants have different scattering length densities, but because of the arrangement of the molecules this is only apparent in the bilayer $\beta(z)$.

single-crystal quartz block and reflected from the quartz-solution interface were recorded as a function of angle of incidence. The off-specular background, including any signal due to scattering from the bulk solution [15], was subtracted to give the reflection coefficient of the surfactant-coated interface. All solutions used were above their critical micelle or aggregation concentration, a condition which leads to a saturated adsorbed film at the solid-solution interface.

The cationic surfactant tetradecyltrimethylammonium bromide (TTAB) forms nearly spherical micellar aggregates consisting of approximately 80 molecules in bulk solution. Small angle neutron-scattering measurements [16] give mi-

FIG. 2. 200×200-nm^2 AFM tip deflection images of (A) spherical TTAB aggregates adsorbed onto quartz from water solution, (B) cylindrical TTAB aggregates adsorbed onto quartz from an aqueous 200mM NaBr solution, and (C) planar DDAB bilayer adsorbed onto quartz from water solution. Long-wavelength undulations visible in (B) and (C) arise from roughness in the underlying quartz.

THE NEUTRON AS A PLANE WAVE PROPAGATING IN FREE SPACE

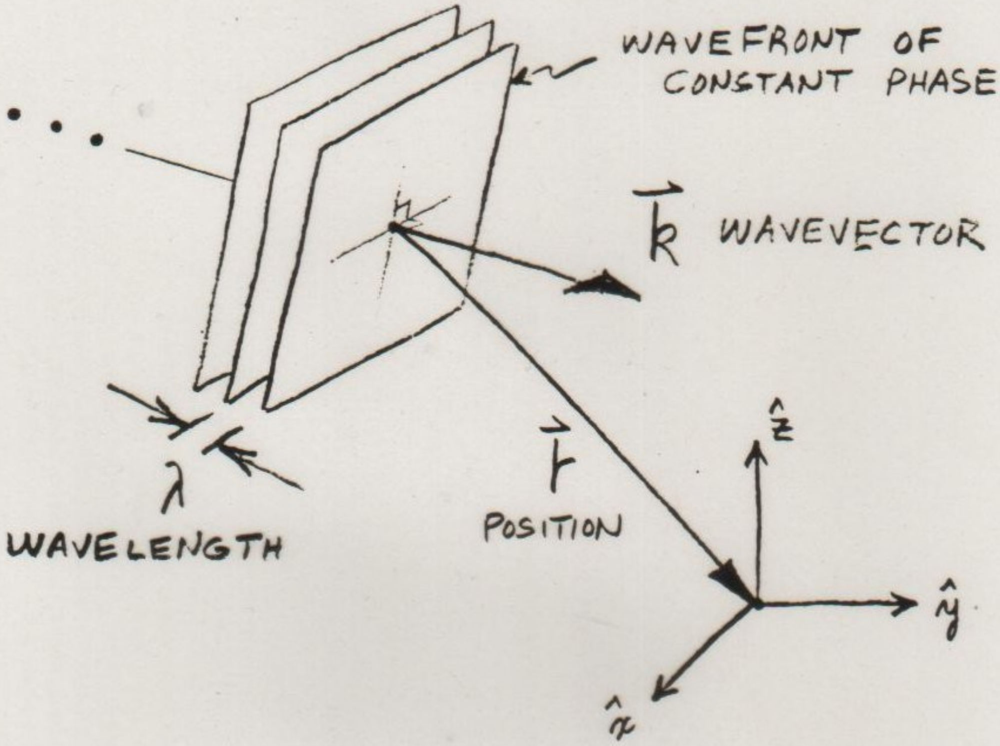

WAVEFUNCTION

$$\boxed{\Psi \propto e^{i\vec{k}_0\cdot\vec{r}}} \qquad \left\{\begin{aligned}\vec{k}_0 &= k_{0x}\hat{x}+k_{0y}\hat{y}+k_{0z}\hat{z}\\ \vec{r} &= x\hat{x}+y\hat{y}+z\hat{z}\end{aligned}\right.$$

FOR $\vec{k}_0$ ALONG $\hat{z}$, FOR EXAMPLE,

$$\Psi \propto \cos\underbrace{(k_{0z}z)}_{=\left(\frac{2\pi}{\lambda}z\right)} + i\,\sin(k_{0z}z)$$

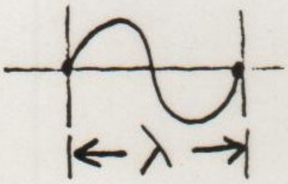

$|\Psi|^2 \propto$ PROBABILITY OF THE NEUTRON BEING THERE

FOR ELASTIC INTERACTIONS
TOTAL ENERGY OF THE
NEUTRON IS CONSTANT

TOTAL ENERGY = KINETIC ENERGY
+ POTENTIAL ENERGY

= CONSTANT

WAVE EQUATION OF MOTION
(SCHROEDINGER EQUATION)

$$\Bigg[\underbrace{\frac{-\hbar^2}{2m}\nabla^2}_{K.E.} + \underbrace{V(\vec{r})}_{P.E.}\Bigg]\Psi = \underbrace{E}_{T.E.}\Psi$$

$$\nabla^2 = \frac{\partial^2}{\partial x^2} + \frac{\partial^2}{\partial y^2} + \frac{\partial^2}{\partial z^2}$$

IN VACUUM

$$K.E._0 = \frac{\hbar^2 k_0^2}{2m}$$

IN THE CONTINUUM LIMIT

$$V(\vec{r}) = \frac{2\pi\hbar^2}{m} \sum_{j=1} N_j b_j = \frac{2\pi\hbar^2}{m}\rho$$

NUMBER OF ATOMS OF TYPE j PER UNIT VOLUME

COHERENT SCATTERING "LENGTH" OF ATOM j

$(b = \mathrm{Re}\, b + i\, \mathrm{Im}\, b)$

ρ = "SCATTERING LENGTH DENSITY" (SLD)

IN VACUUM:

$$E_0 = \frac{\hbar^2 k_0^2}{2m} + 0$$

IN A MATERIAL MEDIUM:

$$E = \frac{\hbar^2 k^2}{2m} + \frac{2\pi\hbar^2}{m}\rho$$

CONSERVATION OF ENERGY REQUIRES $E_0 = E$

$$\therefore \quad k^2 = k_0^2 - 4\pi\rho$$

THUS

$$\left[\nabla^2 + k^2\right]\Psi = 0$$

NOTE REFRACTIVE INDEX $n \equiv \frac{k}{k_0}$:

$$n^2 = 1 - \frac{4\pi\rho}{k_0^2}$$

REFLECTION FROM AN IDEAL FILM OR SLAB OF MATERIAL

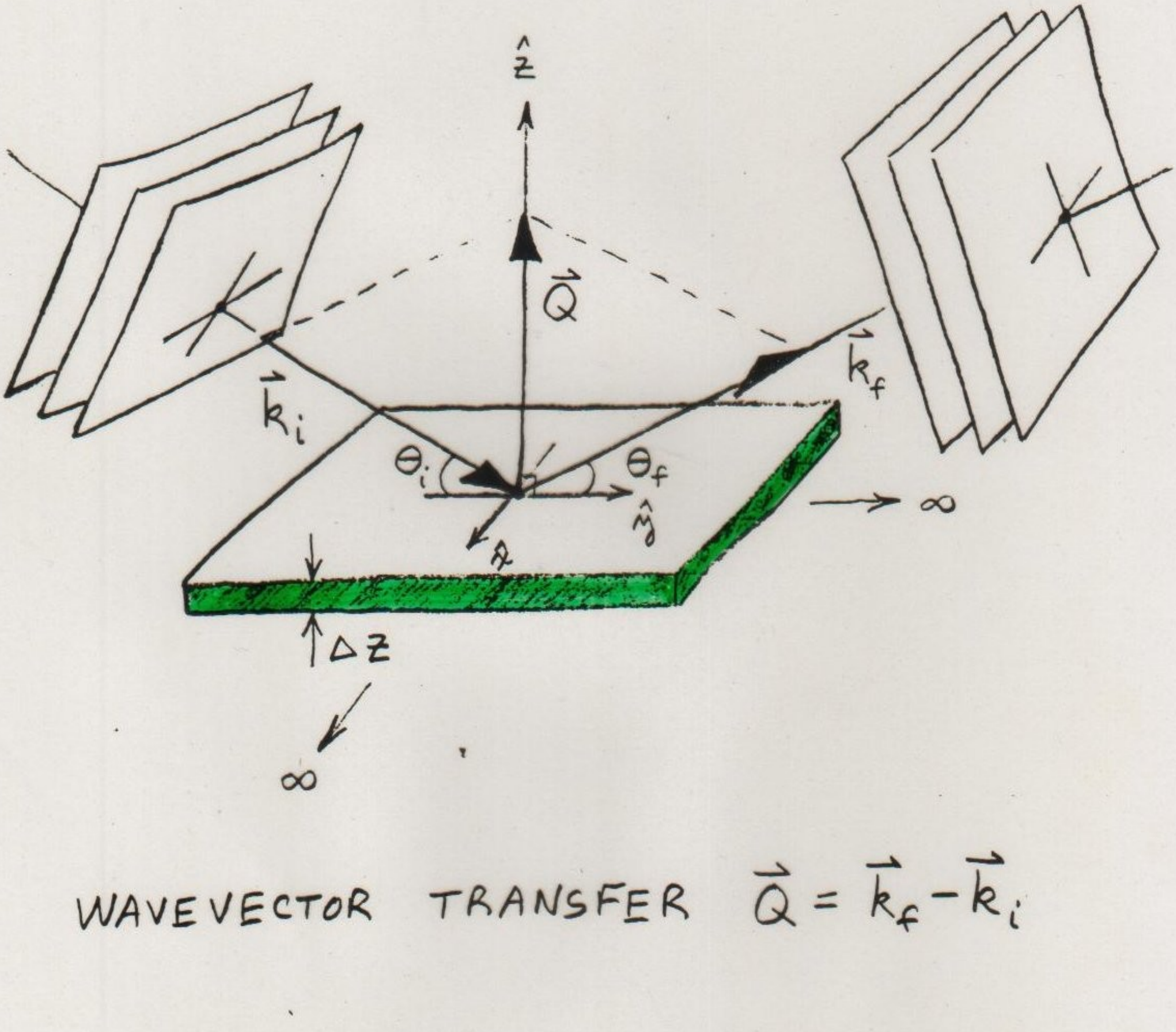

WAVEVECTOR TRANSFER $\vec{Q} = \vec{k}_f - \vec{k}_i$

$\rho = \rho(z)$ ONLY

EXPANDING $k^2 = k_0^2 - 4\pi\rho$,

$$k_x^2 + k_y^2 + k_z^2 + 4\pi\rho = k_{0x}^2 + k_{0y}^2 + k_{0z}^2 .$$

NOW IF $\rho = \rho(z)$ ONLY, THEN

$\frac{\partial \rho}{\partial x}$ AND $\frac{\partial \rho}{\partial y}$, WHICH ARE PROPORTIONAL TO THE GRADIENTS OF THE POTENTIAL OR FORCES IN THE RESPECTIVE DIRECTIONS, ARE EQUAL TO ZERO. THUS, NO FORCE ACTS ALONG THESE DIRECTIONS TO CHANGE k_x AND k_y. THEN

$k_x = k_{0x}$ AND $k_y = k_{0y}$ ARE "CONSTANTS OF THE MOTION".

SUBSTITUTING $\Psi(\vec{r}) = e^{ik_{0x}x} e^{ik_{0y}y} \psi(z)$ INTO $[\nabla^2 + k^2]\Psi = 0$ GIVES

$$\left[\frac{\partial^2}{\partial z^2} + k_z^2\right]\psi(z) = 0$$

AND $\therefore$ $k_z^2 = k_{0z}^2 - 4\pi\rho(z)$.

BECAUSE THERE IS NO CHANGE IN THE POTENTIAL IN THE X- OR Y- DIRECTIONS, THERE CAN BE NO MOMENTUM CHANGE IN THESE DIRECTIONS EITHER

THE IDEAL SLAB GEOMETRY WITH $\rho = \rho(z)$ ONLY GIVES RISE TO THE COHERENT "SPECULAR" REFLECTION OF A PLANE WAVE WHICH IS DESCRIBED BY A ONE-DIMENSIONAL WAVE EQUATION :

$$\boxed{\left[\frac{\partial^2}{\partial z^2} + k_{0z}^2 - 4\pi\rho(z)\right]\Psi_{(z)} = 0}$$

IN THIS CASE $\theta_i = \theta_f \equiv \theta$,

$|\vec{k}_i| = |\vec{k}_f|$ AND $Q = 2k\sin\theta$

$= 2k_z$

ALSO, $n_z^2 \equiv 1 - \dfrac{4\pi\rho(z)}{k_{0z}^2}$

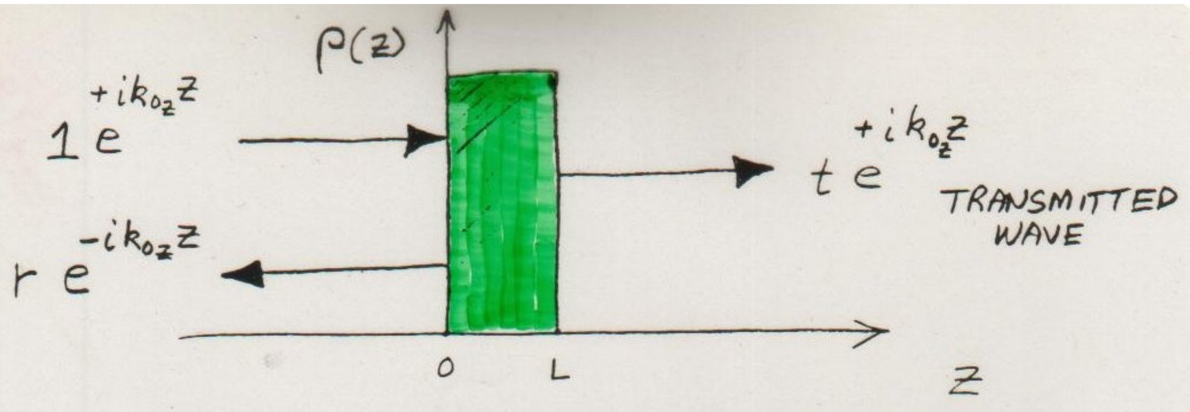

$$Q = 2k_{oz}$$

FROM THE WAVE EQUATION, IT IS POSSIBLE TO FIND A SOLUTION FOR THE REFLECTION AMPLITUDE IN INTEGRAL FORM (SEE ARTICLE PAGES) :

$$r(Q) = \frac{4\pi}{iQ}\int_{-\infty}^{+\infty} \Psi(z)\,\rho(z)\,e^{+ik_{oz}z}\,dz$$

WHAT IS LOCALIZED AT z IN THE SLD PROFILE $\rho(z)$ IN "REAL" SPACE, IS DISTRIBUTED OVER THE REFLECTION AMPLITUDE $r(Q)$ IN THE RELATED SCATTERING OR "RECIPROCAL" SPACE

$$M_j = \begin{bmatrix} \cos\delta_j & \frac{1}{n_{x_j}}\sin\delta_j \\ -n_{x_j}\sin\delta_j & \cos\delta_j \end{bmatrix} \tag{11}$$

with $\delta_j = k_{ox}n_{xj}\Delta_j$, with n_{sx} and n_{ox} corresponding to the substrate and incident medium, respectively. The jth matrix M_j corresponds to the jth slab of thickness Δ_j wherein the scattering density is assumed to be constant and equal to ρ_j. The amplitude of the incident wave is assumed to be unity. The transmission and reflectivity are $T^*T = |T|^2$ and $R^*R = |R|^2$, respectively, and can be obtained directly from Equation (9).

Thus, for a given model potential, it is straightforward to calculate the expected reflectivity. Unfortunately, the converse of this statement is not necessarily true, as will be discussed in more detail in Section 4.

At this point it is useful to consider an alternate derivation of the reflectivity from which the Born approximation (corresponding to the kinematic limit which is discussed below) and other useful results can be directly obtained. Suppose that there exist two arbitrary but different density profiles $\rho_1(x)$ and $\rho_2(x)$ for which the corresponding, separate reflectivities are to be calculated. In each case we take the incident wave to propagate from left to right. We then have to solve the following pair of equations (derived from equations 6 and 7):

$$\psi_j''(x) + [k_{o_x}^2 - 4\pi\rho_j(x)]\,\psi_j(x) = 0 \qquad j = 1,2 \tag{12}$$

for $-\infty < x < \infty$ where $\psi_1(x)$ and $\psi_2(x)$ are the exact solutions in each case. From these we can construct the Wronskian function

$$W(x) \equiv W[\psi_1(x), \psi_2(x)] = \psi_1(x)\psi_2'(x) - \psi_1'(x)\psi_2(x). \tag{13}$$

Differentiating both sides of eq. (13) and using eq. (12) we obtain

$$W'(x) = -\psi_1(x)4\pi\rho_{12}(x)\psi_2(x) \tag{14}$$

where

$$\rho_{12}(x) \equiv \rho_1(x) - \rho_2(x) \tag{15}$$

Equation (14) tells us that W(x) is a constant over intervals where the two density profiles coincide, $\rho_1(x) = \rho_2(x)$, which is a property we will exploit to obtain a formula relating the reflectivities for each profile. First, assume that $\rho_1 \neq \rho_2(x)$ only within an interval $\ell_1 < x < \ell_2$. We allow subintervals of (ℓ_1, ℓ_2) where $\rho_1(x) = \rho_2(x)$, but we demand finite ℓ_1 and ℓ_2 such that $\rho_1(x) = \rho_2(x)$ for all $x < \ell_1$ and for all $x > \ell_2$. We also assume that the wave is incident in vacuum so for $x < \ell_1$, $\rho_1(x) = \rho_2(x) = 0$. The wavefunctions for $x < \ell_1$ are then

$$\psi_j(x) = e^{ik_{o_x}x} + R_j e^{-ik_{o_x}x} \tag{16}$$

where R_1 and R_2 are the reflection amplitudes for each problem. Similarly, we assume that each density profile has a common substrate so that for $x > \ell_2$, $\rho_1(x) = \rho_2(x) = \rho(\infty)$. The wavefunctions for $x > \ell_2$ are then

$$\psi_j(x) = T_j\, e^{iKx} \tag{17}$$

where

$$K = \sqrt{k_{o_x}^2 - 4\pi\rho(\infty)} \tag{18}$$

and T_1 and T_2 are the transmission amplitudes in each problem. Now we see that for the given pair of profile functions $\rho_1(x)$ and $\rho_2(x)$, W(x) is uniquely determined everywhere and varies with x only in (ℓ_1, ℓ_2), where $\rho_1(x)$ and $\rho_2(x)$ can differ. Substituting (17) into (13) we obtain

$$W(x) = 0 \tag{19}$$

for all $x \geq \ell_2$, since $\psi_1(x)$ and $\psi_2(x)$ are proportional to one another (linearly dependent) in this region. However, substituting (16) into (13) we get

$$W(x) = 2ik_{o_x}(R_1 - R_2) \tag{20}$$

for all $x \leq \ell_1$, which is a complex constant. Finally, for $\ell_1 < x < \ell_2$ we integrate both sides of equation (14) to obtain

$$\int_{\ell_1}^{\ell_2} W'(x)dx = W(\ell_2) - W(\ell_1) = -\alpha_{12} \tag{21}$$

where

$$\alpha_{12} = \int_{\ell_1}^{\ell_2} \psi_1(x) 4\pi\rho_{12}(x)\psi_2(x)dx \quad . \tag{22}$$

Now W(x) is continuous everywhere since $\psi_j(x)$ and $\psi_j'(x)$ are. Thus, evaluating (19) and (20) at $x = \ell_2$ and $x = \ell_1$, respectively, we find $W(\ell_2) = 0$ and $W(\ell_1) = 2ik_{ox}(R_1-R_2)$. Thus, from equation (21) we get

$$R_1 = R_2 + \frac{\alpha_{12}}{iQ} \tag{23}$$

where again $Q = 2k_{ox}$ is the wavevector transfer. Equation (23) is the general formula we set out to derive and is a handy starting point for exact treatments as well as approximation schemes.

For example, consider any $\rho(x)$ which vanishes identically for $x < \ell_1$ and for $x > \ell_2$. Then, in equation (23) we can set $\rho_1(x) = \rho(x)$, $\psi_1(x) = \psi(x)$, and $R_1 = R$ whereas for the "other" density profile we take $\rho_2(x) = 0$ everywhere so that $\psi_2(x) = \exp(ik_{ox}x)$ and $R_2 = 0$. Combining equations (22) and (23) then gives the exact solution of the reflectivity for an arbitrary scattering density profile $\rho(x)$:

$$R = \frac{4\pi}{iQ} \int_{-\infty}^{+\infty} \psi(x)\rho(x)e^{ik_{o_x}x}dx \tag{24}$$

where we have formally extended the integration over all x, though only the region where $\rho(x) \neq 0$ contributes. Although it may not be obvious from the derivation, equation (24) also holds if we allow $\rho(x)$ to be nonzero as $x \rightarrow \infty$, as long as the integral exists. Note that (24) requires, to be exact, the exact wavefunction $\psi(x)$ wherever $\rho(x) \neq 0$. The corresponding expression for the reflectivity $|R|^2$, is

$\Psi(z)$ INSIDE THE MEDIUM IS GENERALLY UNKNOWN:

BORN APPROXIMATION REPLACES $\Psi(z)$ WITH THE INCIDENT WAVE FUNCTION $e^{+ik_{0z}z}$ BASED ON THE ASSUMPTION THAT $\Psi(z)$ IS NOT SIGNIFICANTLY DISTORTED FROM THE FREE SPACE FORM (WEAK INTERACTION): THEN

FOURIER TRANSFORM

$$\boxed{r(Q) \simeq \frac{4\pi}{iQ}\int_{-\infty}^{+\infty} \rho(z)\, e^{iQz}\, dz}$$

FOR A REAL POTENTIAL $\rho(z)$

$$\mathrm{Re}\; r(Q) \simeq \frac{4\pi}{Q}\int_{-\infty}^{+\infty} \rho(z) \sin(Qz)\, dz$$

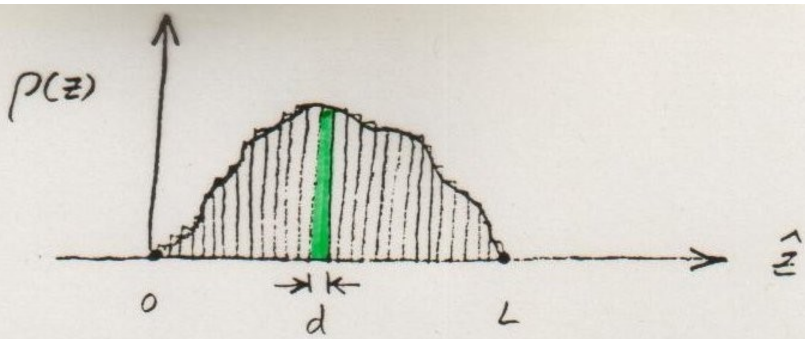

ARBITRARY POTENTIAL DIVIDED INTO RECTANGULAR SLABS OF WIDTH d AND CONSTANT ρ

THEN

(BORN APPROX.)

$$\text{Re}\, r(Q) \simeq \frac{4\pi}{Q}\int_0^L \rho(z)\sin(Qz)\,dz$$

BECOMES

$$\text{Re}\, r(Q_j) \simeq \frac{4\pi}{Q_j}\sum_{\ell=1}^{N}\int_{(\ell-1)d}^{\ell d}\rho_\ell \sin(Q_j z)\,dz$$

$$= -\frac{4\pi}{Q_j^2}\sum_{\ell=1}^{N}\rho_\ell\left[\cos(Q_j z)\right]_{(\ell-1)d}^{\ell d}$$

SET OF Rer FOR DIFFERENT VALUES OF Q OR θ

$$\left\{\begin{aligned}
\text{Re}\, r_1 &= \mathcal{C}_{11}\rho_1 + \mathcal{C}_{12}\rho_2 + \cdots + \mathcal{C}_{1N}\rho_N\\
\text{Re}\, r_2 &= \mathcal{C}_{21}\rho_1 + \mathcal{C}_{22}\rho_2 + \cdots + \mathcal{C}_{2N}\rho_N\\
&\vdots\\
\text{Re}\, r_N &= \mathcal{C}_{N1}\rho_1 + \mathcal{C}_{N2}\rho_2 + \cdots + \mathcal{C}_{NN}\rho_N
\end{aligned}\right.$$

SOLVE SIMULTANEOUS EQUATIONS FOR ρ's GIVEN Rer's

e.g., SVD, EIGENVALUE PROBLEM FORMULATION, ...

$$\underbrace{\mathrm{Re}\; r_{BA}(Q)\left[\frac{Q^2}{8\pi \,\mathrm{SIN}\left(\frac{Qd}{2}\right)}\right]}_{\equiv\, \mathcal{F}(Q)} = \sum_{j=1}^{N} \rho_j \,\mathrm{SIN}\left[\frac{(2j-1)Qd}{2}\right]$$

$$\int_0^{\pi} \sin m\theta \,\sin n\theta \,d\theta = \begin{cases} 0 & m, n \text{ INTEGERS, } m \neq n \\ \frac{\pi}{2} & m, n \text{ INTEGERS, } m = n \end{cases}$$

ORTHOGONALITY

$$\boxed{\rho_j = \frac{d}{4\pi^2}\int_0^{\frac{\pi}{d}} Q^2\, \mathrm{Re}\; r_{BA}(Q)\, \frac{\mathrm{SIN}\left[\frac{(2j-1)Qd}{2}\right]}{\mathrm{SIN}\left(\frac{Qd}{2}\right)}\, dQ}$$

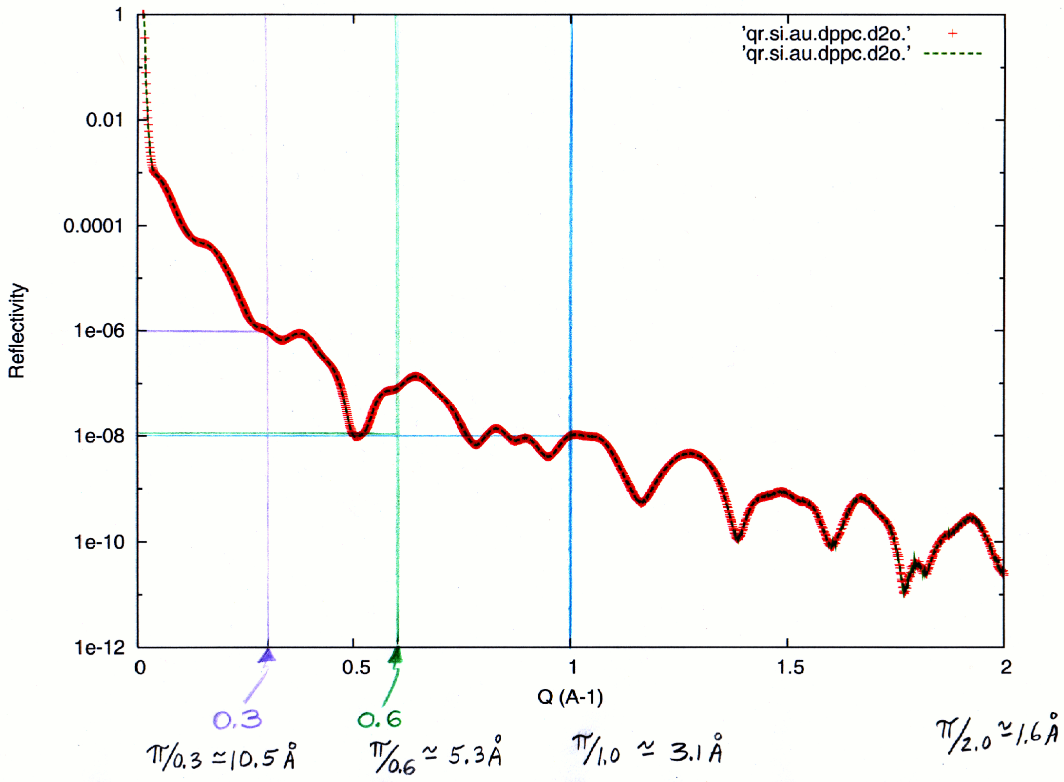
'qr.si.au.dppc.d2o.'
'qr.si.au.dppc.d2o.'
Reflectivity
1
0.01
0.0001
1e-06
1e-08
1e-10
1e-12
0
0.5
1
1.5
2
Q (A-1)
0.3
0.6
π/0.3 ≃ 10.5 Å
π/0.6 ≃ 5.3 Å
π/1.0 ≃ 3.1 Å
π/2.0 ≃ 1.6 Å

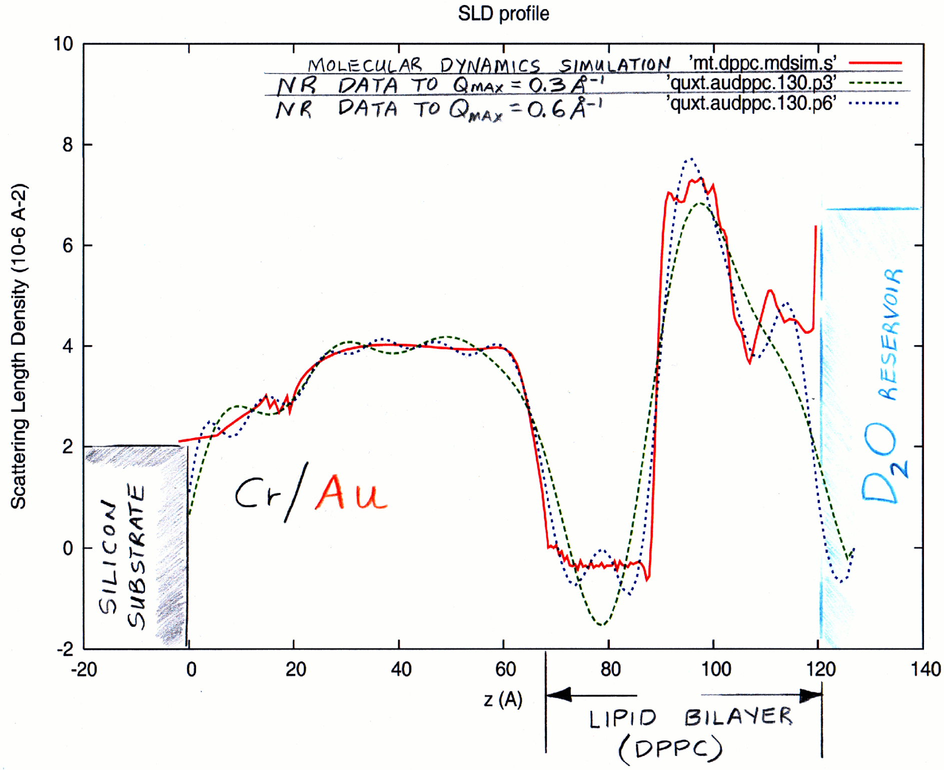
SLD profile
MOLECULAR DYNAMICS SIMULATION 'mt.dppc.mdsim.s'
NR DATA TO QMAX = 0.3 Å-1 'quxt.audppc.130.p3'
NR DATA TO QMAX = 0.6 Å-1 'quxt.audppc.130.p6'
Scattering Length Density (10-6 A-2)
10
8
6
4
2
0
-2
-20
0
20
40
60
80
100
120
140
z (A)
SILICON SUBSTRATE
Cr/Au
D2O RESERVOIR
LIPID BILAYER
(DPPC)

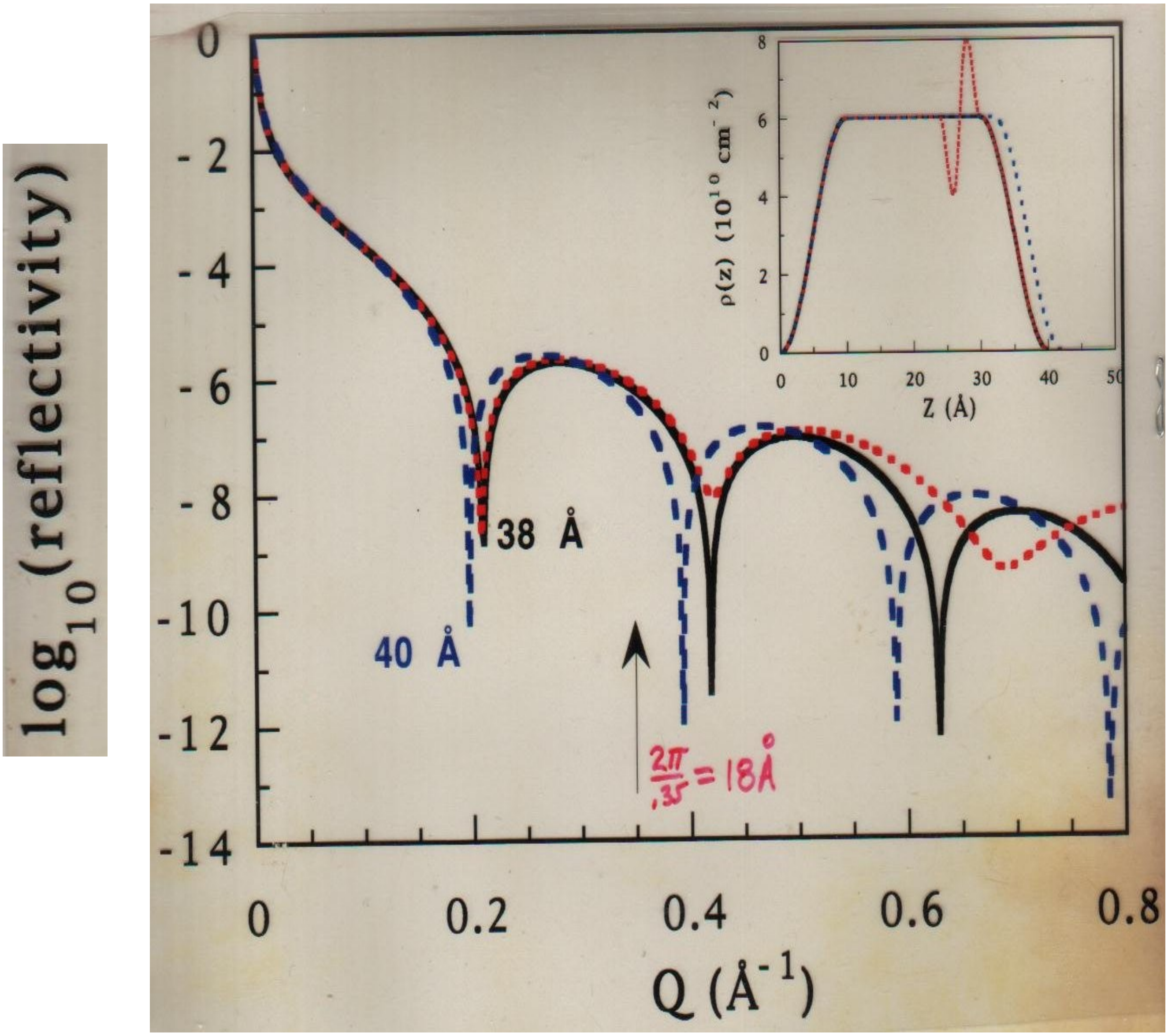

Solid, long-dash, and short-dash neutron reflectivity curves corresponding to their respective scattering length density profiles shown in the inset. This series of curves and profiles illustrates the sensitivity of the reflectivity to the overall film thickness at reflectivities approaching 10-7 whereas detailed features such as the oscillation in the long-dash profile can only be accurately discerned at reflectivities an order of magnitude or so lower, at Q-values corresponding to 2 pi/ width of the feature.

"REFLECTIVITY" REGIME

CRYSTAL "DIFFRACTION" REGIME

LOW Q : HIGHER SENSITIVITY FOR COMPOSITION PROFILE

HIGH Q : HIGHER SENSITIVITY FOR STRAIN OR LATTICE SPACING PROFILE

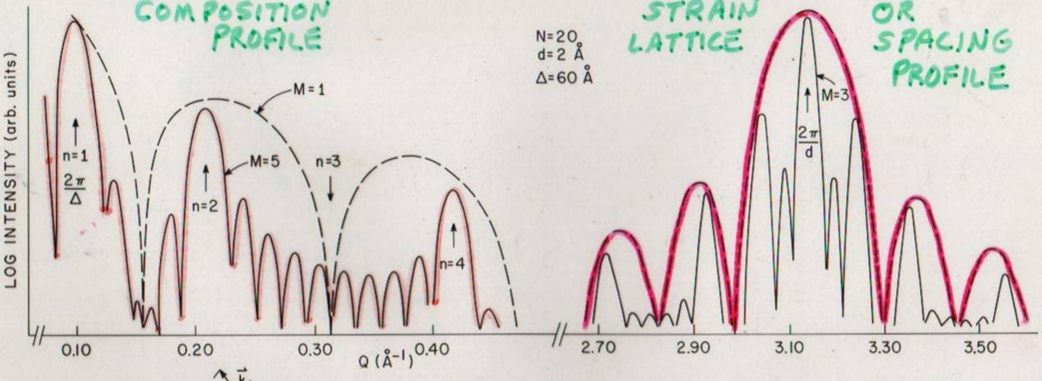

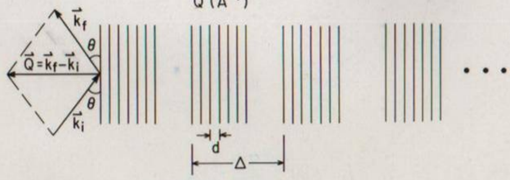

$$|R|^2_{KIN} = \left(\frac{4\pi}{Q}\right)^2 \left| \sum_{m=1}^{M} \sum_{n=1}^{N} \rho\, e^{iQ(nd+m\Delta)} \right|^2$$

$$= \left(\frac{4\pi}{Q}\right)^2 \rho^2 \left| \frac{\sin(NQd/2)}{\sin(Qd/2)} \right|^2 \left| \frac{\sin(MQ\Delta/2)}{\sin(Q\Delta/2)} \right|^2$$

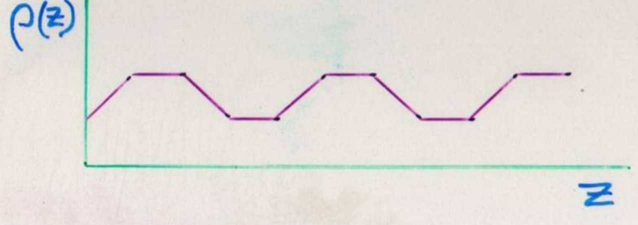

PROBLEM: BORN APPROXIMATION FAILS AT SUFFICIENTLY SMALL Q — MUST THEN USE EXACT THEORY

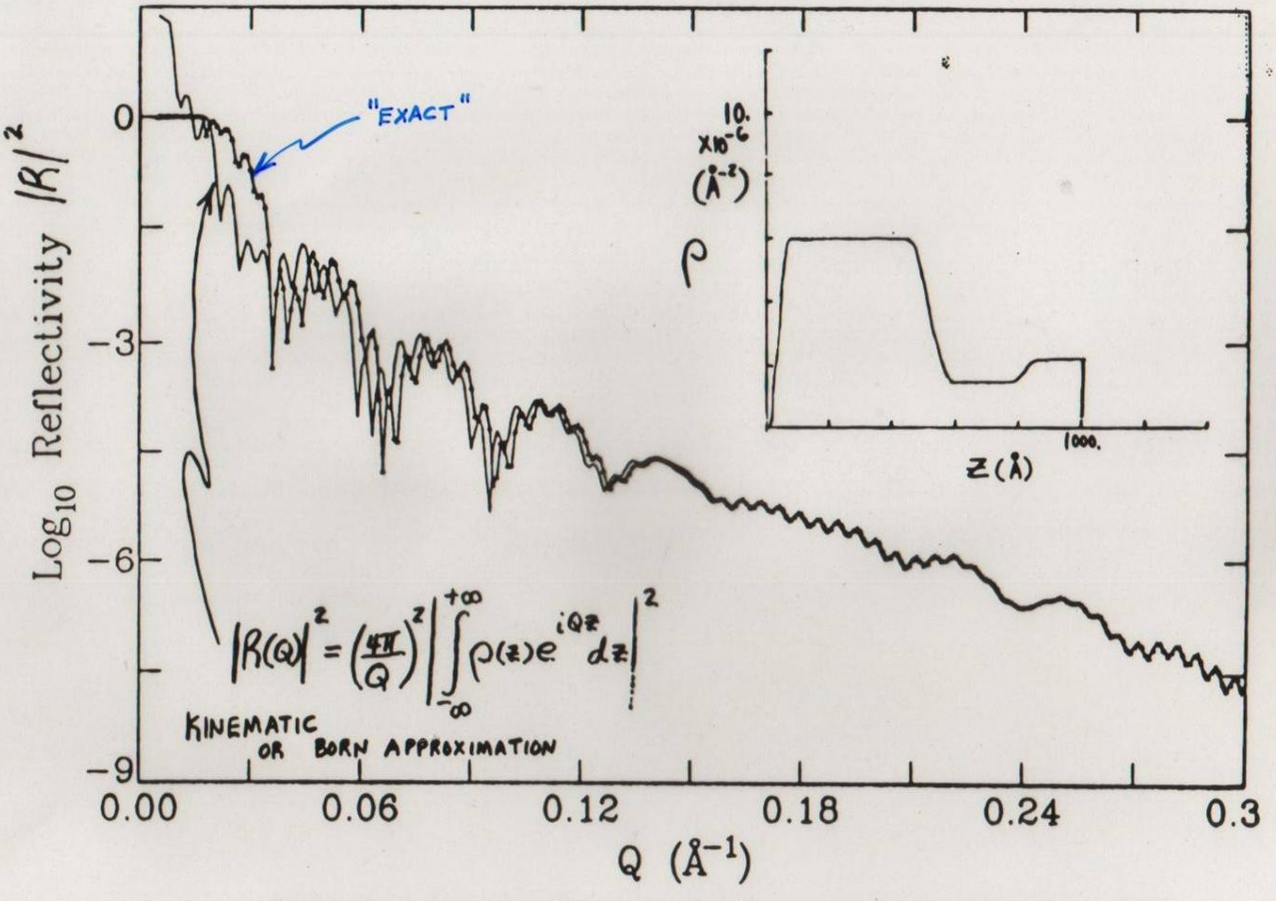

Comparison between kinematic (line) and dynamic (triangle + line) plus-state reflectivities for a density profile similar to that of Fig.2 as described in the text.

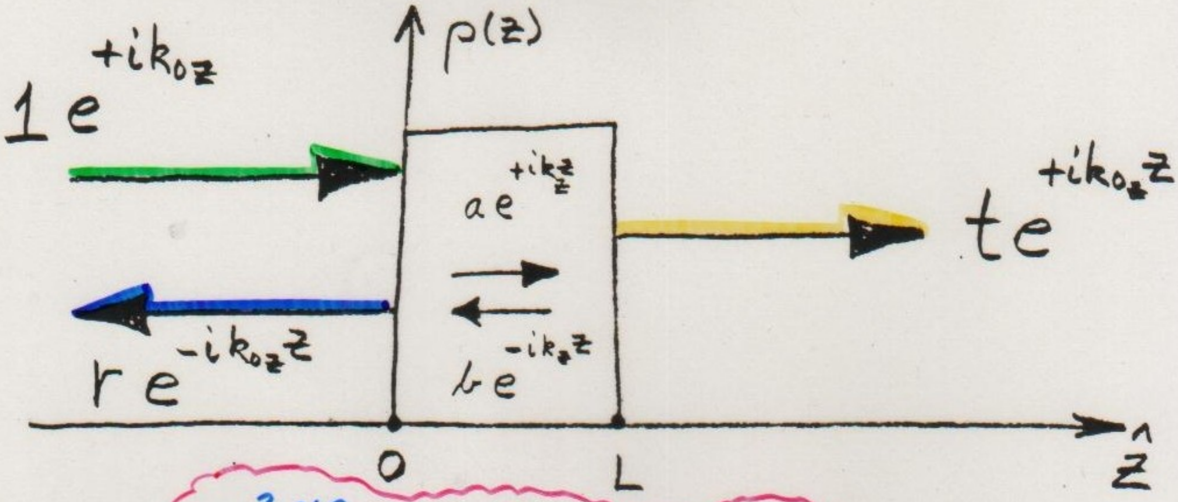

$$\boxed{\frac{\partial^2 \psi(z)}{\partial z^2} + k_z^2\, \psi(z) = 0}$$

CONSERVATION OF MOMENTUM AND PARTICLE NUMBER REQUIRE THAT $\dfrac{\partial \psi(z)}{\partial z}$ AND $\psi(z)$

BE CONTINUOUS AT THE BOUNDARIES $z=0$ & $z=L$

$$\begin{pmatrix} t \\ it \end{pmatrix} e^{ik_{0z}L} = \begin{pmatrix} A & B \\ C & D \end{pmatrix} \begin{pmatrix} 1+r \\ i(1-r) \end{pmatrix}$$

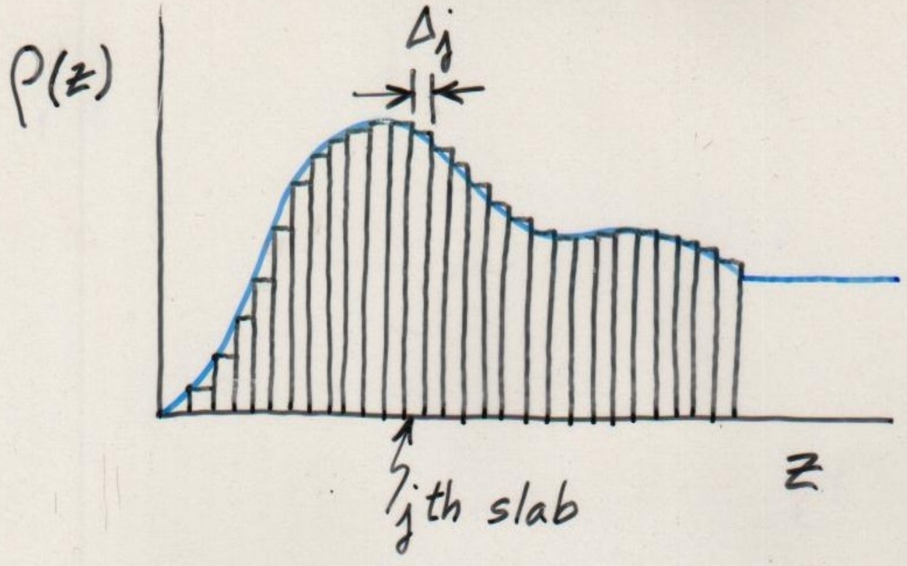

$$\begin{pmatrix} A & B \\ C & D \end{pmatrix} = \begin{pmatrix} a_N & b_N \\ c_N & d_N \end{pmatrix} \begin{pmatrix} a_{N-1} & b_{N-1} \\ c_{N-1} & d_{N-1} \end{pmatrix} \cdots \begin{pmatrix} a_2 & b_2 \\ c_2 & d_2 \end{pmatrix} \begin{pmatrix} a_1 & b_1 \\ c_1 & d_1 \end{pmatrix}$$

$$\begin{pmatrix} a_j & b_j \\ c_j & d_j \end{pmatrix} = \begin{pmatrix} \cos \delta_j & \frac{1}{n_{z_j}} \sin \delta_j \\ -n_{z_j} \sin \delta_j & \cos \delta_j \end{pmatrix}$$

$$\delta_j = k_{0z} n_{z_j} \Delta_j$$

$$= k_{z_j} \Delta_j$$

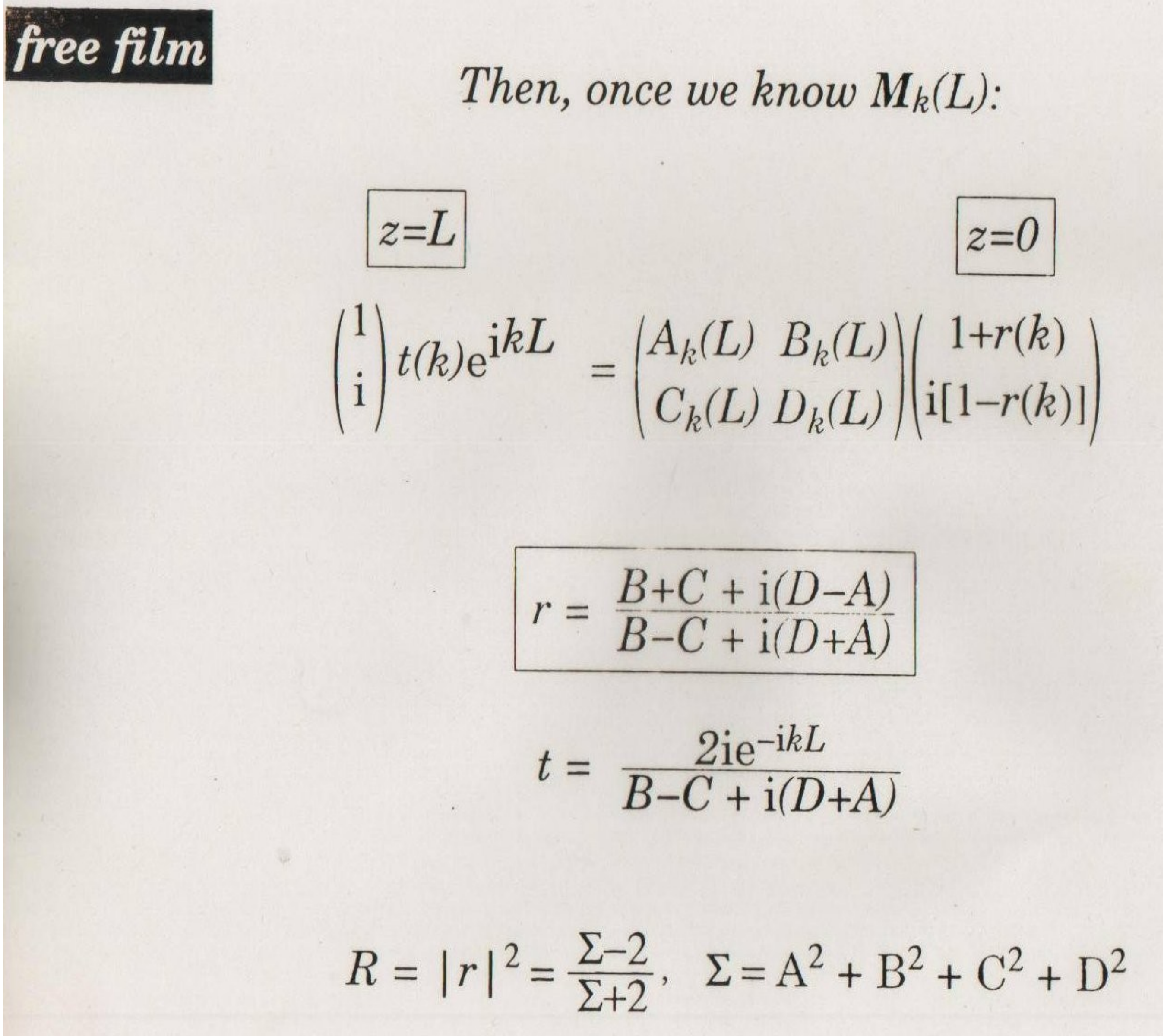

free film

Then, once we know $\mathbf{M}_k(L)$*:*

$\boxed{z=L}$ $\qquad\qquad\qquad\qquad$ $\boxed{z=0}$

$$\begin{pmatrix} 1 \\ \mathrm{i} \end{pmatrix} t(k)\mathrm{e}^{\mathrm{i}kL} = \begin{pmatrix} A_k(L) & B_k(L) \\ C_k(L) & D_k(L) \end{pmatrix} \begin{pmatrix} 1+r(k) \\ \mathrm{i}[1-r(k)] \end{pmatrix}$$

$$\boxed{r = \frac{B+C+\mathrm{i}(D-A)}{B-C+\mathrm{i}(D+A)}}$$

$$t = \frac{2\mathrm{i}\mathrm{e}^{-\mathrm{i}kL}}{B-C+\mathrm{i}(D+A)}$$

$$R = |r|^2 = \frac{\Sigma-2}{\Sigma+2}, \quad \Sigma = \mathrm{A}^2 + \mathrm{B}^2 + \mathrm{C}^2 + \mathrm{D}^2$$

(Courtesy of Norm Berk)

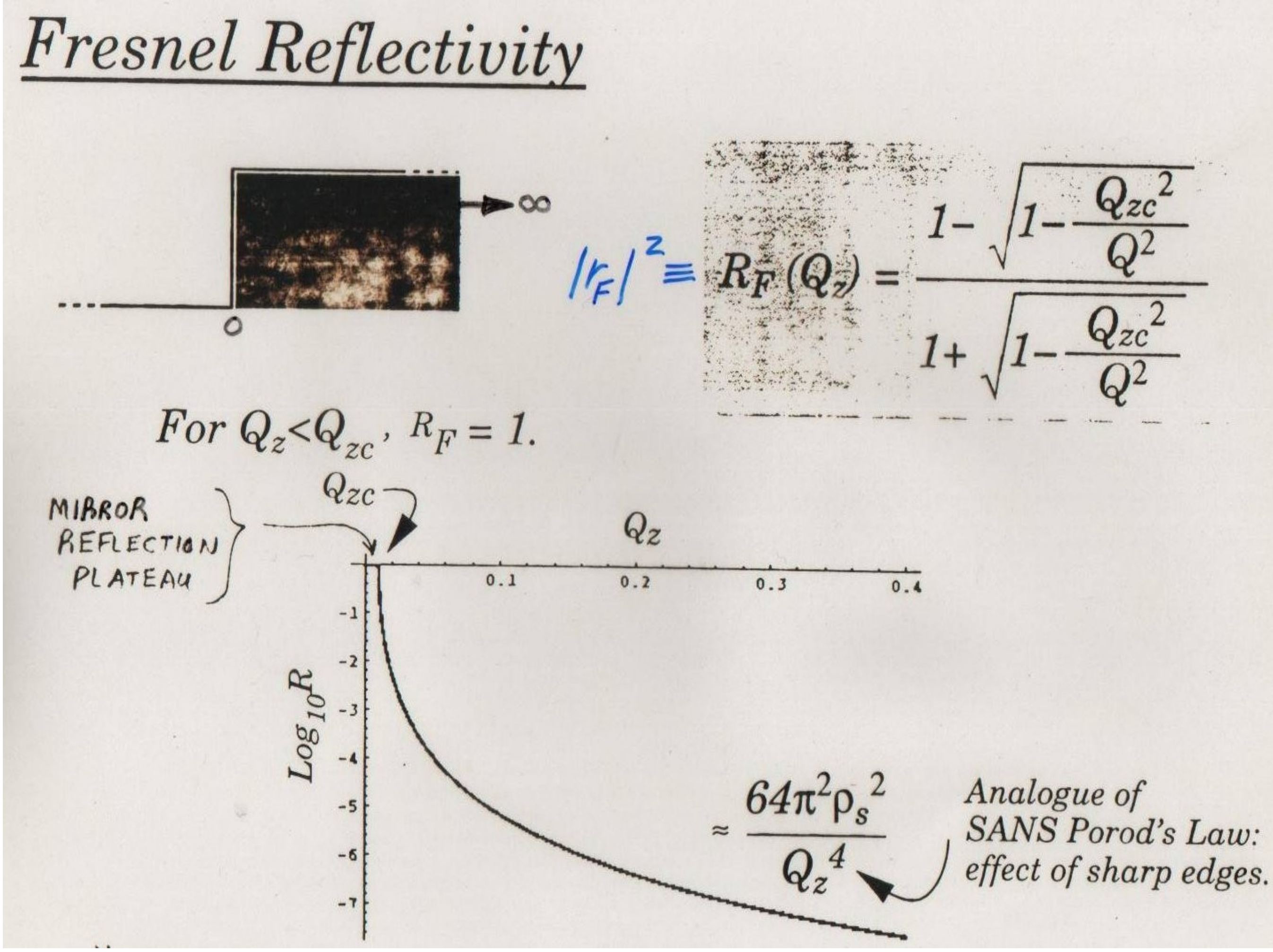

Fresnel Reflectivity

$$|r_F|^2 \equiv R_F(Q_z) = \frac{1-\sqrt{1-\frac{Q_{zc}^2}{Q^2}}}{1+\sqrt{1-\frac{Q_{zc}^2}{Q^2}}}$$

For $Q_z<Q_{zc}$, $R_F = 1$.

MIRROR REFLECTION PLATEAU

$$\approx \frac{64\pi^2\rho_s^2}{Q_z^4}$$

Analogue of SANS Porod's Law: effect of sharp edges.

Qzc = SQRT(16*pi*rho) (Courtesy of Norm Berk)

"*Soft*" *substrate*

Smooth transition:

interlayer diffusion
roughness

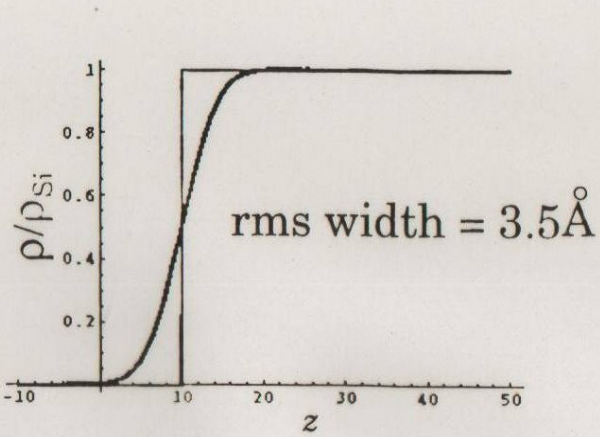

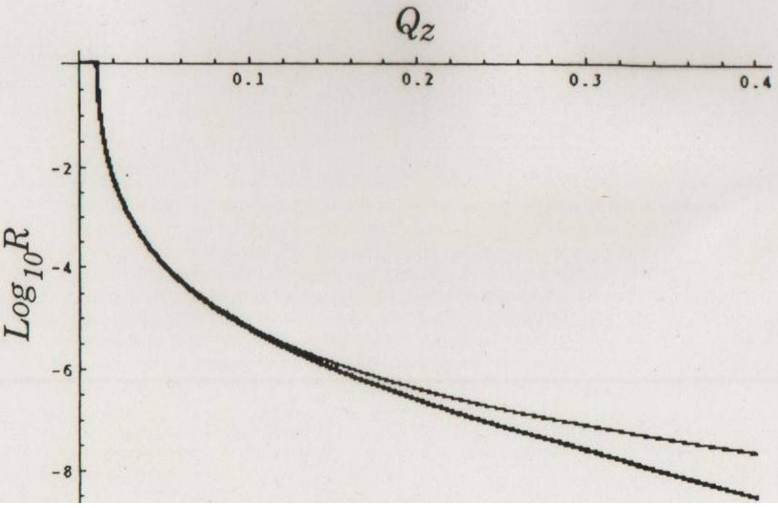

(N.F. BERK)

Uniform slab

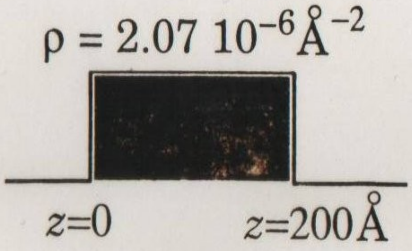

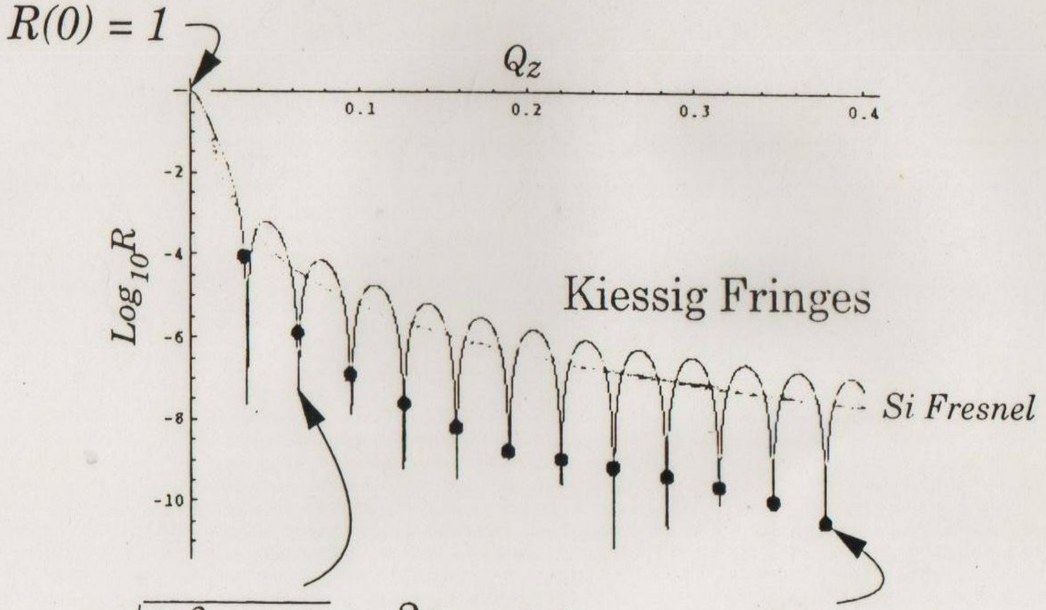

$\sqrt{Q_z^2 - 16\pi\rho} = \frac{2\pi}{L}$ m=1,2,...

$\frac{2\pi}{L}$ m=1,2,...

(Kinematical)

(N.F. BERK)

Multilayer on Si

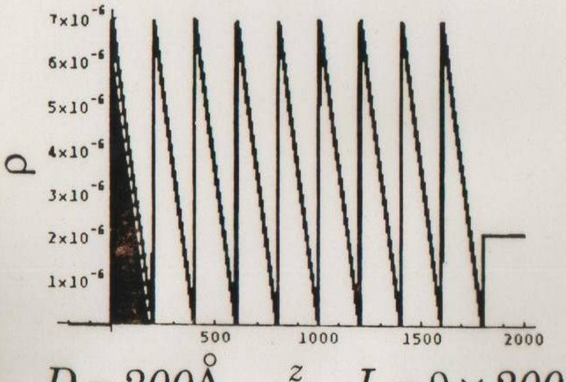

$D = 200\text{Å}$ $\qquad$ $L = 9 \times 200\text{Å}$

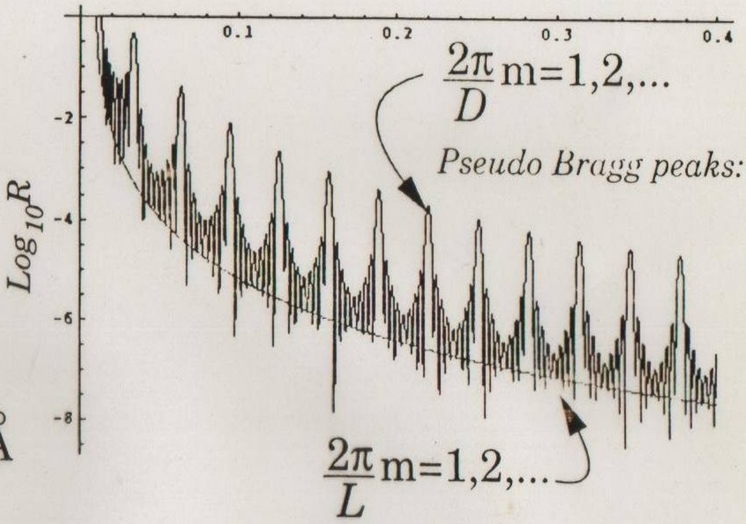

$\frac{2\pi}{D}$ m=1,2,...

Pseudo Bragg peaks:

$\frac{2\pi}{L}$ m=1,2,...

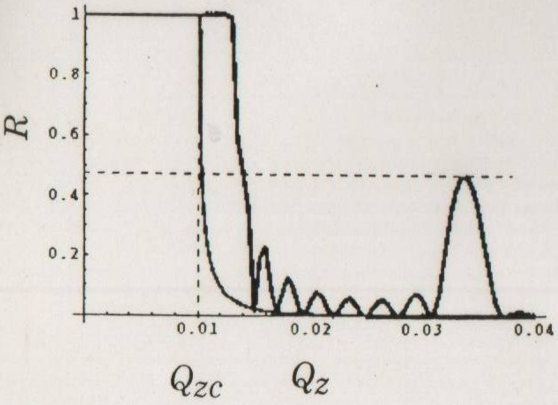

$L = 18 \times 200\text{Å}$

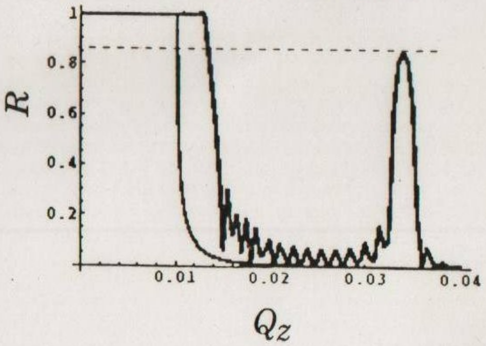

(N.F. BERK)

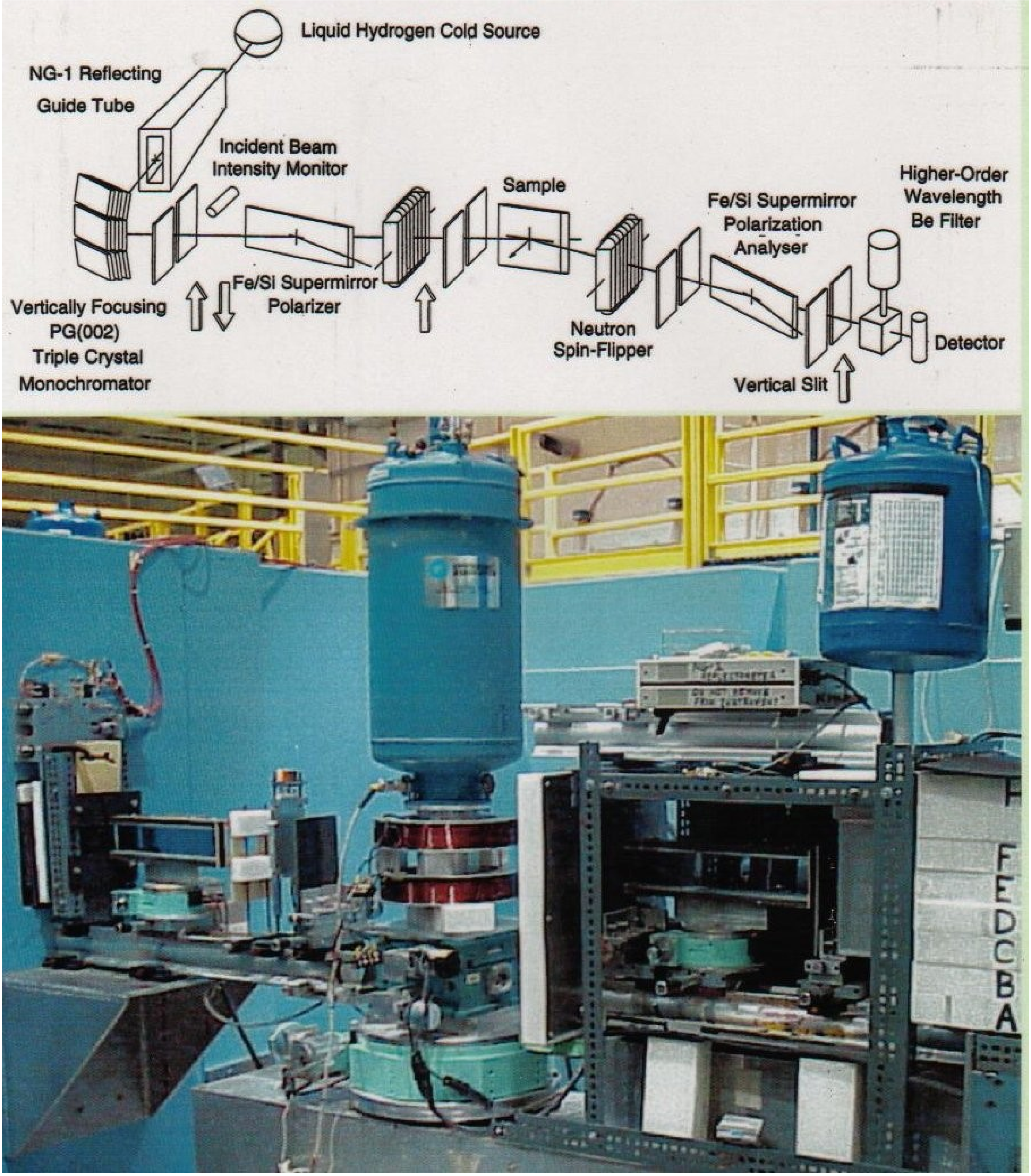

Polarized neutron reflectometer at NIST

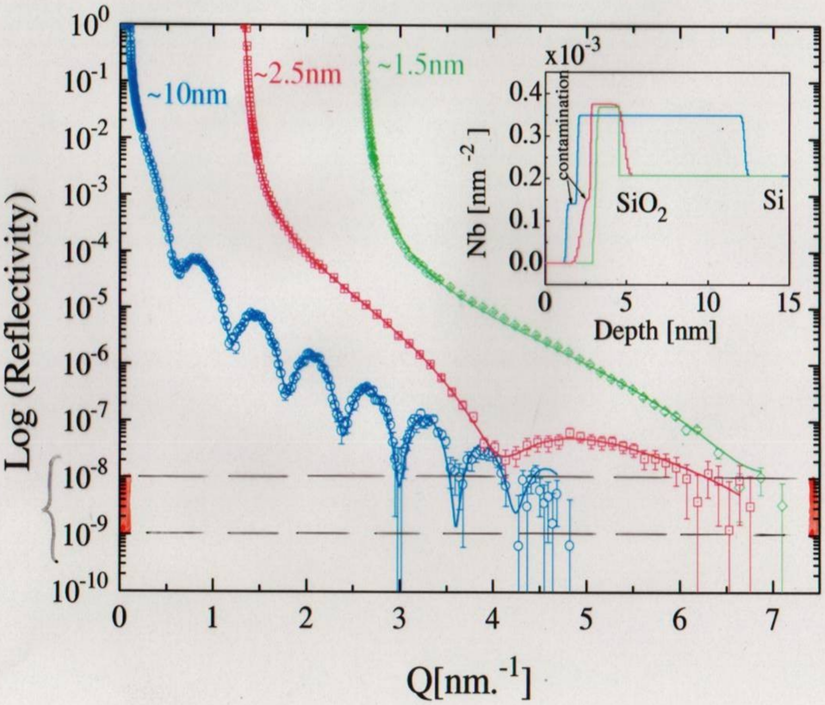

Log (Reflectivity)
10^0
10^{-1}
10^{-2}
10^{-3}
10^{-4}
10^{-5}
10^{-6}
10^{-7}
10^{-8}
10^{-9}
10^{-10}
~10nm
~2.5nm
~1.5nm
0
1
2
3
4
5
6
7
Q[nm.$^{-1}$]
x10^{-3}
Nb [nm $^{-2}$]
0.4
0.3
0.2
0.1
0.0
contamination
SiO$_2$
Si
0
5
10
15
Depth [nm]

J. DURA et a.l.

$$Q = \frac{4\pi \sin\theta}{\lambda}$$

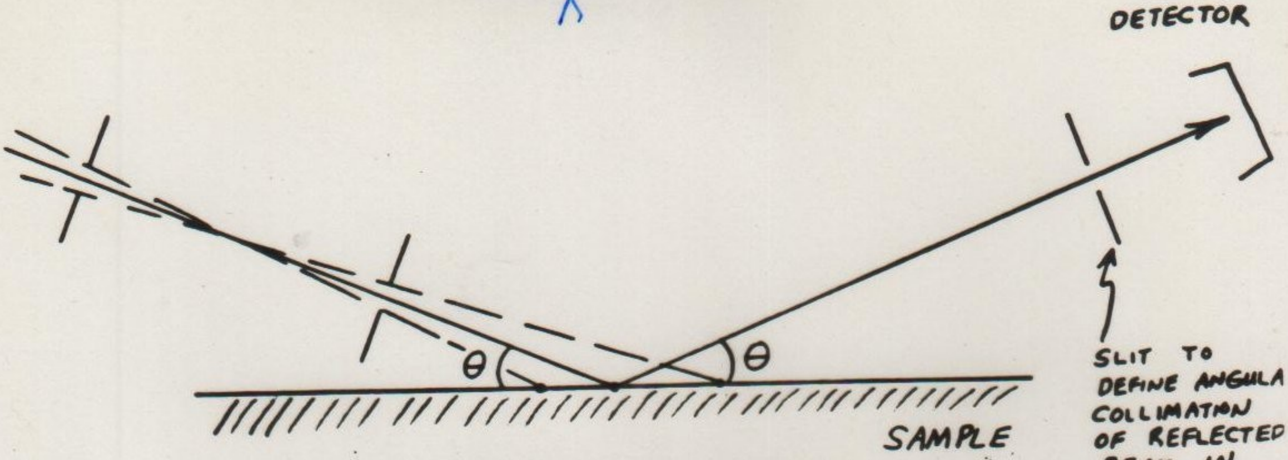

SLIT TO DEFINE ANGULA COLLIMATION OF REFLECTED BEAM IN NONSPECULAR OR TRANSVER Q-SCANS

$$\Delta Q_{\text{LONGITUDINAL}} \simeq \frac{\Delta\lambda}{\lambda} Q + \sqrt{\left(\frac{4\pi}{\lambda}\right)^2 - Q^2}\ \Delta\theta$$

$$\text{TYPICAL VALUES} \left\{ \begin{array}{l} \dfrac{\Delta\lambda}{\lambda} \simeq 0.01 \\ \Delta\theta \simeq 1 \text{ min of arc} \end{array} \right.$$

$$\text{KEEP } \frac{\Delta Q}{Q} \simeq \text{CONSTANT}$$

$$R_{\text{OBS.}}(Q_0) \simeq \left(\frac{0.9394}{\Gamma}\right) \int_{-\Gamma}^{+\Gamma} R_{\text{ACT.}}(Q)\, e^{-\left(\frac{2.7725}{\Gamma^2}\right)(Q-Q_0)^2}\, dQ$$

(ASSUMING A GAUSSIAN DISTRIBUTION OF Q-VALUES)

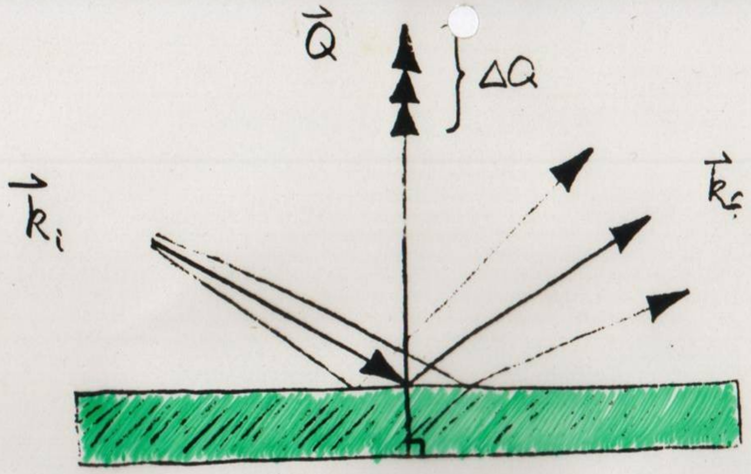

FLAT
SUBSTRATE

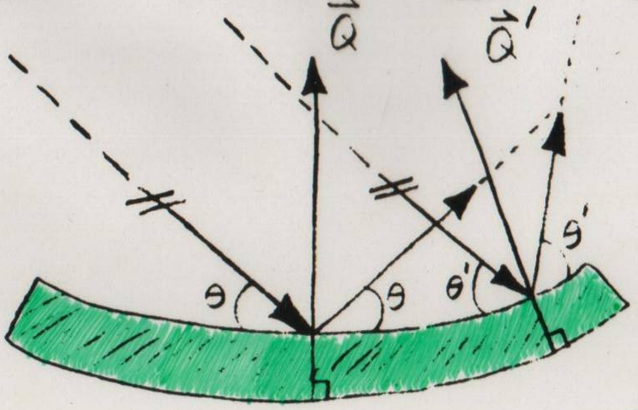

CURVED
SUBSTRATE

IF ρ IS NOT EXACTLY $\rho(z)$, i.e., SOME VARIATIONS EXIST IN THE (X, Y)- PLANE, THEN

$$r_{BORN} \simeq \frac{4\pi}{iQ} \int_{-\infty}^{+\infty} \langle \rho(x,y,z) \rangle_{x,y} \, e^{iQz} \, dz$$

ON SPECULAR "RIDGE" WHERE $\vec{Q} = Q_z \hat{z}$

WHERE

$$\langle \rho(x,y,z) \rangle_{x,y} = \frac{1}{A} \int_{-\infty}^{+\infty} \int_{-\infty}^{+\infty} \rho(x,y,z) \, dx dy$$

$= \bar{\rho}(z)$ ONLY

& A = NORMALIZING AREA OF THE (X,Y)- PLANE

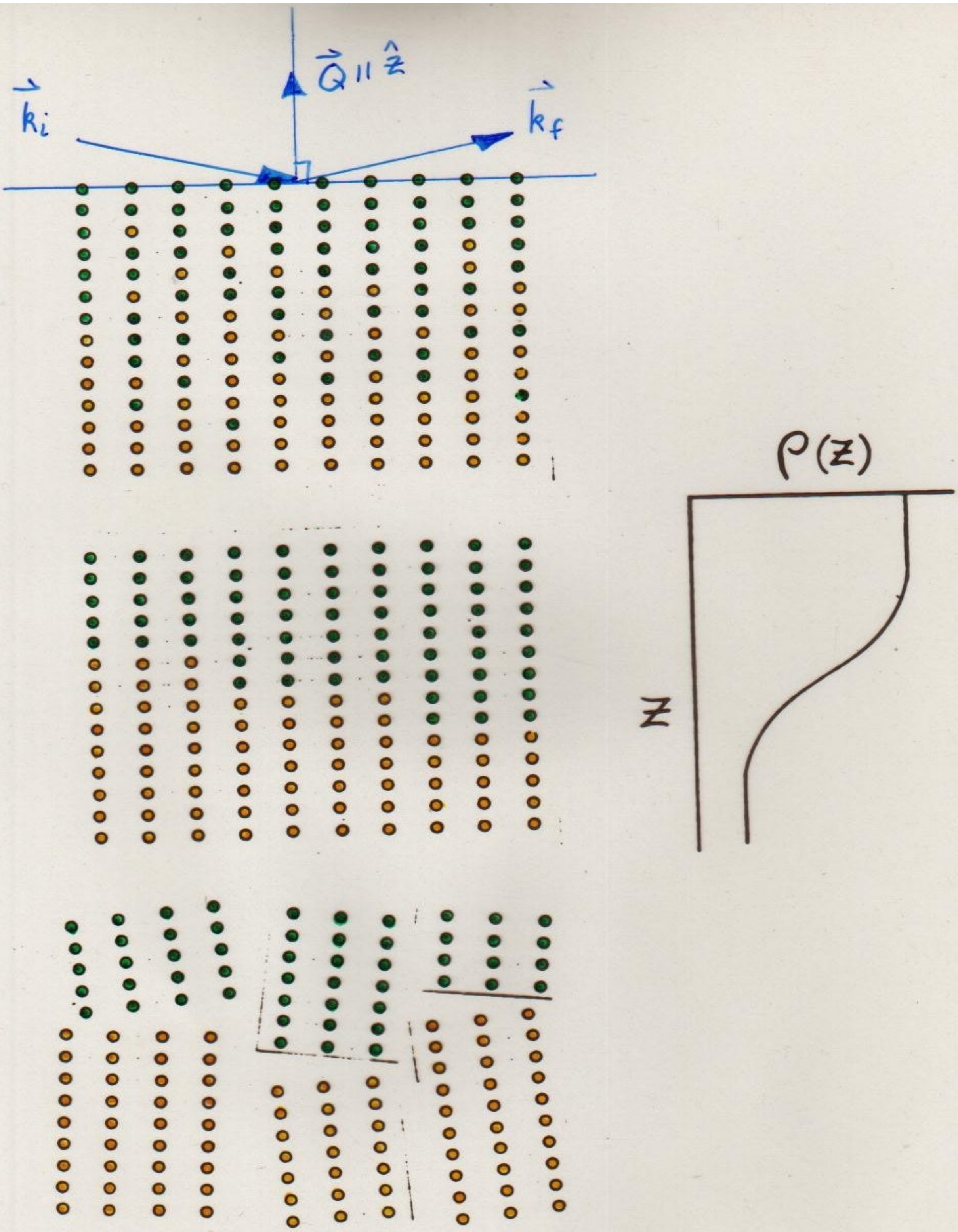

POSSIBLE MICROSTRUCTURES CORRESPONDING TO INTERFACIAL ROUGHNESS

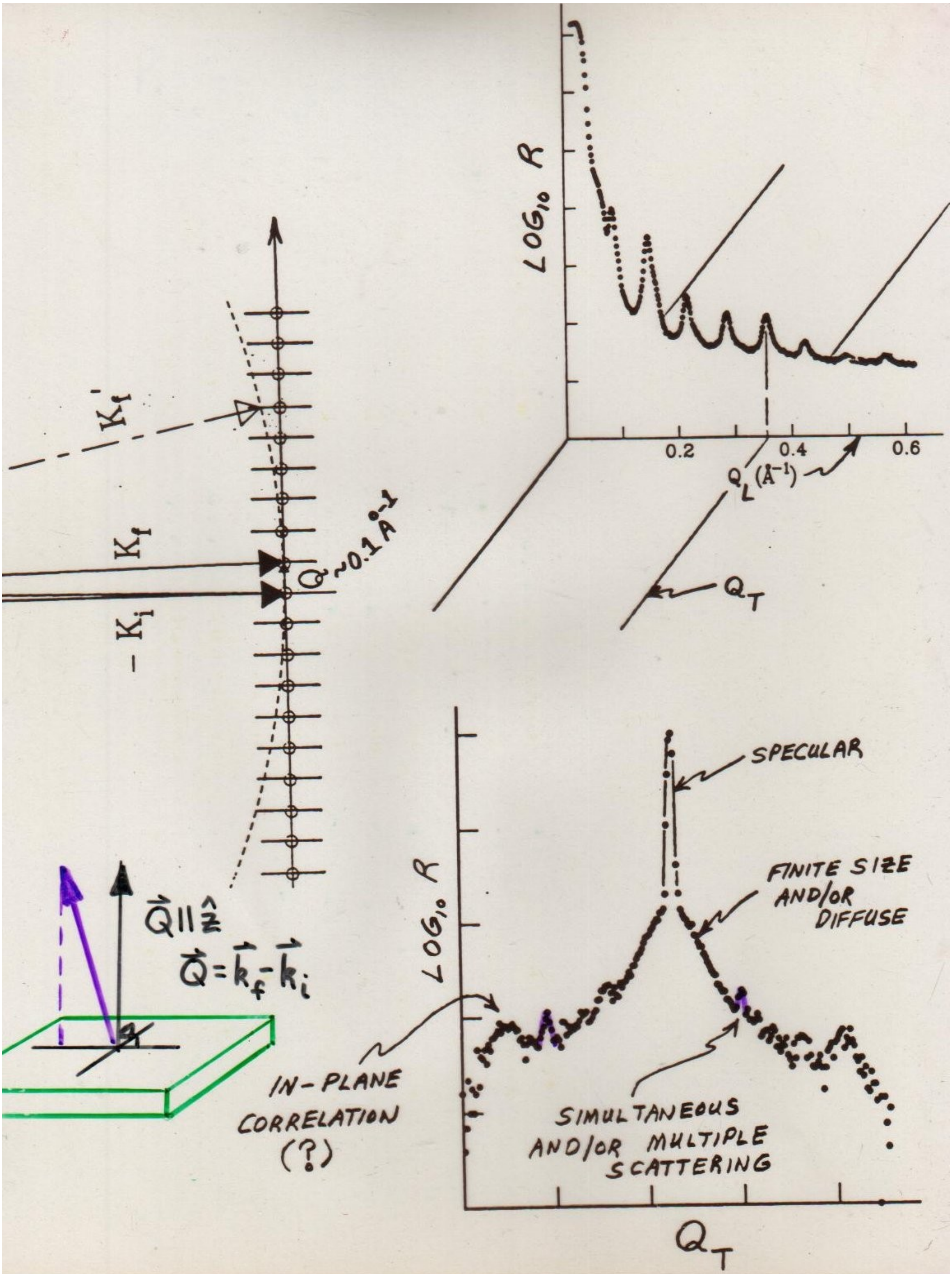

LOG₁₀ R
0.2
0.4
0.6
Q_L (Å⁻¹)
Q_T
K_f'
K_f
- K_i
Q ~0.1 Å⁻¹
Q ∥ ẑ
Q = k_f - k_i
SPECULAR
FINITE SIZE AND/OR DIFFUSE
LOG₁₀ R
IN-PLANE CORRELATION (?)
SIMULTANEOUS AND/OR MULTIPLE SCATTERING
Q_T

Diblock copolymer lamellar nanostructures – R.Jones, B.Berry, and K.Yager (NIST Polymer Division) and S.Satija, J.Dura, B.Maranville et al. (NCNR).

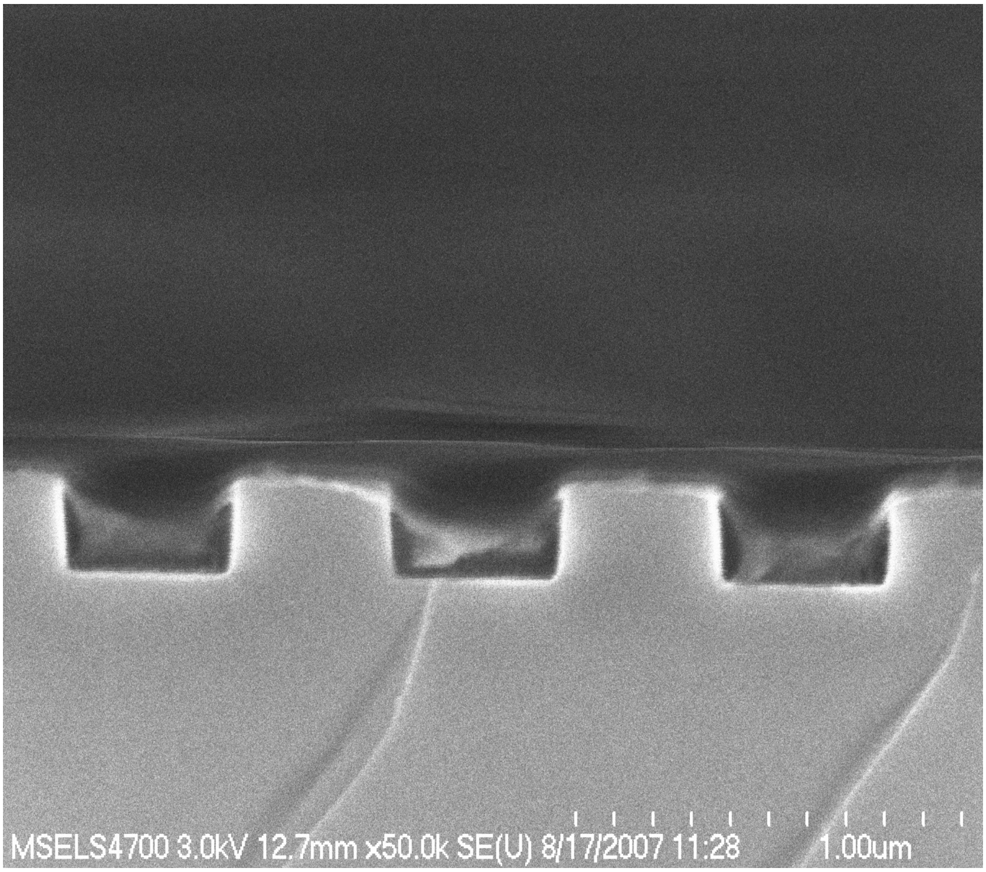

Fig 1. Side-view scanning-electron micrograph of laser-interfe
with 400 nm channels, spaced by 400 nm for a total repeat dis

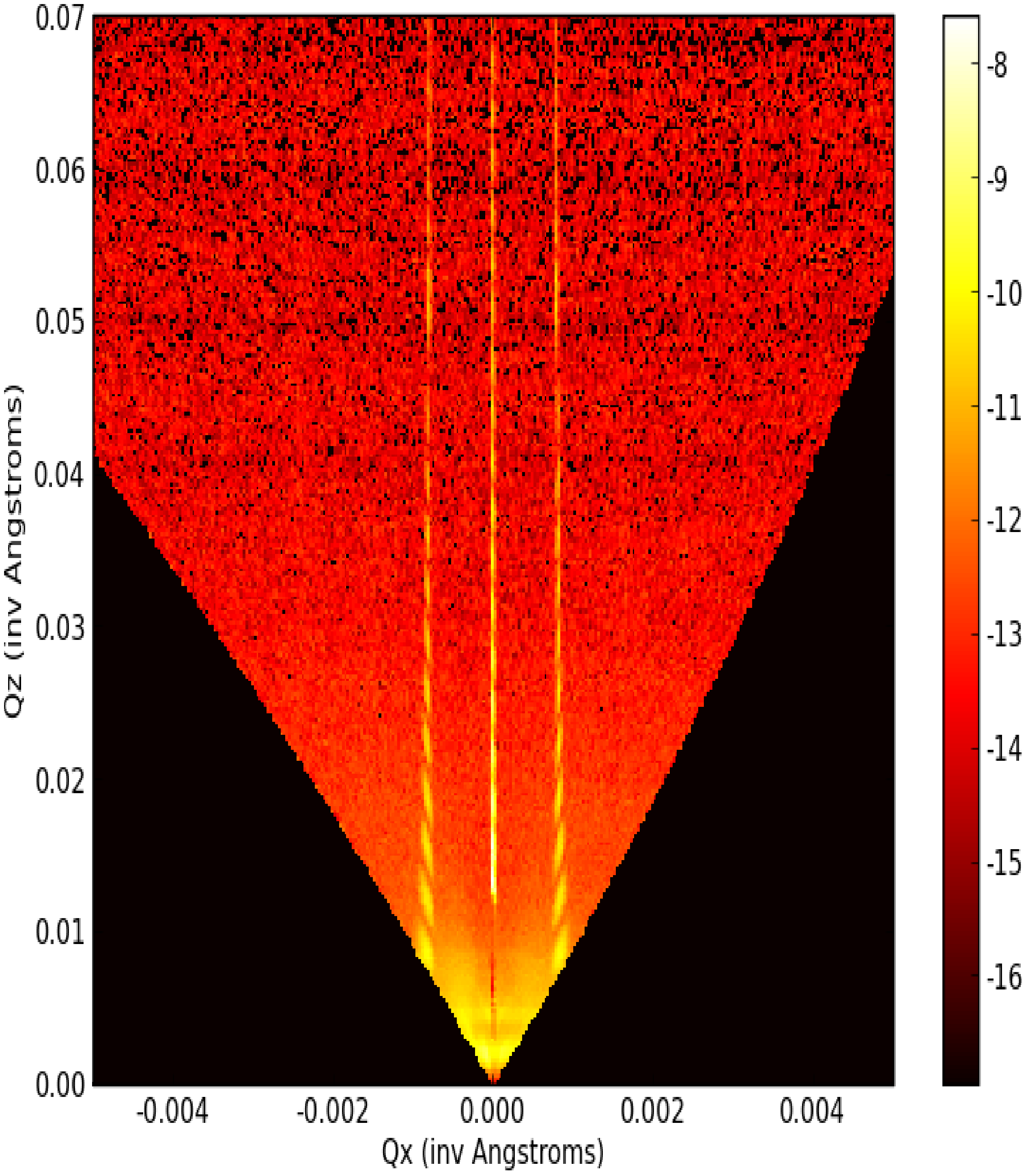

Neutron diffraction from silicon with channels but without polymer.

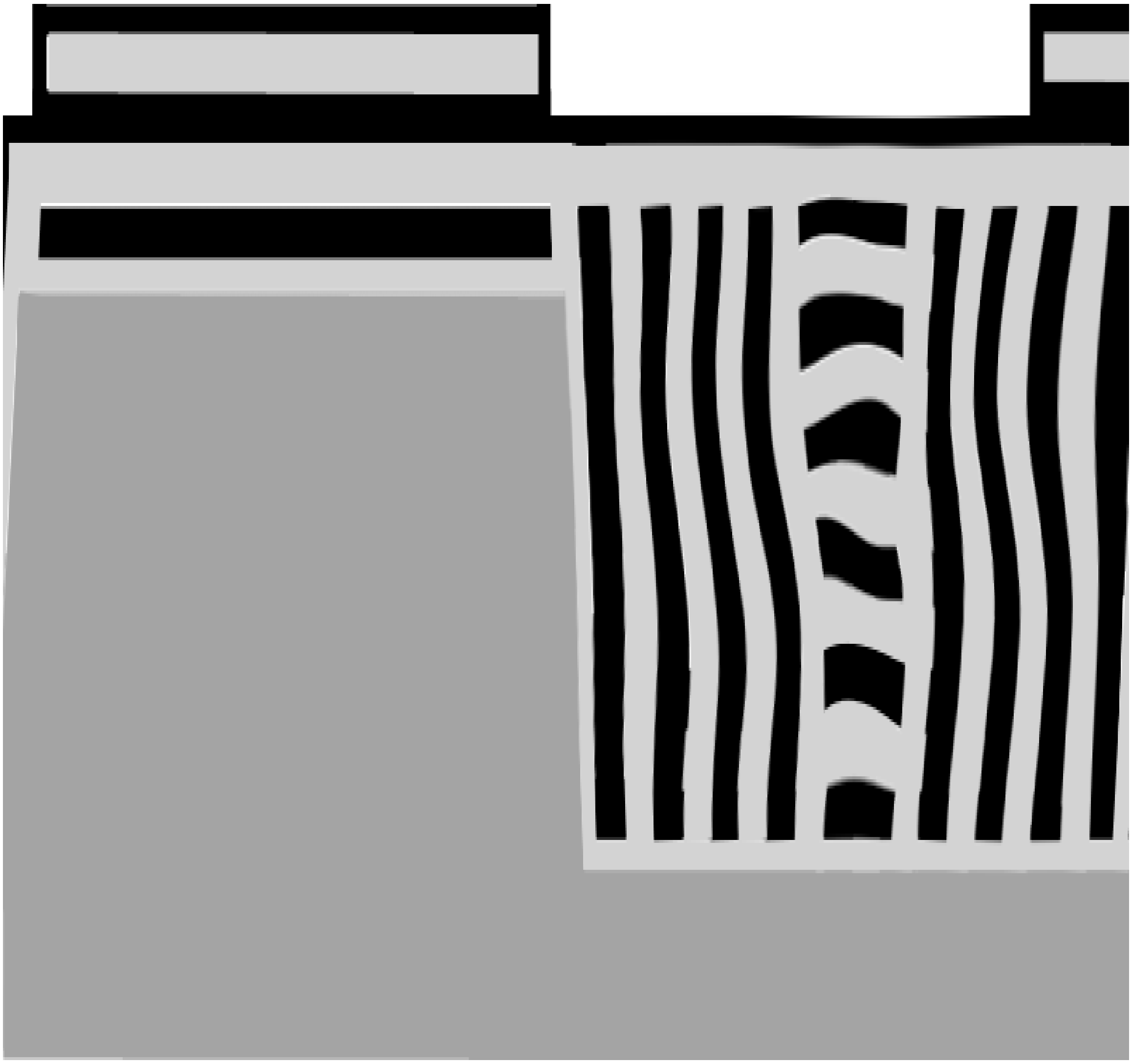

Fig 2. Diagram of expected orientation of lan
Silicon substrate with etched channels is disp
corresponding to the two polymer component

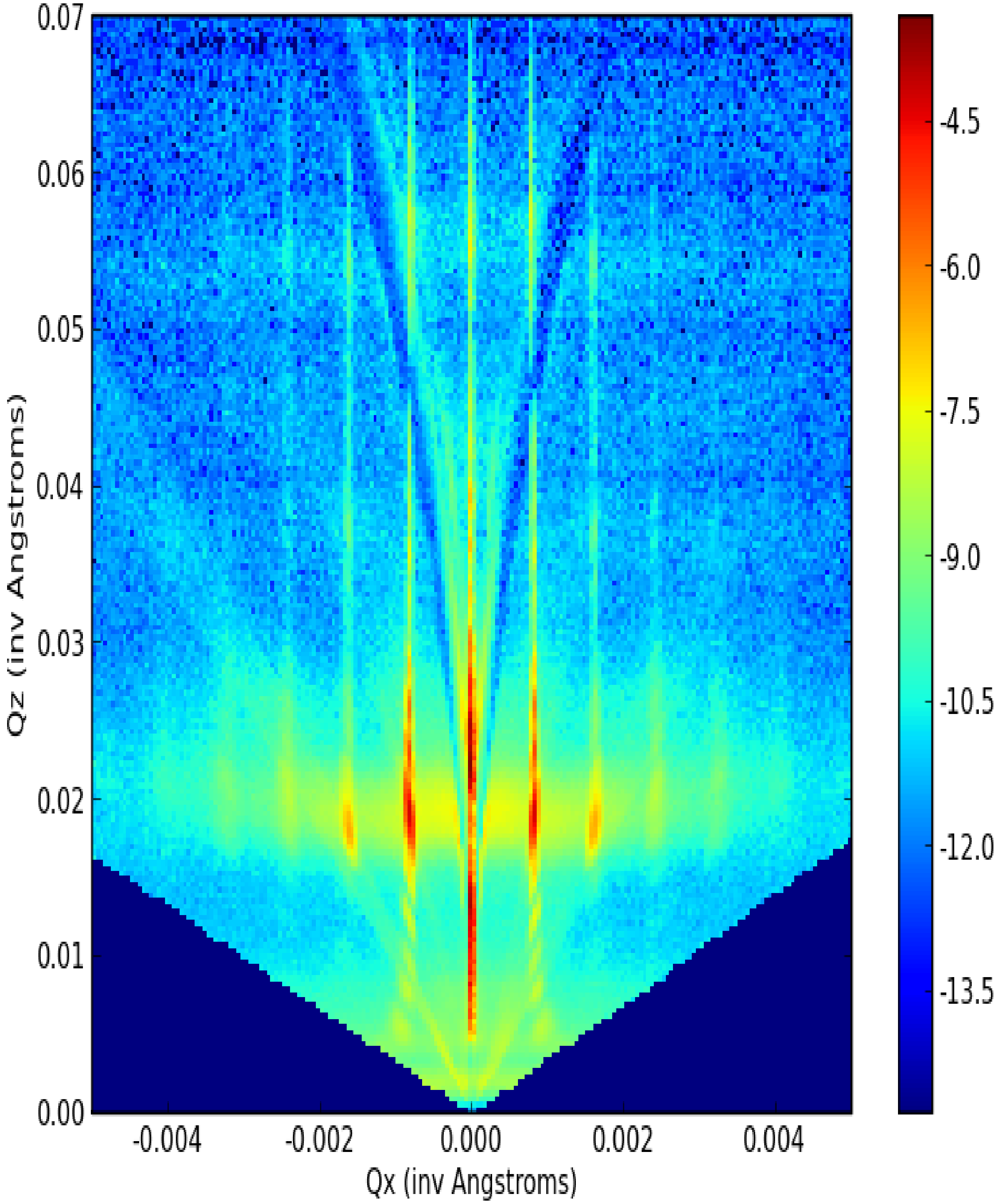

Neutron diffraction from Si channels filled with ordered diblock copolymer.

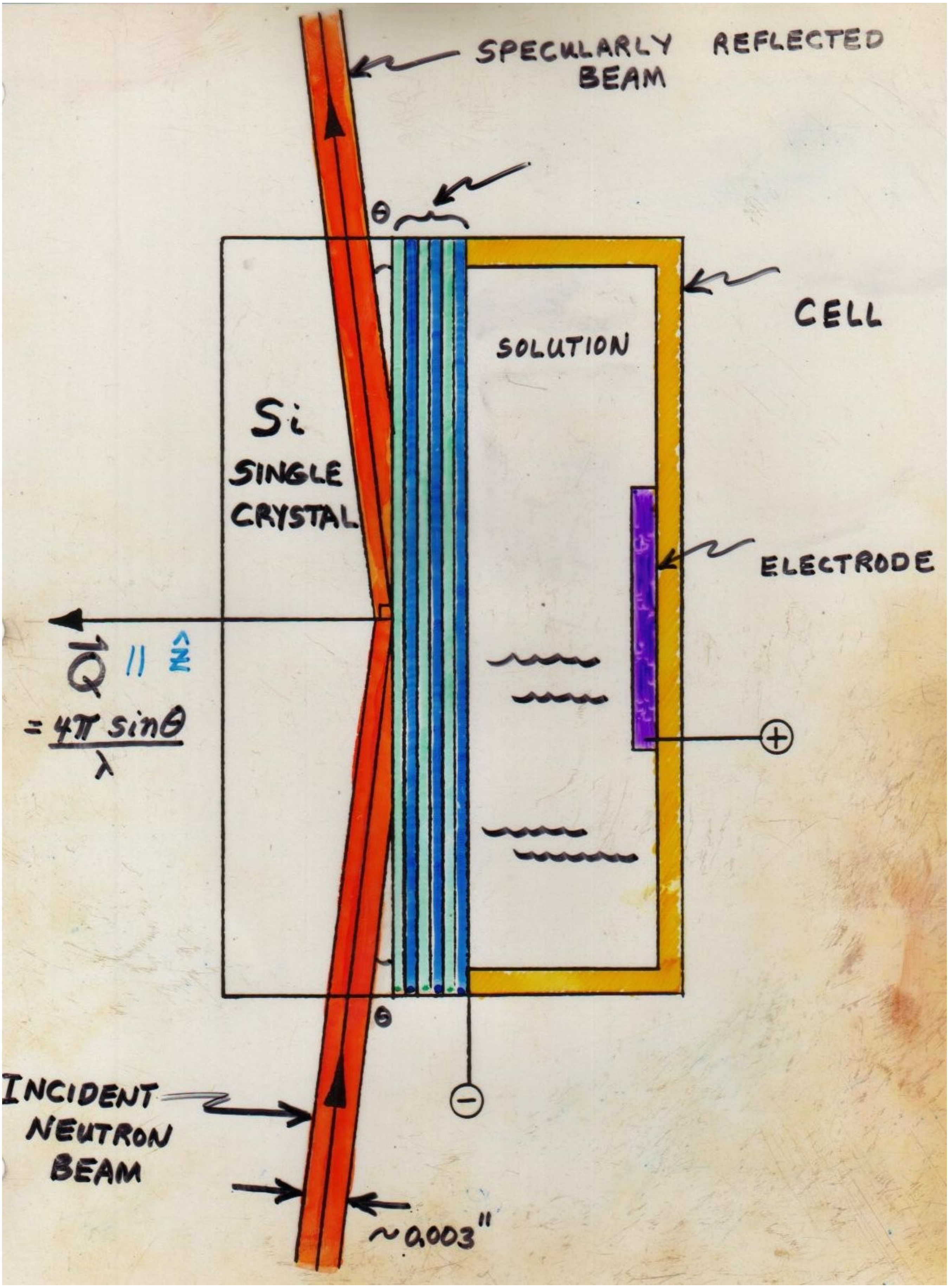
SPECULARLY REFLECTED BEAM
θ
CELL
SOLUTION
Si
SINGLE CRYSTAL
ELECTRODE
$\vec{Q} \parallel \hat{z}$
$= \frac{4\pi \sin\theta}{\lambda}$
$\oplus$
θ
$\ominus$
INCIDENT NEUTRON BEAM
~0.003"

Part 2: The Phase problem, Direct Inversion and Simultaneous Fitting

<> ambiguous SLD profiles from reflected *intensities*

<> measurement of reflection *amplitude* via references yields unique solution -- one-to-one correspondence with SLD profile

<> given the reflection amplitude, exact, first-principles inversion to obtain unique SLD profile for specular reflection is possible

<> simultaneous fitting of multiple composite (sample + reference) reflectivity data sets can lead to unambiguous solution as well

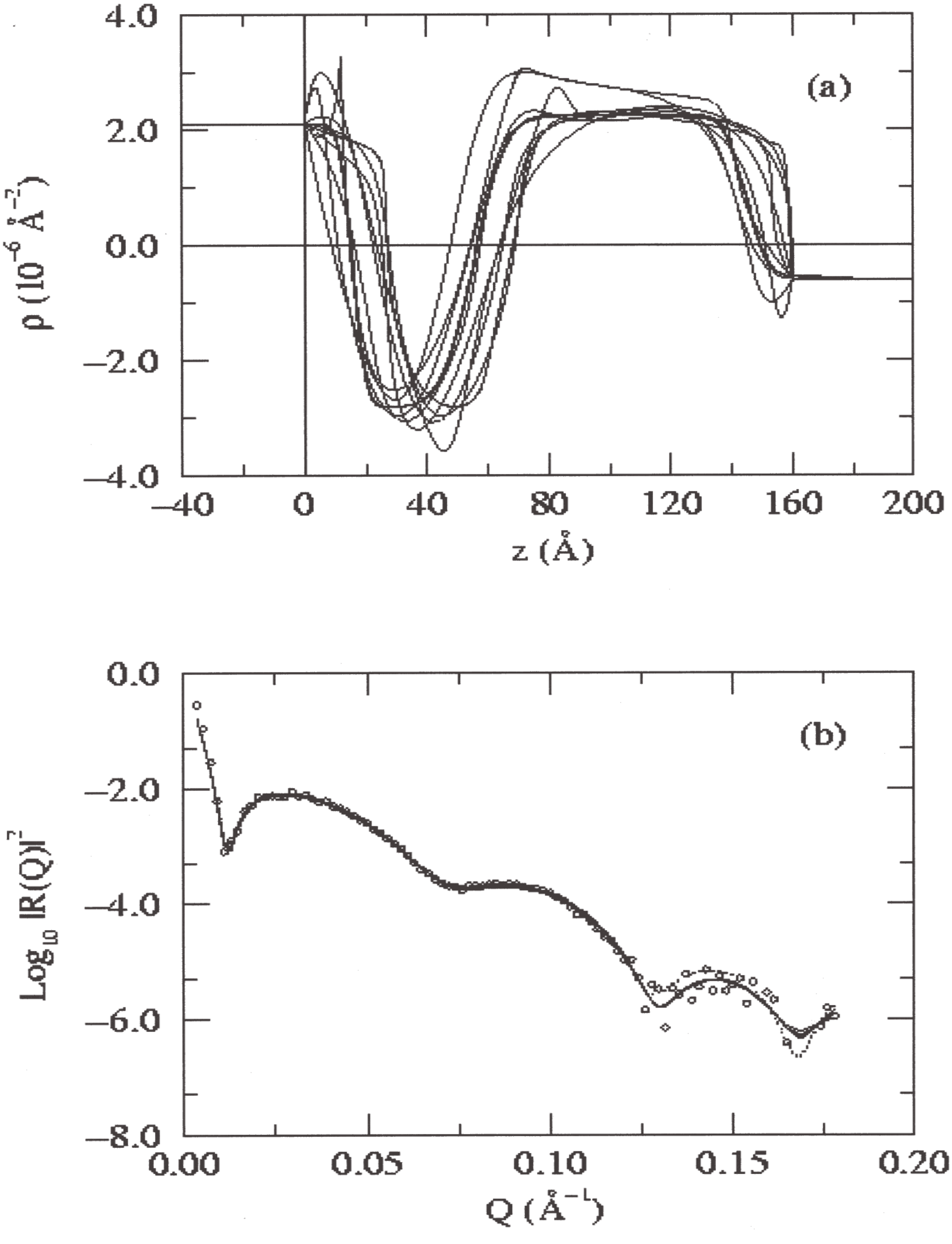

Repeated fits of reflectivity data from a Ti/TiO film system on a Si substrate in contact with an aqueous reservoir (Berk et al.).

TiO in situ: Wiesler, et al.

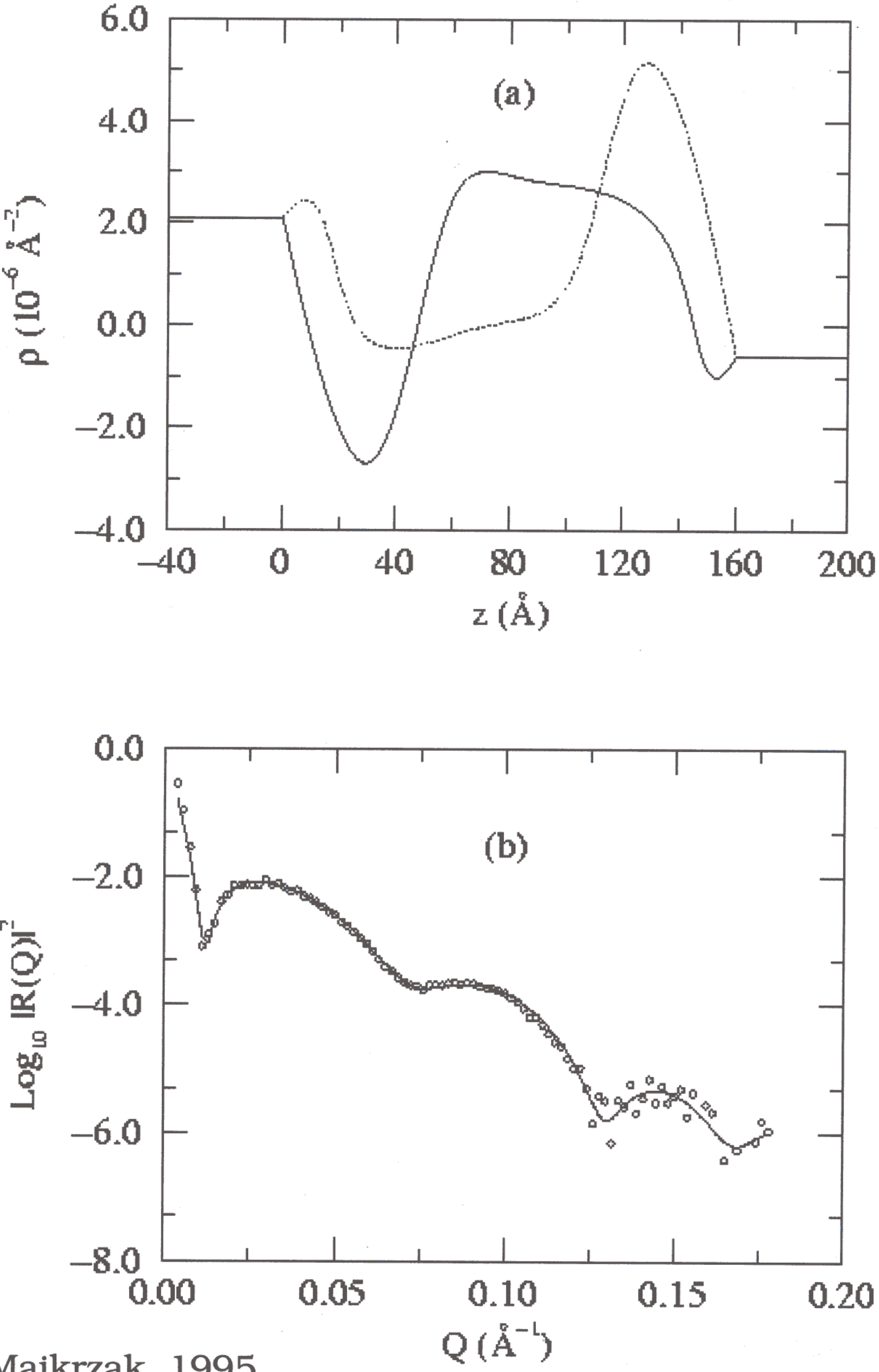

Berk & Majkrzak, 1995

Inverting reflectivity

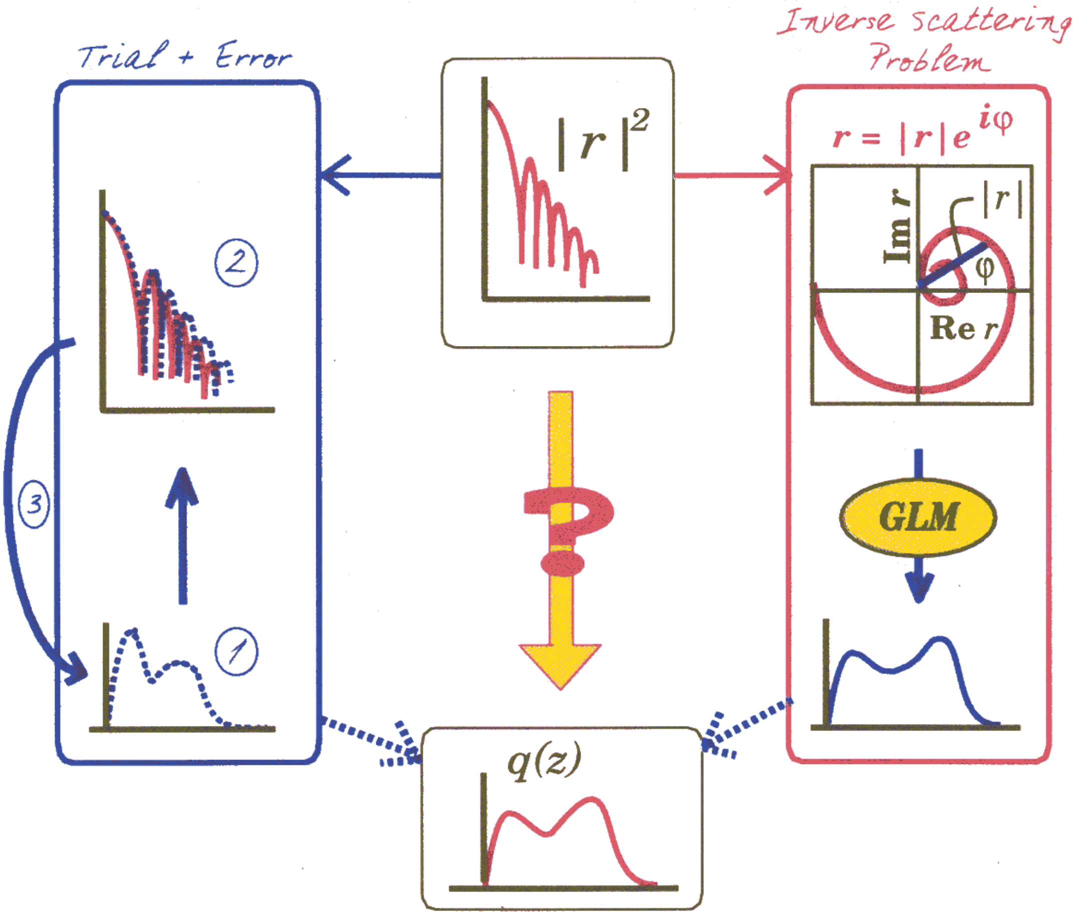

Phase determination

C.F. Majkrzak and N.F. Berk, Phys. Rev. B **52**, 10827 (1995).
V.–O. de Haan, et al., Phys. Rev. B **52**, 10830 (1995).

H. Leeb, H.R. Lipperheide and G. Reiss, this conference.

Logarithmic dispersion

W.L. Clinton, Phys. Rev. B **48**, 1 (1993).

Tunneling times

H. Fiedeldey, H.R. Lipperheide, et al., Phys. Lett. A **170**, 347 (1992).

Pseudo–inversion

S.K. Sinha, et al., *Surface X–Ray and Neutron Scattering*, 85 (Springer, 1992).
C.F. Majkrzak, N.F. Berk, et al., SPIE Proc. **1738**, 282 (1992).

Phase Determination with 3 References

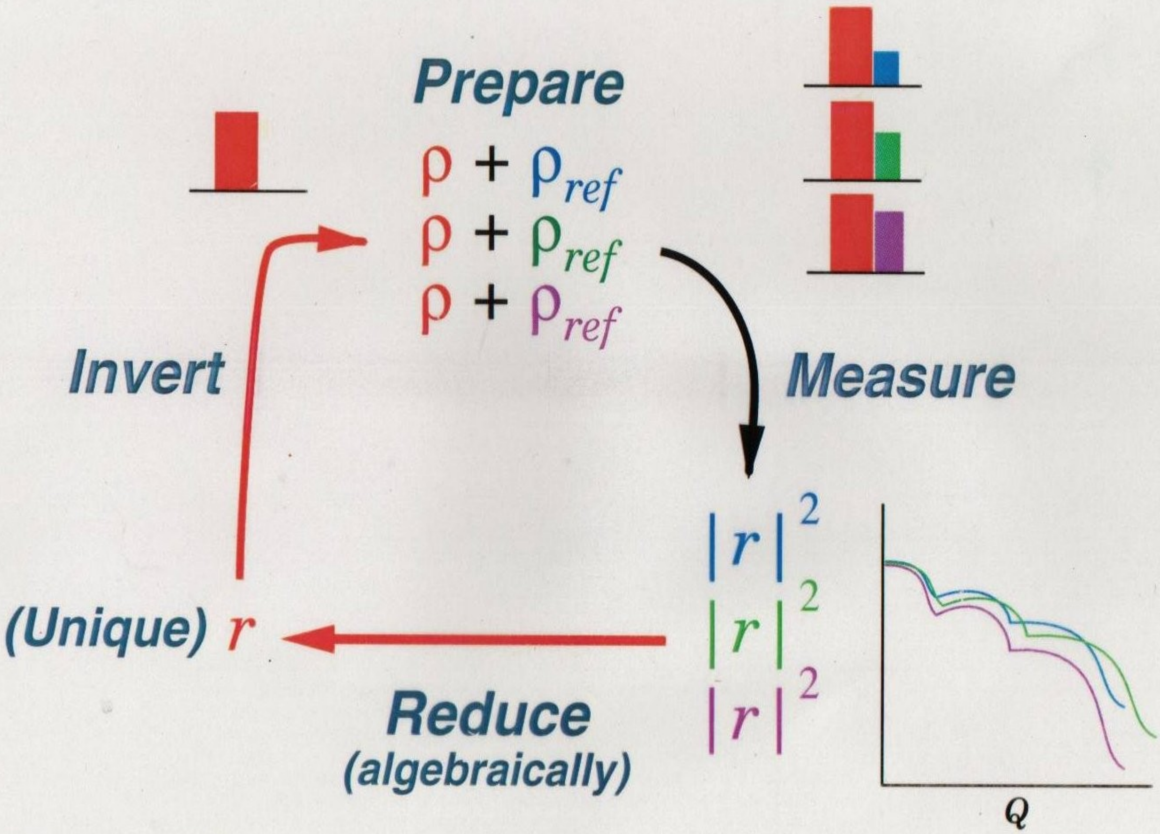

Prepare

$\rho + \rho_{ref}$

$\rho + \rho_{ref}$

$\rho + \rho_{ref}$

Measure

$|r|^2$

$|r|^2$

$|r|^2$

Reduce
(algebraically)

(Unique) r

Invert

Majkrzak & Berk, 1995
de Haan, et al., 1995

FORMALISM ALLOWS A COMPOSITE POTENTIAL TO BE EXPRESSED AS A PRODUCT:

$$\underbrace{\begin{pmatrix} A & B \\ C & D \end{pmatrix}}_{\text{COMPOSITE (1,2,3)}} = \underbrace{\begin{pmatrix} a & b \\ c & d \end{pmatrix}}_{\underline{\text{UNKNOWN}}} \underbrace{\begin{pmatrix} w & x \\ y & z \end{pmatrix}}_{\text{REFERENCE (1,2,3)}}$$

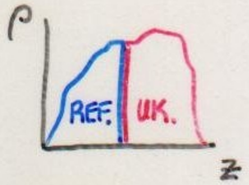

$$|R(Q)|^2 = |R_1(Q)|^2,\ |R_2(Q)|^2, \text{ and } |R_3(Q)|^2$$

$$\Sigma_i \equiv 2\left[\frac{1+|R_i|^2}{1-|R_i|^2}\right] = A_i^2 + B_i^2 + C_i^2 + D_i^2$$

$$A_i^2 = a^2w_i^2 + b^2y_i^2 + 2abw_iy_i$$

$$C_i^2 = c^2w_i^2 + d^2y_i^2 + 2cdw_iy_i$$

$$B_i^2 = a^2x_i^2 + b^2z_i^2 + 2abx_iz_i$$

$$D_i^2 = c^2x_i^2 + d^2z_i^2 + 2cdx_iz_i$$

(INDEPENDENTLY AT EACH Q)

$$\Sigma_i = \overbrace{(w_i^2 + x_i^2)}^{\text{REF.}}\underline{\alpha} + \overbrace{(y_i^2 + z_i^2)}^{\text{REF.}}\underline{\beta} + 2\overbrace{(w_iy_i + x_iz_i)}^{\text{REF.}}\underline{\gamma}$$

SOLVE FOR UNKNOWNS α, β, AND γ TO GET

$\alpha = a^2 + c^2$

$\beta = b^2 + d^2$

$\gamma = ab + cd$

$i = 1, 2, 3$

$$\boxed{R_{\text{UNKNOWN}} = \frac{(\beta - \alpha) - 2i\gamma}{2 + \beta + \alpha}}$$

FOURIER TRANSFORM OF THE COMPLEX REFLECTION AMPLITUDE

$$\mathcal{R}(z) = \frac{1}{\pi}\,\mathrm{Re}\int_{0}^{\infty} r(k_z)\, e^{ik_z z}\, dk_z$$

GELFAND LEVITAN MARCHENKO INTEGRAL EQUATION

$$K(z,y) + \mathcal{R}(z+y) + \int_{-z}^{+z} K(z,x)\,\mathcal{R}(x+y)\,dx = 0$$

SCATTERING LENGTH DENSITY

$$\rho(z) = 2\frac{d\,K(z,z)}{dz}$$

GIVEN THE COMPLEX REFLECTION AMPLITUDE, THE SCATTERING LENGTH DENSITY ρ CAN BE OBTAINED FROM AN EXACT, FIRST PRINCIPLE INVERSION FOR A REAL POTENTIAL OF FINITE EXTENT —— AND THE SOLUTION IS UNIQUE!

NO FITTING, NO ADJUSTABLE PARAMETERS

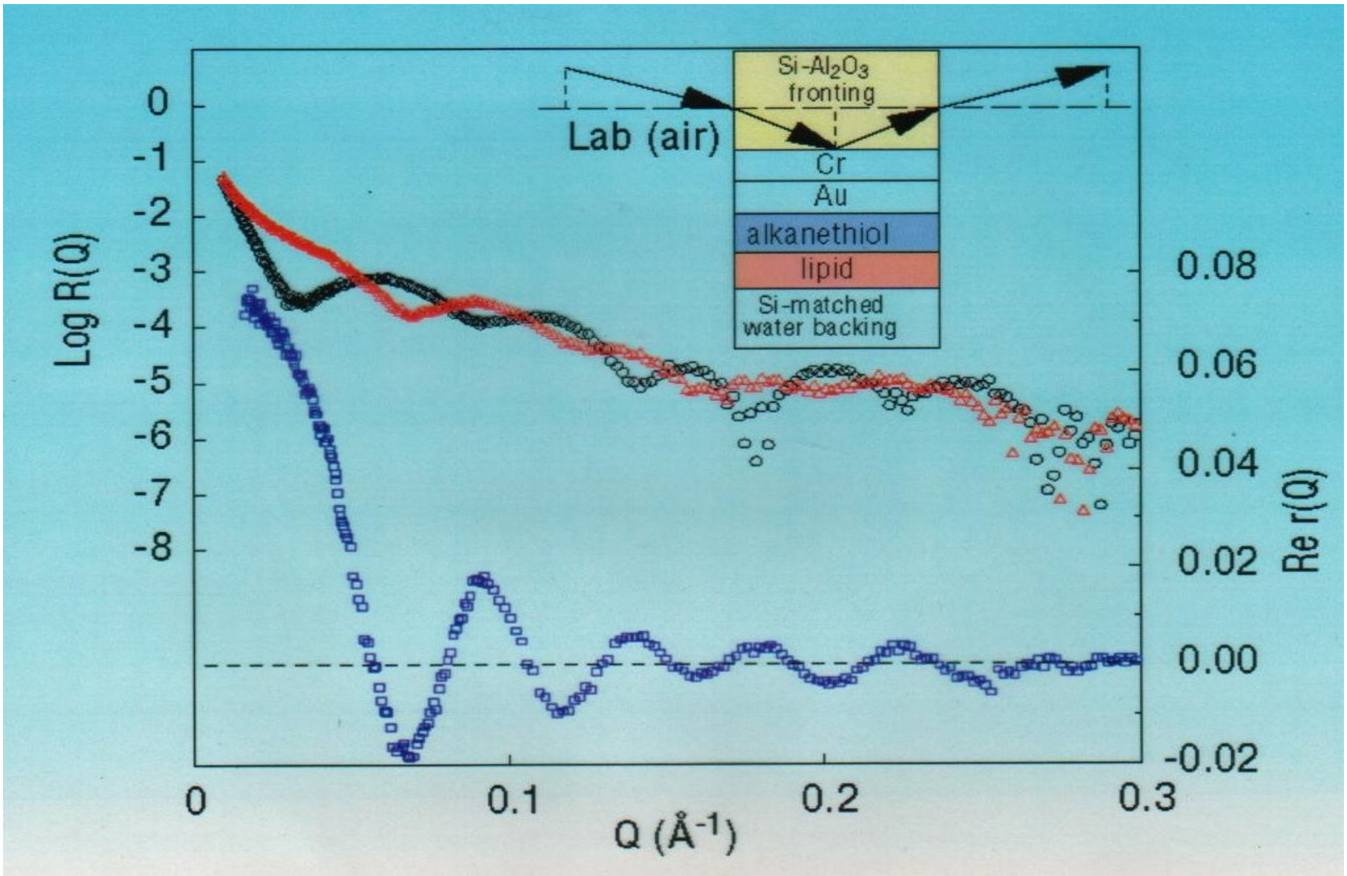
Si-Al$_2$O$_3$
fronting
Lab (air)
Cr
Au
alkanethiol
lipid
Si-matched
water backing
Log R(Q)
0
-1
-2
-3
-4
-5
-6
-7
-8
Re r(Q)
0.08
0.06
0.04
0.02
0.00
-0.02
0
0.1
0.2
0.3
Q (Å^{-1})

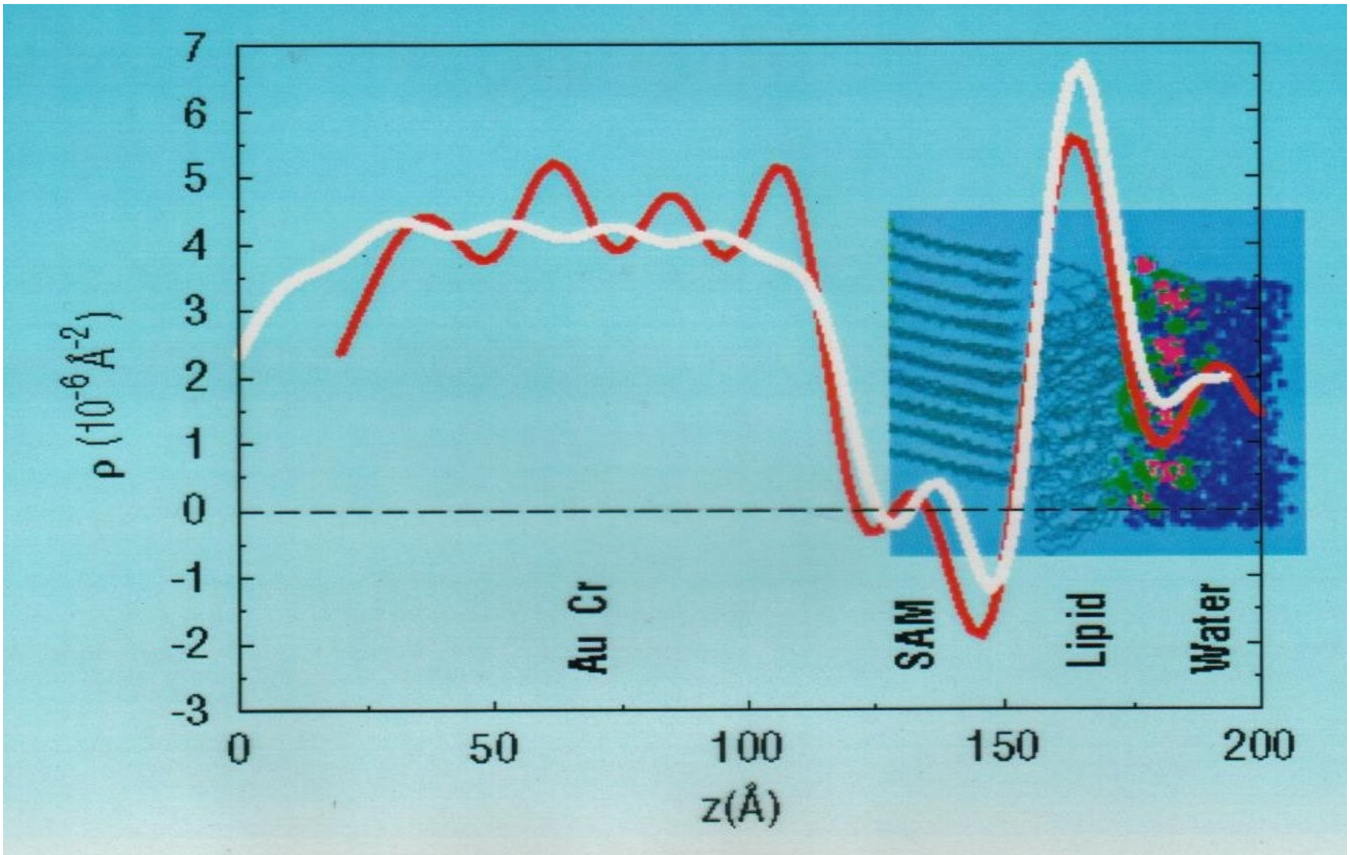
ρ (10^{-6} Å^{-2})
7
6
5
4
3
2
1
0
-1
-2
-3
Au Cr
SAM
Lipid
Water
0
50
100
150
200
z(Å)

UNIQUE DETERMINATION OF BIOMIMETIC MEMBRANE PROFILES BY NEUTRON REFLECTIVITY

New biomimetic membrane materials, of fundamental importance in understanding such key biological processes as molecular recognition, conformational changes, and molecular self-assembly, can be characterized using neutron reflectometry. In particular, scattering length density (SLD) depth profiles along the normal to the surface of a model biological bilayer, which mimics the structure and function of a genuine cell membrane, can be deduced from specular neutron reflectivity data collected as a function of wavevector transfer Q. Specifically, this depth profile can be obtained by numerically fitting a computed to a measured reflectivity. The profile generating the best fitting reflectivity curve can then be compared to cross-sectional slices of the film's chemical composition predicted, for example, by molecular dynamics simulations [1]. However, the uniqueness of a profile obtained by conventional analysis of the film's reflectivity alone cannot be established definitively without additional information. In practice, significantly different SLD profiles have been shown to yield calculated reflectivity curves with essentially equivalent goodness-of-fit to measured data [2], as illustrated in Fig. 1.

The existence of multiple solutions, only one of which can be physical, is especially problematic in cases where a key additional piece of structural or compositional information is lacking as can happen in the investigation of these biological membrane systems.

Why this inherent uncertainty? The neutron specular reflection amplitude for a model SLD can be computed exactly from first principles; the square of its modulus gives the measurable reflectivity. It is firmly established, however, that the complex amplitude is necessary and sufficient for a unique solution of the inverse problem, that of recovering the SLD from reflection measurements. Unambiguous inversion requires both the magnitude and phase of reflection. Once these are known, practical methods [3] exist for extracting the desired SLD.

In fact, considerable efforts were made about a quarter century ago to solve the analogous "phase problem" in X-ray crystallography using known constraints on the scattering electron density [4] and by the technique of isomorphic substitution [5]. Variations of the latter approach have been applied to reflectivity, using a known reference layer in a composite film in place of atomic substitutions. These

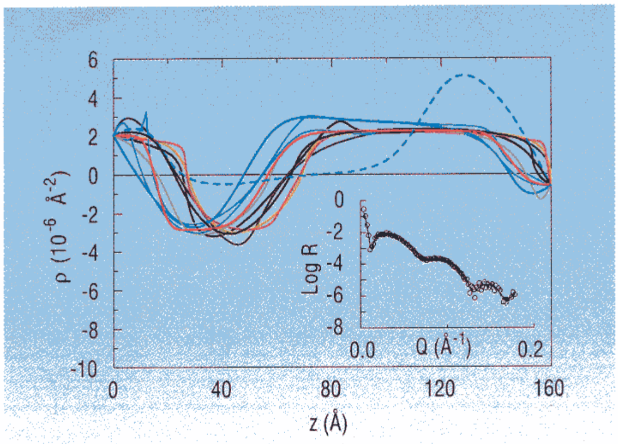

FIGURE 1. Family of scattering length density profiles obtained by model-independent fitting of the reflectivity data in the inset. The profile represented by the blue dashed line is unphysical for this Ti/TiO film system yet generates a reflectivity curve that fits the data with essentially equivalent goodness-of-fit (all the reflectivity curves corresponding to the SLD's shown are plotted in the inset but are practically indistinguishable from one another).

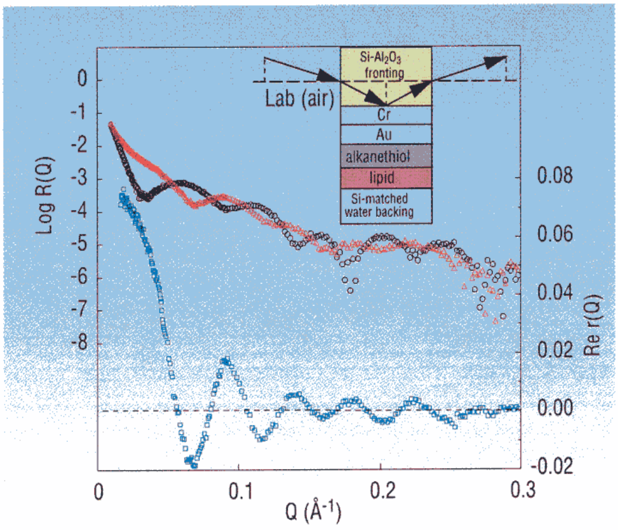

FIGURE 2. Reflectivity curves for the thin film system depicted schematically in the inset, one for a Si fronting (red triangles), the other for Al_2O_3 (black circles). The curve in the lower part of the figure (blue squares) is the real part of the complex reflection amplitude for the films obtained from the reflectivity curves by the method described in the text.

C. F. Majkrzak, N. F. Berk, S. Krueger, J. A. Dura
NIST Center for Neutron Research
National Institute of Standards and Technology
Gaithersburg, MD 20899-8562

C. W. Meuse, V. Silin, J. Woodward, A. L. Plant
NIST Biotechnology Division
National Institute of Standards and Technology
Gaithersburg, MD 20899-8311

M. Tarek
Department of Chemistry
University of Pennsylvania
Philadelphia, PA 19103

solution methods, however, were tied to the Born approximation, which generally is valid in crystal structure determination but which fails catastrophically at low Q (low glancing angles) in reflection from slab-shaped samples such as thin films. Exact inversion requires accurate knowledge of the reflection amplitude over the entire Q-range, especially at low Q.

In this decade the reflection phase problem has been exactly solved using a protocol of three reflectivity measurements on composite films consisting of the film of interest in intimate contact with each of three known reference layers [6, 7]. Subsequently, variations using only two measurements have been shown to partially solve the phase problem, an additional procedure being required to choose between two solution branches, only one of which is physical [8, 9]. In the past year [10], an exact solution has been found for a two measurement strategy in which the film surround, either the fronting (incident) or backing (transmitting) medium, is varied. This new approach is simpler to apply than reference layer methods and is adaptable to many experiments. Surround variation neutron reflectometry has been successfully applied to the challenging type of biological membrane depth profiling described earlier.

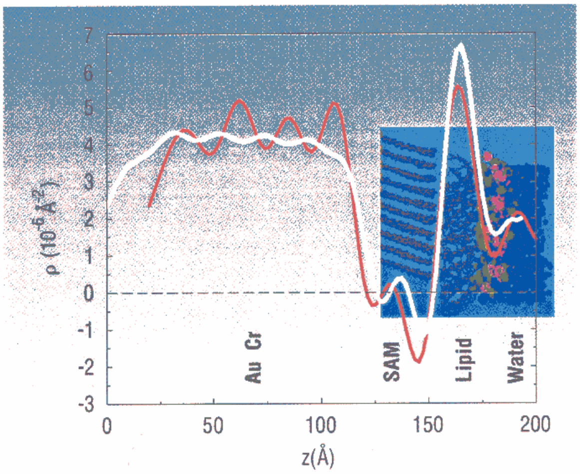

FIGURE 3. SLD profile (red line) resulting from a direct inversion of the Re r of Fig. 2 compared with that predicted by a molecular dynamics simulation (white line) as discussed in the text. The headgroup for the Self-Assembled-Monolayer (SAM) at the Au surface in the actual experiment was ethylene oxide and was not included in the simulation but, rather, modelled separately as part of the Au. Also, the Cr-Au layer used in the model happened to be 20 Å thicker than that actually measured in the experiment.

In Fig. 2 are plotted a pair of neutron reflectivity curves measured for the layered film structure schematically depicted in the upper right inset, one with Si and the other with Al_2O_3 as the fronting medium. The lower part of Fig. 2 shows the real part of the complex reflection amplitude for the multilayer as extracted from the reflectivity data, according to the method described above, and which was subsequently used to perform the inversion to obtain the SLD shown in Fig. 3. For comparison, the SLD predicted by a molecular dynamics simulation is also shown in Fig. 3, in a slightly distorted version, corresponding to a truncated reflectivity data set, which indicates the spatial resolution of an SLD obtainable in practice. This latter SLD was obtained by inversion of the reflection amplitude computed for the exact model SLD, but using values only up to the same maximum Q value (0.3 Å^{-1}) over which the actual reflectivity data sets were collected. Overall, agreement between the experimentally determined profile and the theoretical prediction is remarkable, essentially limited only by the Q-range of the measurement. Surround variation neutron reflectivity thus makes it possible to measure complicated thin film structures without the ambiguity associated with curve fitting. The veridical SLD profile is obtained directly by a first principles inversion.

REFERENCES:

[1] M. Tarek, K. Tu, M.L. Klein, and D. J. Tobias, Biophys. J. **77**, 964 (1999).
[2] N. F. Berk and C. F. Majkrzak, Phys. Rev. B **51**, 11296 (1995).
[3] P. E. Sacks, Wave Motion **18**, 21 (1993).
[4] H. A. Hauptman, Science **233**, 178 (1986).
[5] J. M. Cowley, *Diffraction Physics*, 2nd Ed., (North Holland, Amsterdam, 1990), p. 131.
[6] C. F. Majkrzak and N. F. Berk, Phys. Rev. B **52**, 10825 (1995).
[7] V.O. deHaan, A. A. van Well, S. Adenwalla, and G.P. Felcher, Phys. Rev. B **52**, 10830 (1995).
[8] T. Aktosun and P. E. Sacks, Inverse Problems **14**, 211 (1998).
[9] C. F. Majkrzak and N. F. Berk, Physica B **267-268**, 168 (1999).
[10] C. F. Majkrzak and N. F. Berk, Phys. Rev. B **58**, 15416 (1998).

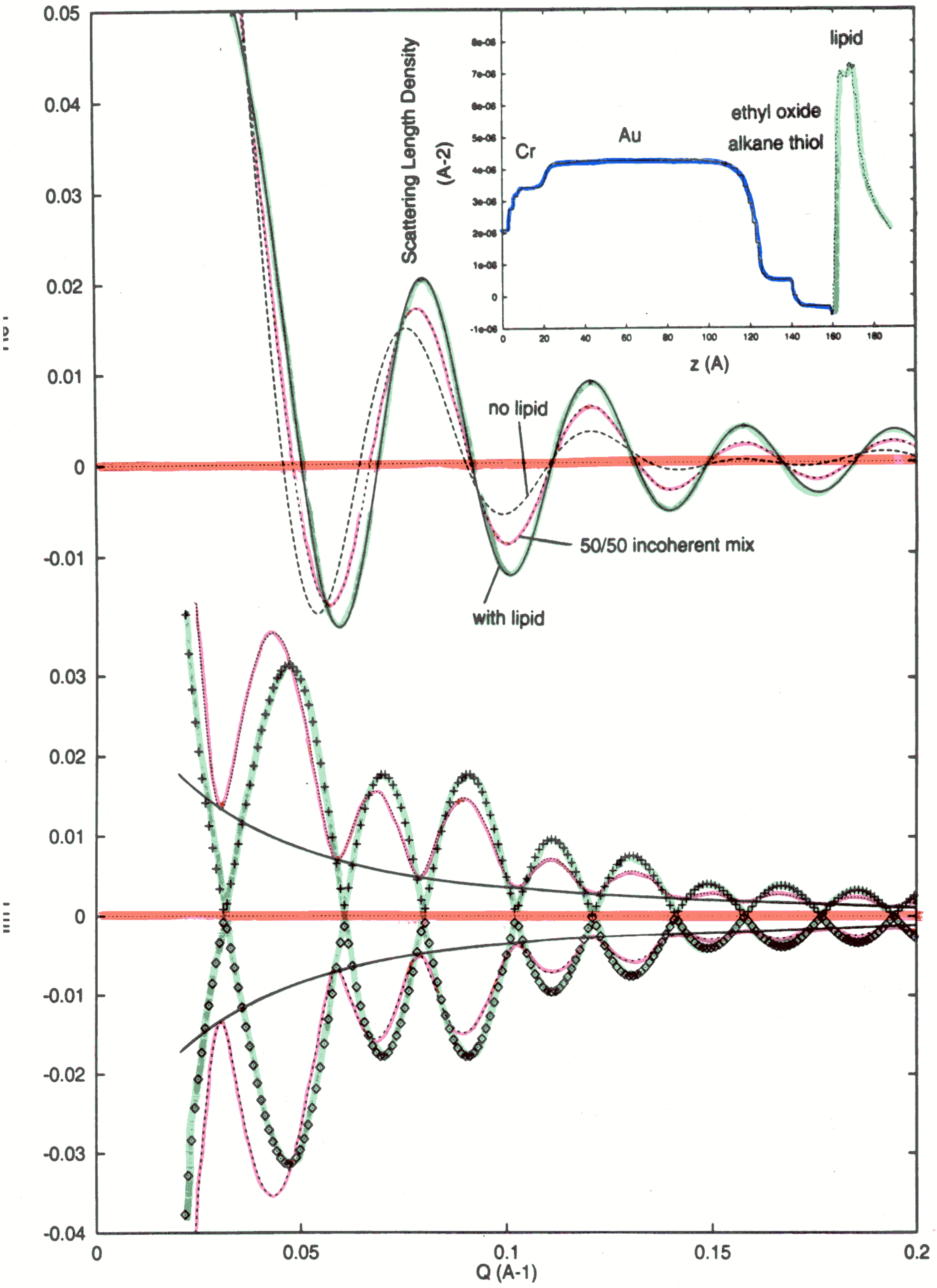
0.05
0.04
0.03
0.02
0.01
0
-0.01
Scattering Length Density
(A-2)
8e-08
7e-08
6e-08
5e-08
4e-08
3e-08
2e-08
1e-08
0
-1e-08
0
20
40
60
80
100
120
140
160
180
z (A)
Cr
Au
ethyl oxide
alkane thiol
lipid
no lipid
50/50 incoherent mix
with lipid
0.03
0.02
0.01
0
-0.01
-0.02
-0.03
-0.04
0
0.05
0.1
0.15
0.2
Q (A-1)

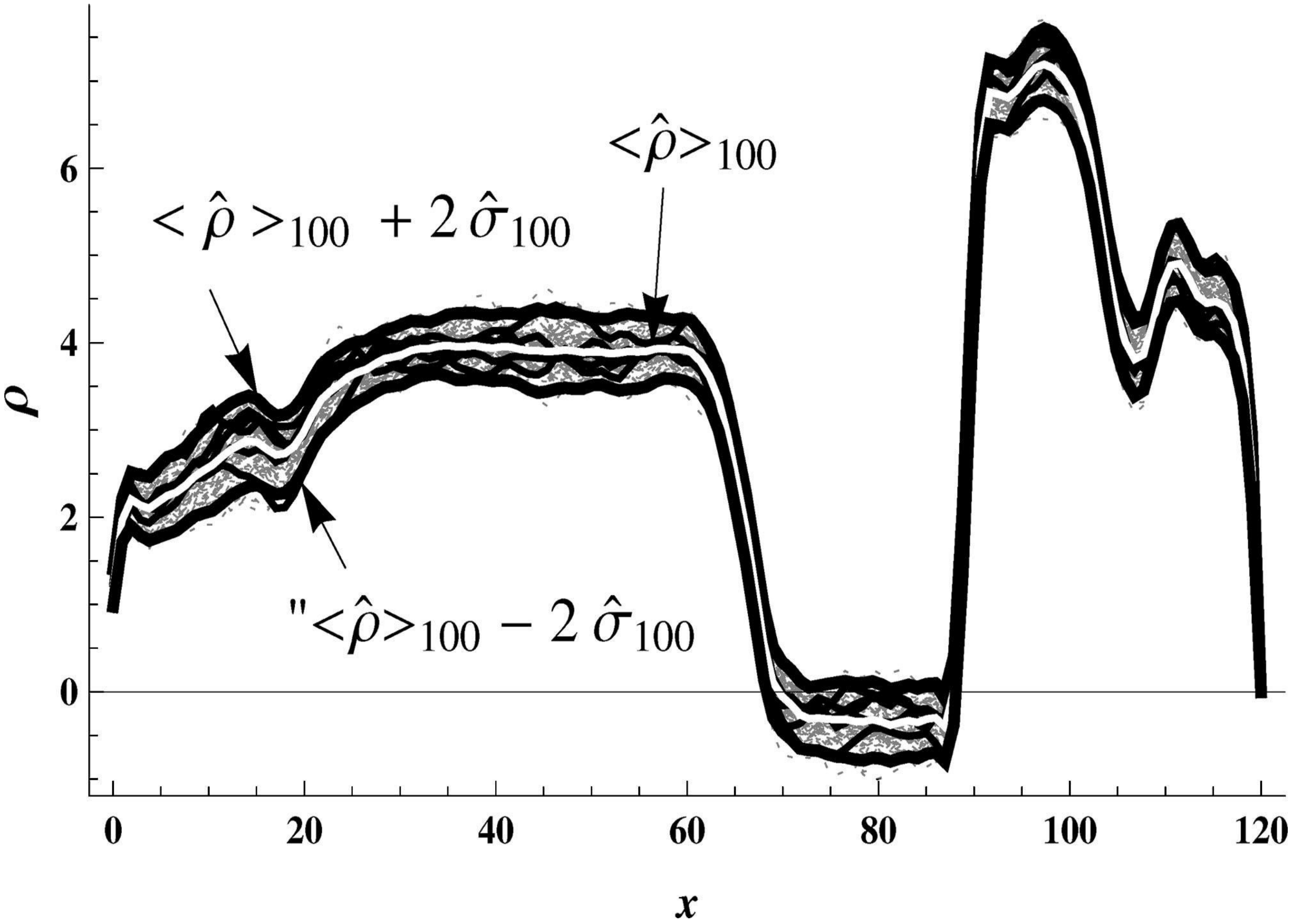

“Statistical Analysis of Phase-Inversion Neutron Specular Reflectivity”, N.F.Berk and C.F.Majkrzak, *Langmuir* **25**, 4132 (2009).

Part 3: Applications of NR to studies of the nano-scale structure of thin film materials

<> Soft condensed matter:

- -- polymers
- -- bio-membranes
- -- organic photo-voltaic films
- . . .

<> Hard condensed matter:

- -- magnetic materials (to be discussed in a following lecture)
- -- chemical interdiffusion (e.g., 58Ni/62Ni)
- -- metal hydrides
- . . .

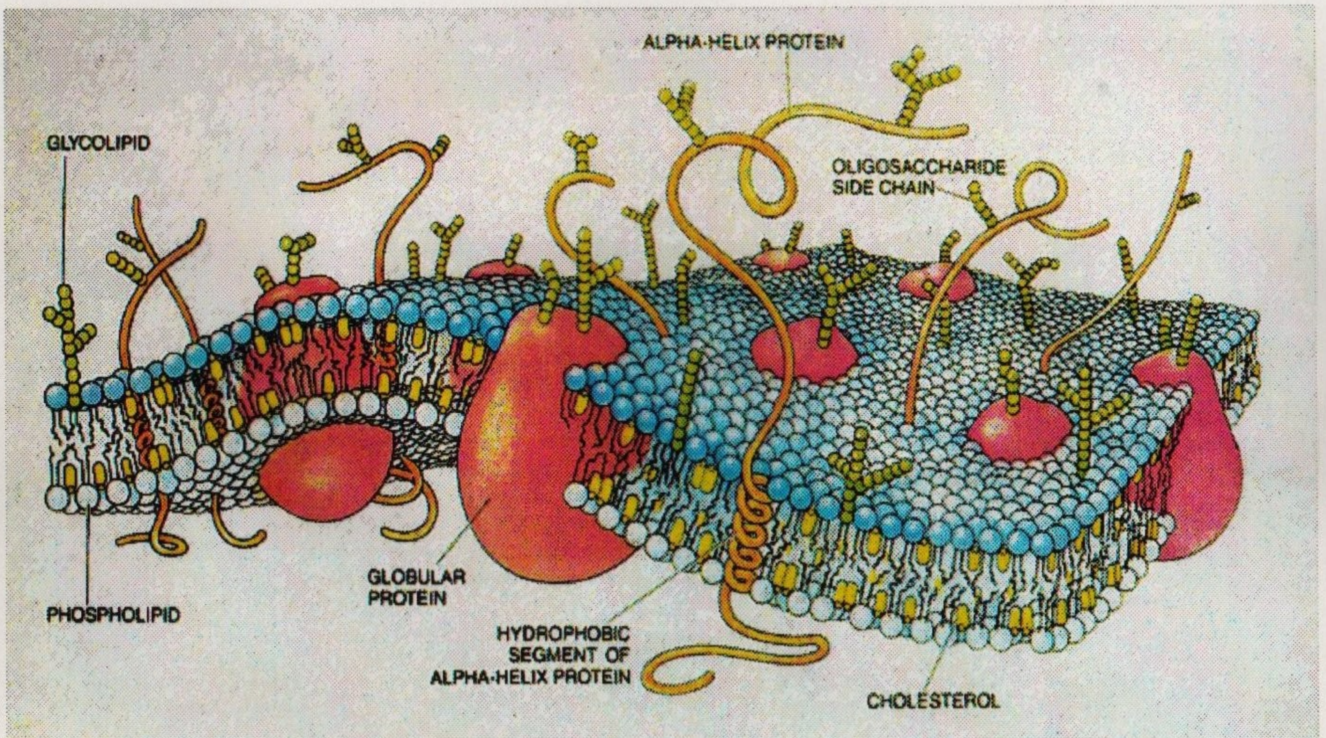

BORROWED FROM SCIENTIFIC AMERICAN

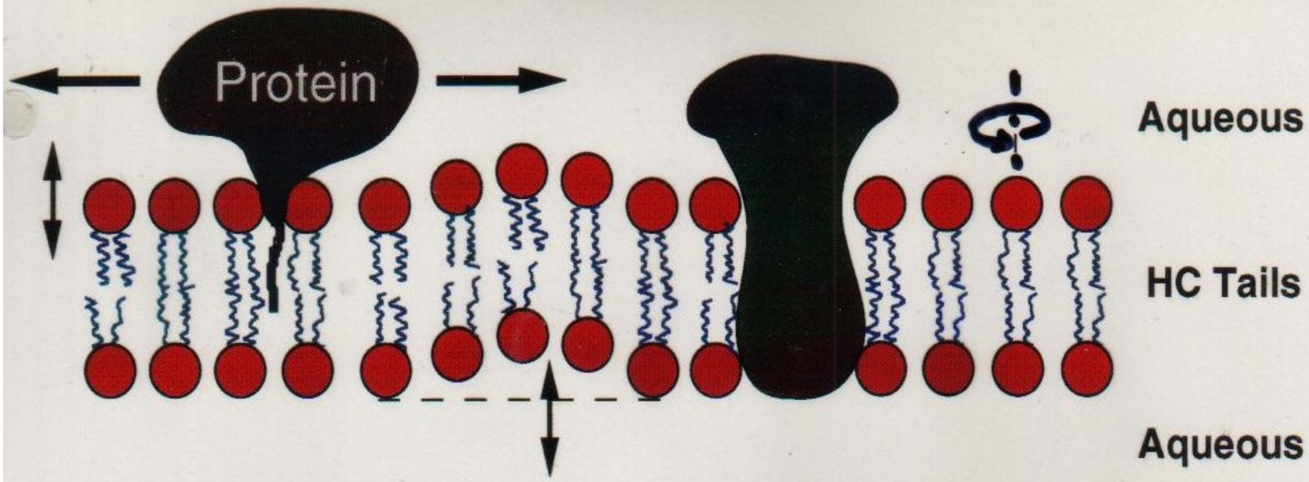

Supported Lipid Bilayers

A model system to mimic the structure and dynamics of cell membranes.

Proteins in Lipid Bilayers

- Difficult to characterize by traditional x-ray crystallography.
- Play a crucial role in cell function
  - regulate ion and nutrient transport
  - engage in binding, signalling and cell recognition
  - participate in cell fusion events.

Biosensors (Anne Plant & coworkers)

Melittin in Hybrid Bilayer Membranes

S. Krueger, A. Plant, et al., NIST
(Langmuir)

- pore-forming toxin
- used as model membrane peptide
- active in HBMs

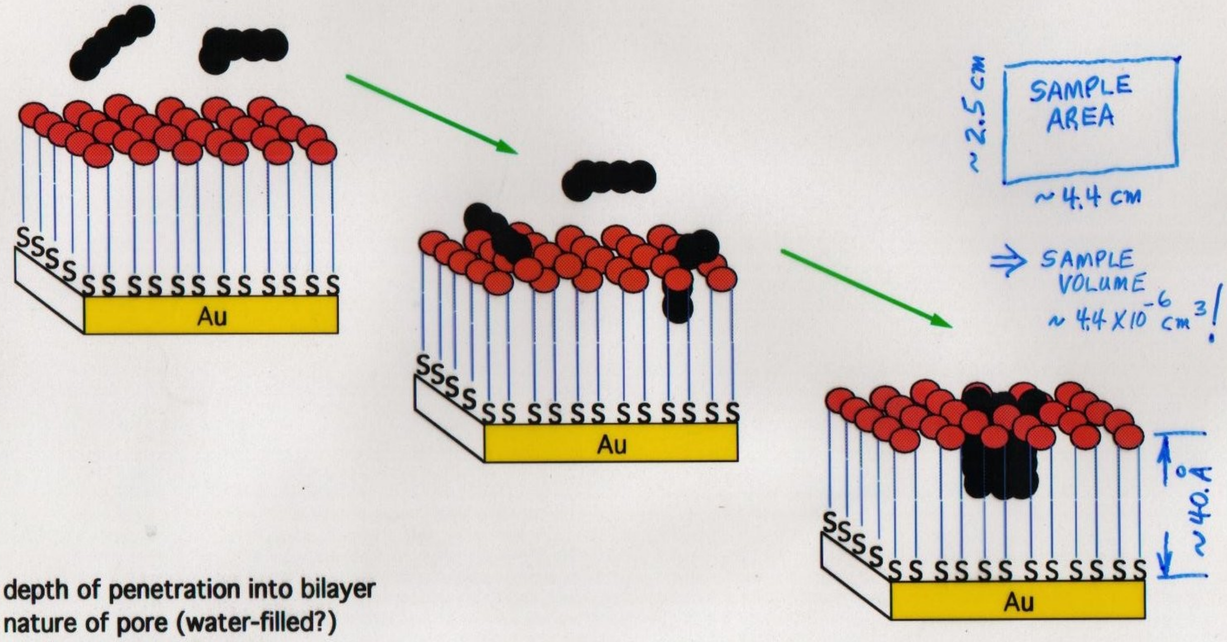

⇒ SAMPLE VOLUME
~ 4.4×10^{-6} cm^3!

- depth of penetration into bilayer
- nature of pore (water-filled?)
- conformational changes
- random or ordered distribution?
- influence on surrounding lipids (location,conformation)

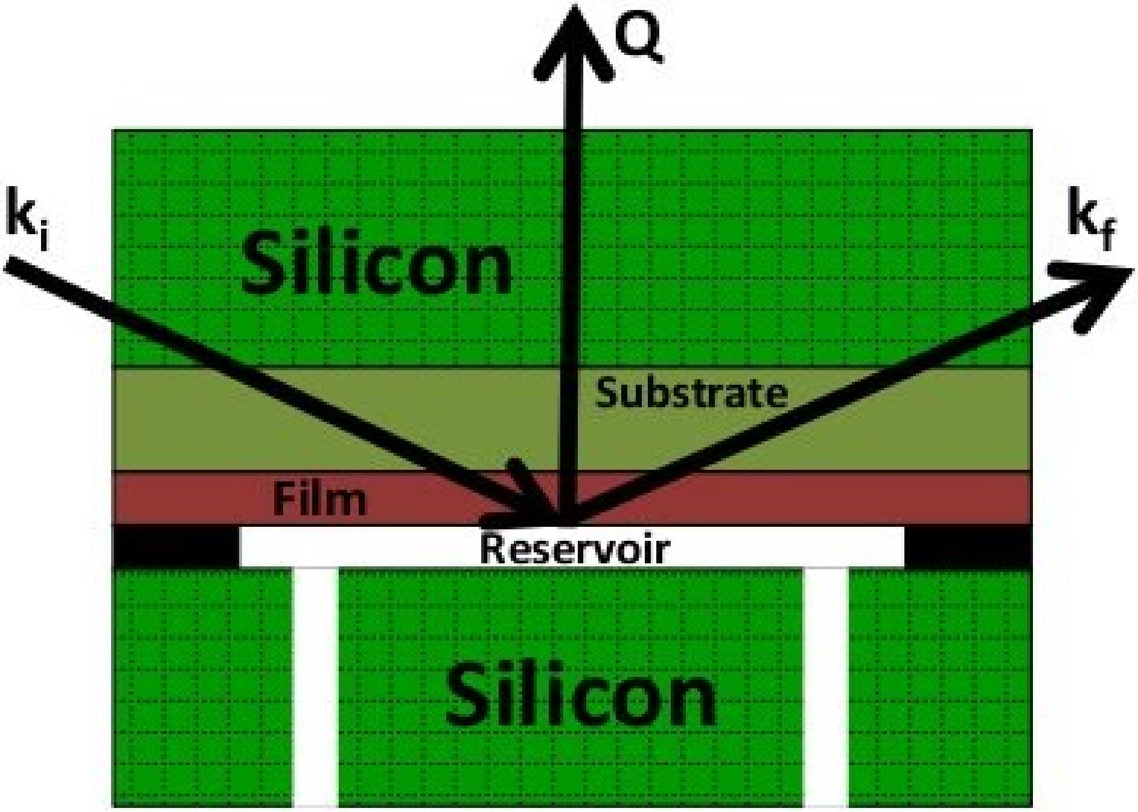
Q
k_i
k_f
Silicon
Substrate
Film
Reservoir
Silicon

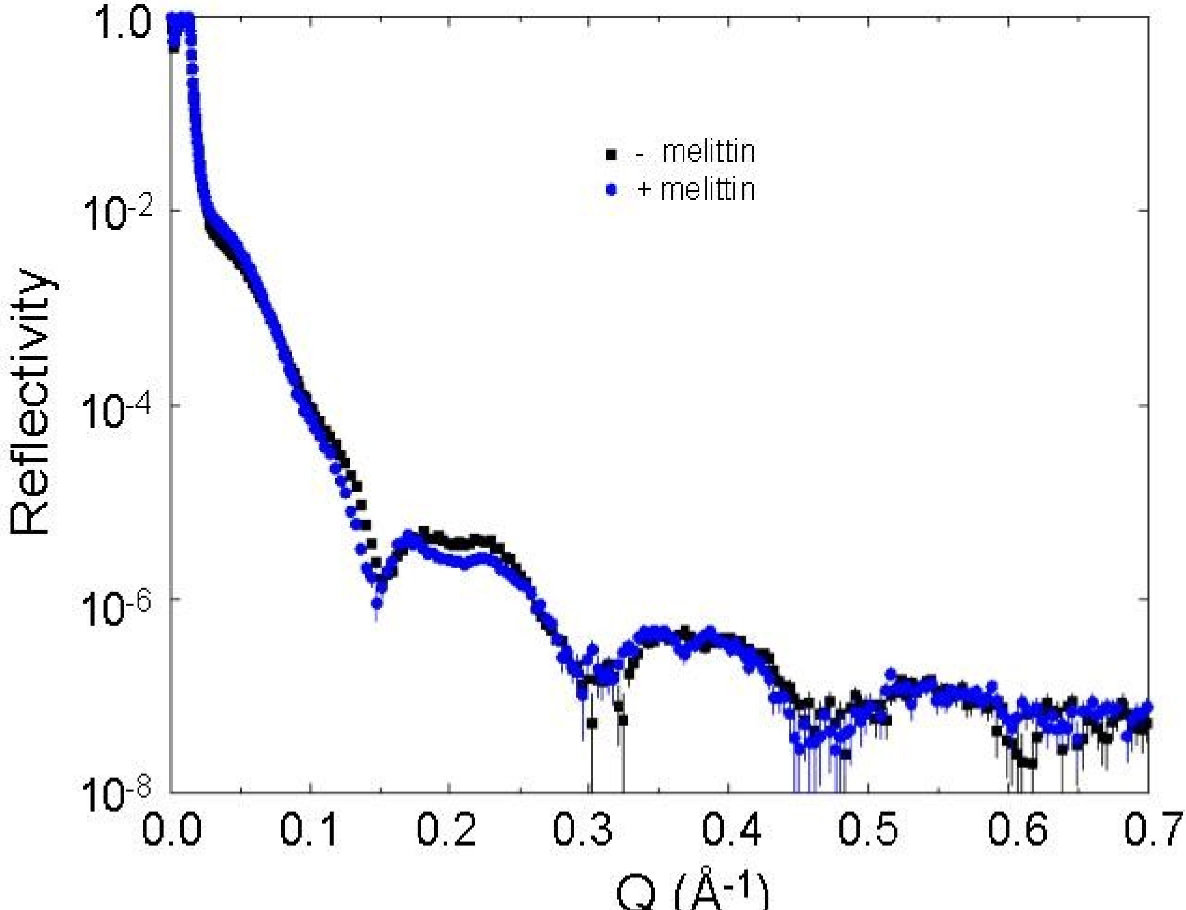
1.0
10-2
10-4
10-6
10-8
Reflectivity
0.0
0.1
0.2
0.3
0.4
0.5
0.6
0.7
Q (Å-1)
■ - melittin
● + melittin

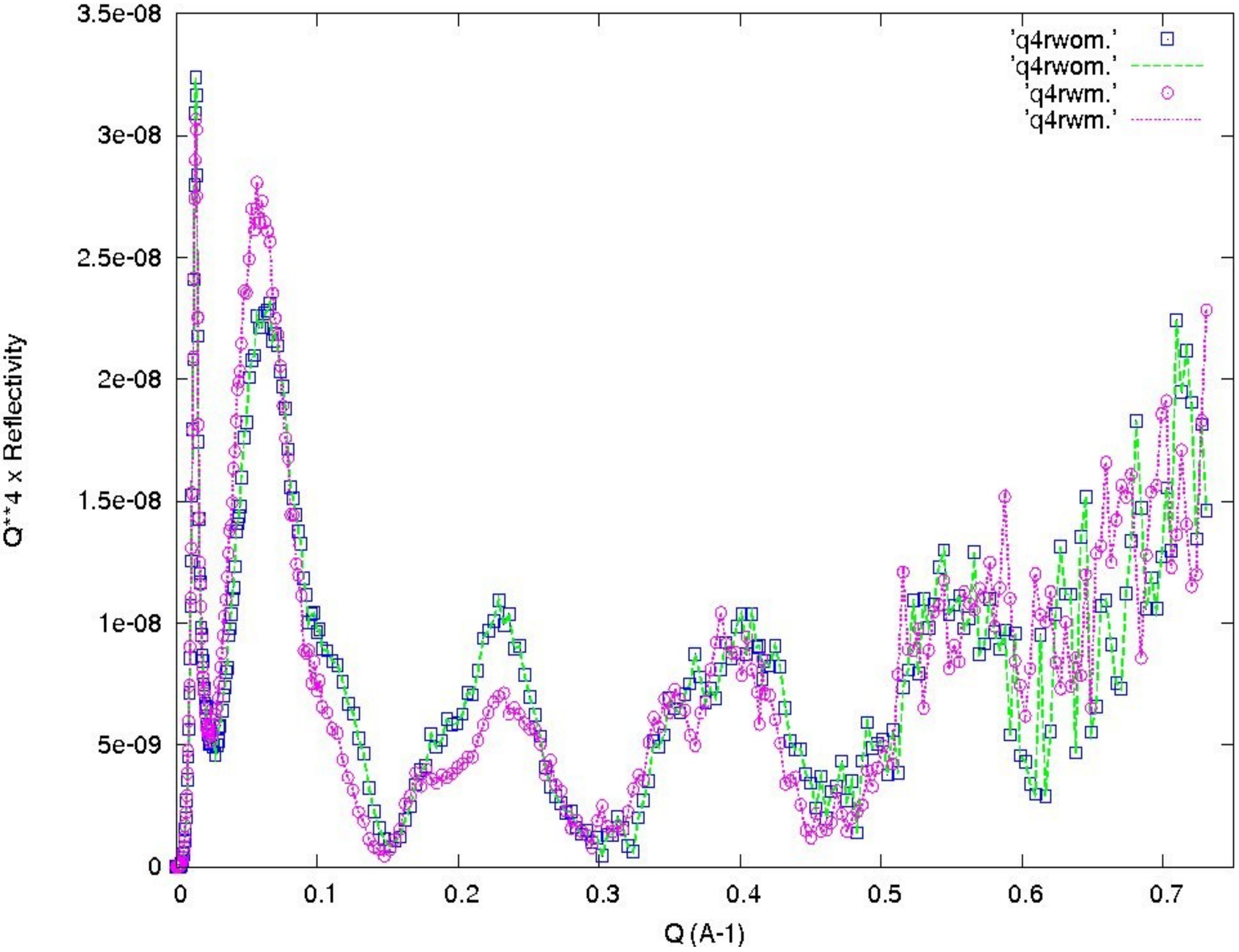

'q4rwom.'
'q4rwom.'
'q4rwm.'
'q4rwm.'
Q**4 x Reflectivity
Q (A-1)
3.5e-08
3e-08
2.5e-08
2e-08
1.5e-08
1e-08
5e-09
0
0
0.1
0.2
0.3
0.4
0.5
0.6
0.7

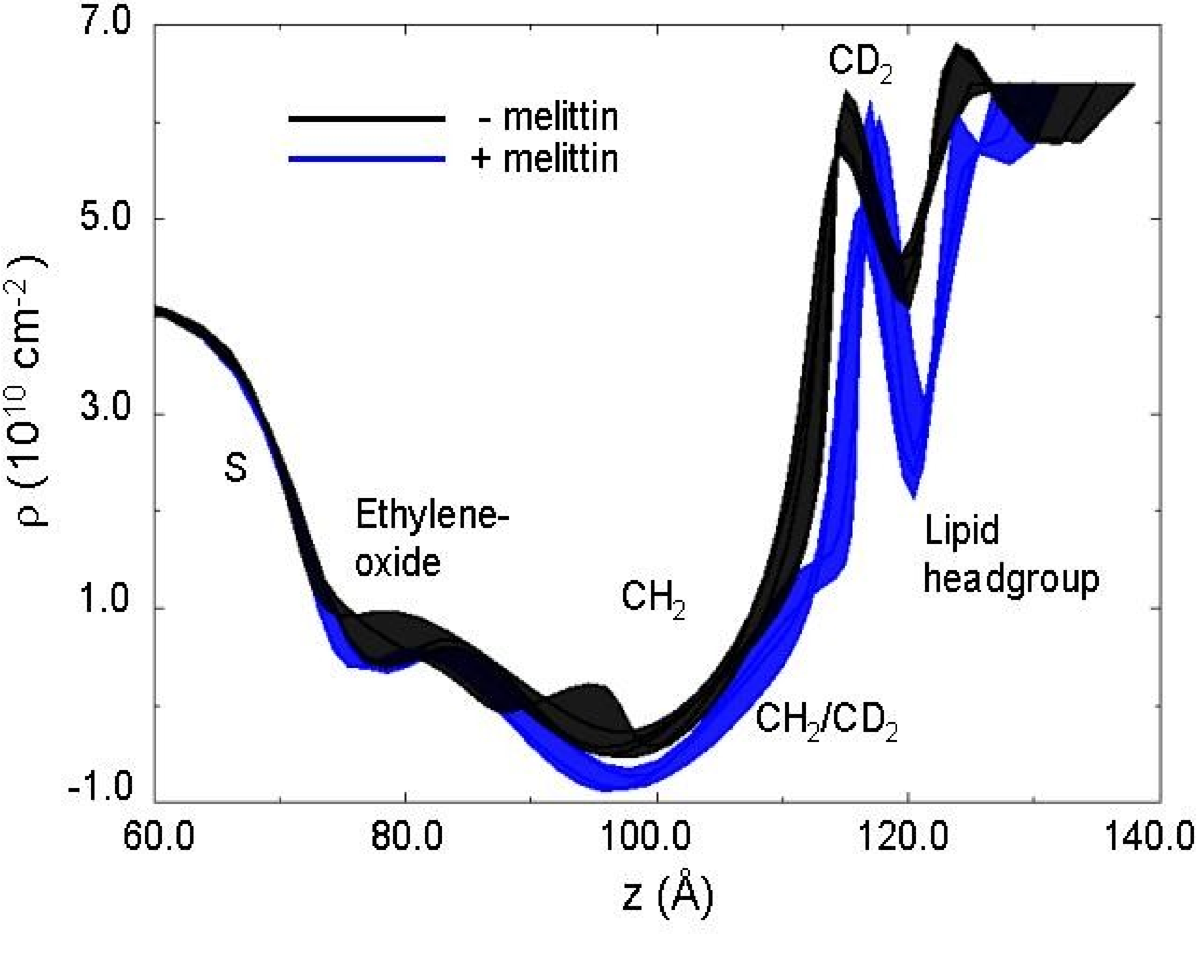
7.0
5.0
3.0
1.0
-1.0
ρ (10^{10} cm^{-2})
60.0
80.0
100.0
120.0
140.0
z (Å)
- melittin
+ melittin
S
Ethylene-
oxide
CH$_2$
CH$_2$/CD$_2$
CD$_2$
Lipid
headgroup

S. KRUEGER, C.F. MAJKRZAK, N.F. BERK, M. TAREK, D. TOBIAS,
V. SILIN, J.A. DURA, C.W. MEUSE, J. WOODWARD, A.L. PLANT
(Langmuir)

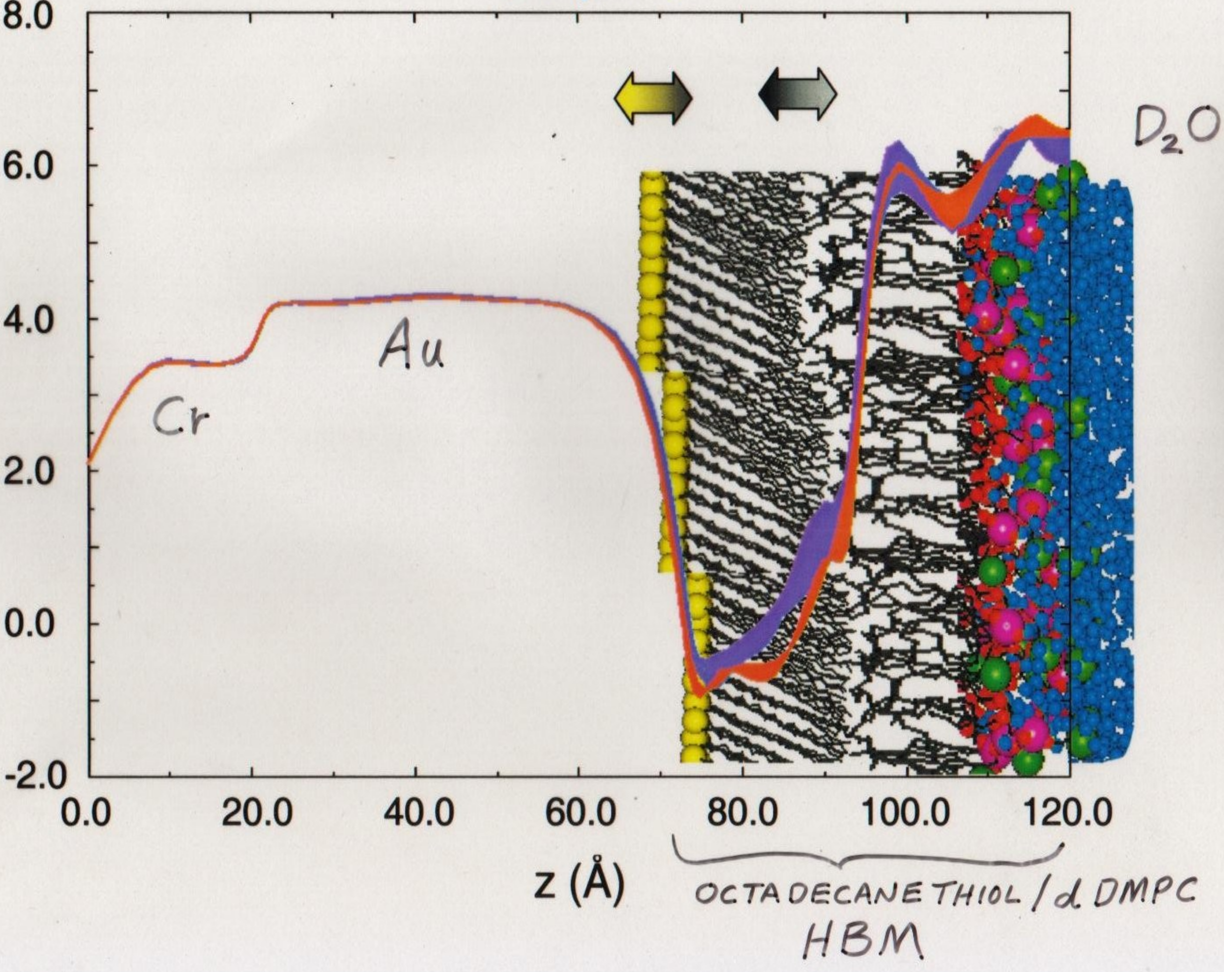

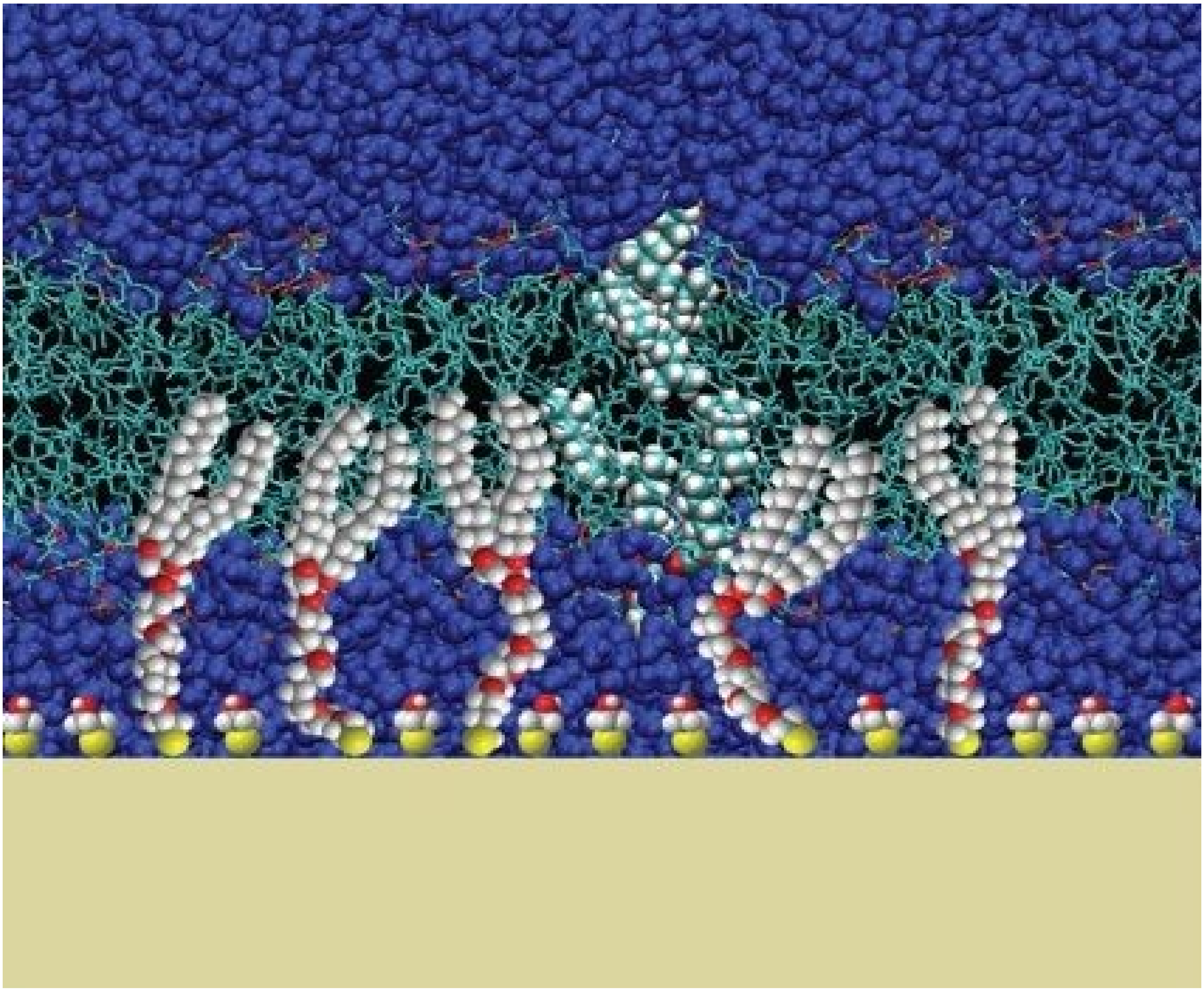

Schematic representation of tethered bilayer being used as a support for trans-membrane type proteins in structural studies using NR (Courtesy David Vanderah et al.).

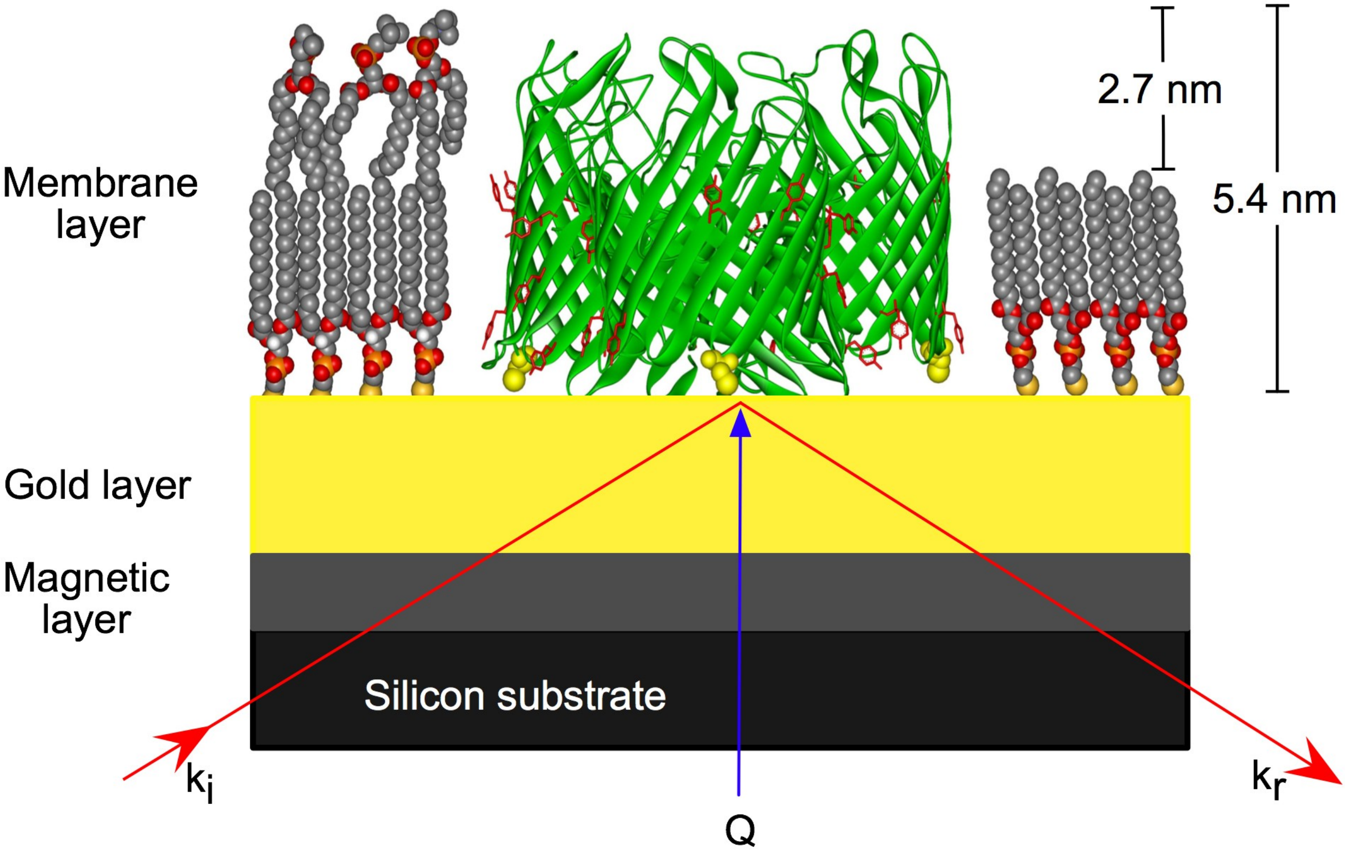

(From work of Anton Le Brun, Stephen Holt, Jeremy Lakey, et al.)

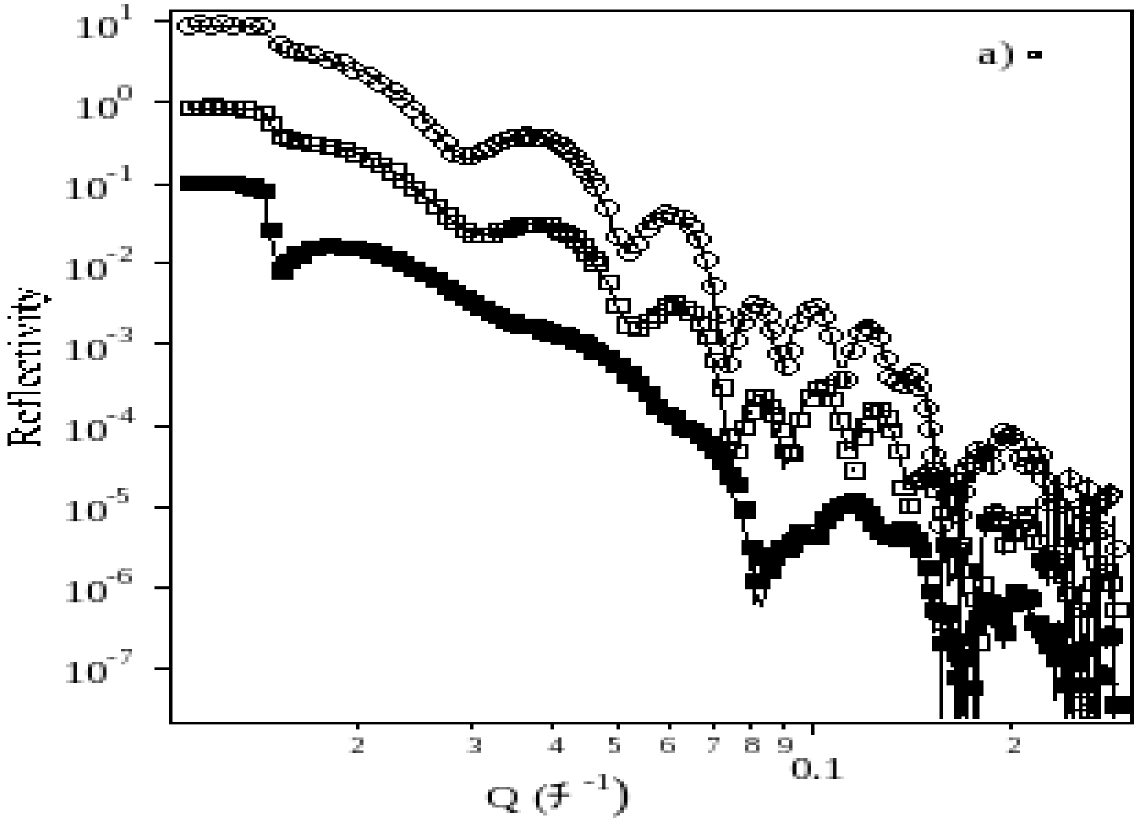
a)
Reflectivity
10^1
10^0
10^{-1}
10^{-2}
10^{-3}
10^{-4}
10^{-5}
10^{-6}
10^{-7}
2
3
4
5
6
7
8
9
0.1
2
Q (Å^{-1})

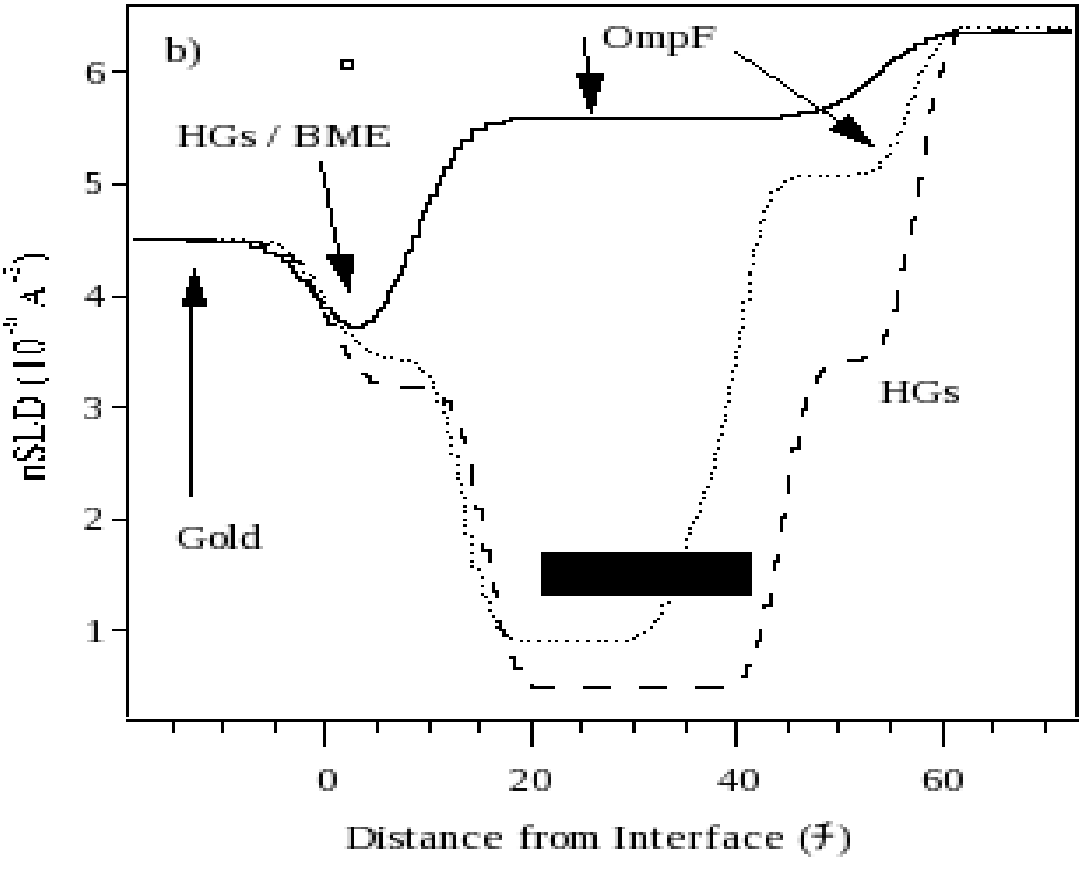
b)
OmpF
HGs / BME
Gold
HGs
nSLD (10^{-6} Å^{-2})
6
5
4
3
2
1
0
20
40
60
Distance from Interface (Å)

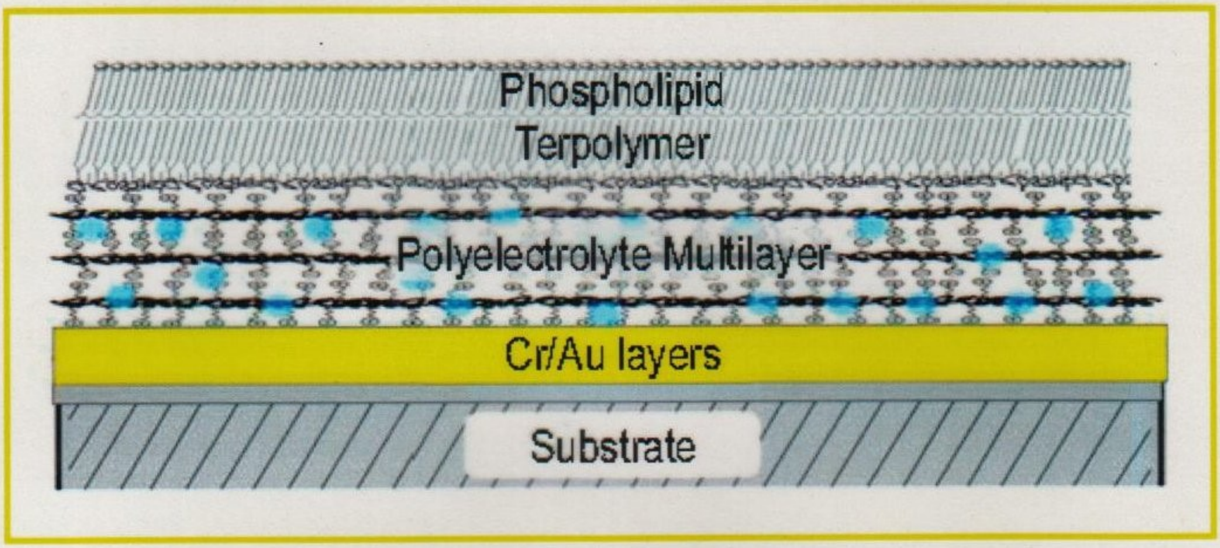

Fig. 1. Schematic diagram of a biomimetic membrane. The phospholipid layer at the top combines with the terpolymer layer to form a membrane-mimic that in turn resides on the water (blue dots) permeable "cushion" polyelectrolyte multilayer. The latter attaches electrostatically to the Au-capped substrate.

(Work of Ursula Perez-Salas, K. Faucher, E. Chaikof, et al.)

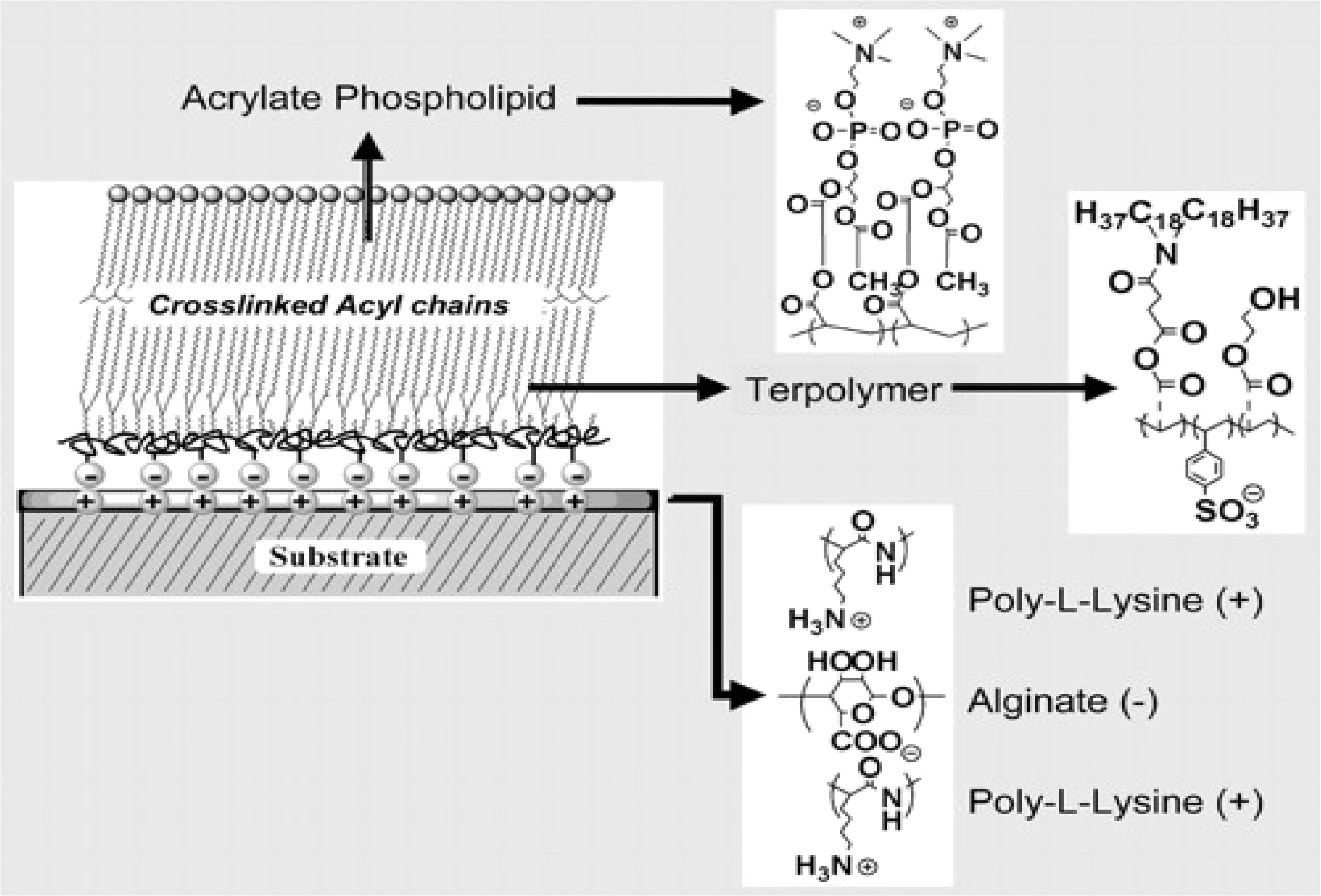
Acrylate Phospholipid
Crosslinked Acyl chains
Terpolymer
Substrate
Poly-L-Lysine (+)
Alginate (-)
Poly-L-Lysine (+)
H37C18C18H37
N
OH
SO3
CH3
CH3
HOOH
COO
H3N
H3N

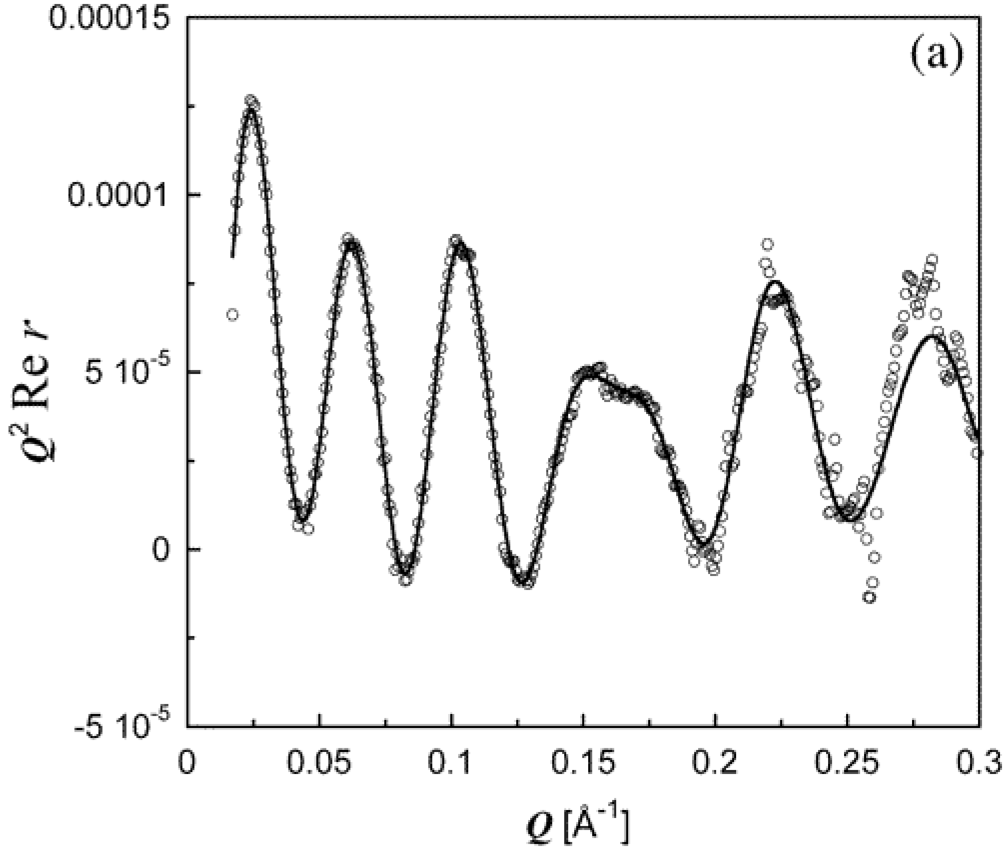
(a)
0.00015
0.0001
5 10⁻⁵
0
-5 10⁻⁵
Q^2 Re r
0
0.05
0.1
0.15
0.2
0.25
0.3
Q [Å⁻¹]

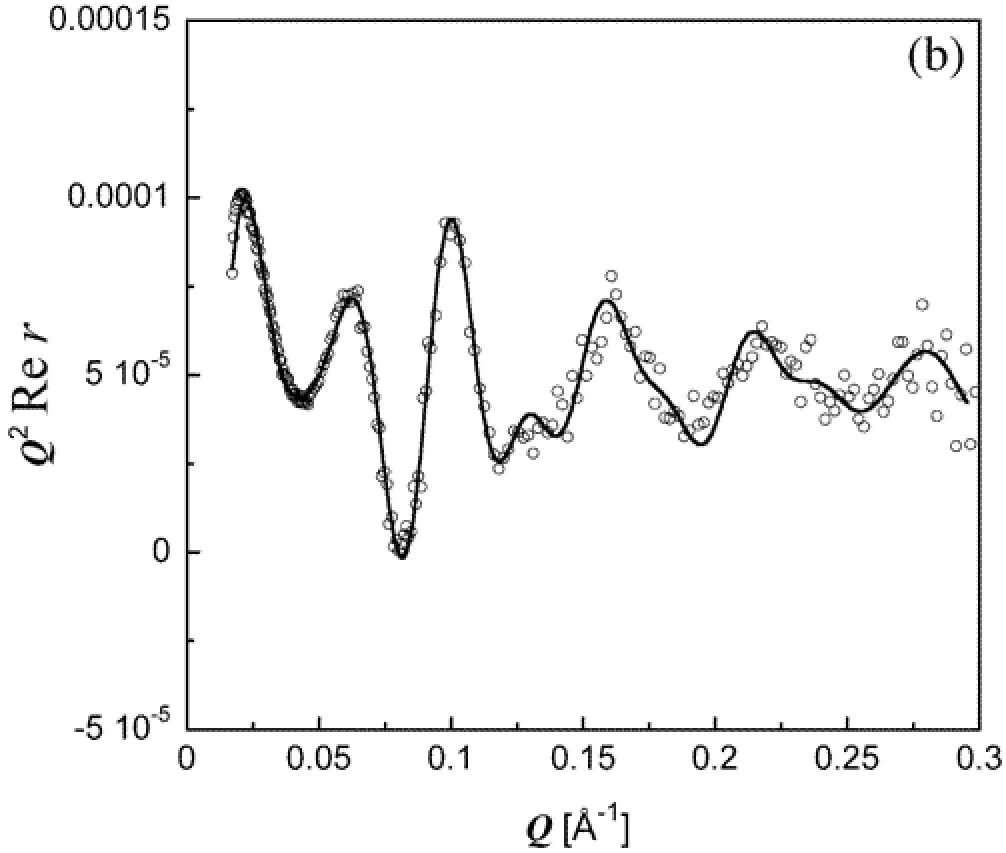
(b)
0.00015
0.0001
5 10⁻⁵
0
-5 10⁻⁵
Q^2 Re r
0
0.05
0.1
0.15
0.2
0.25
0.3
Q [Å⁻¹]

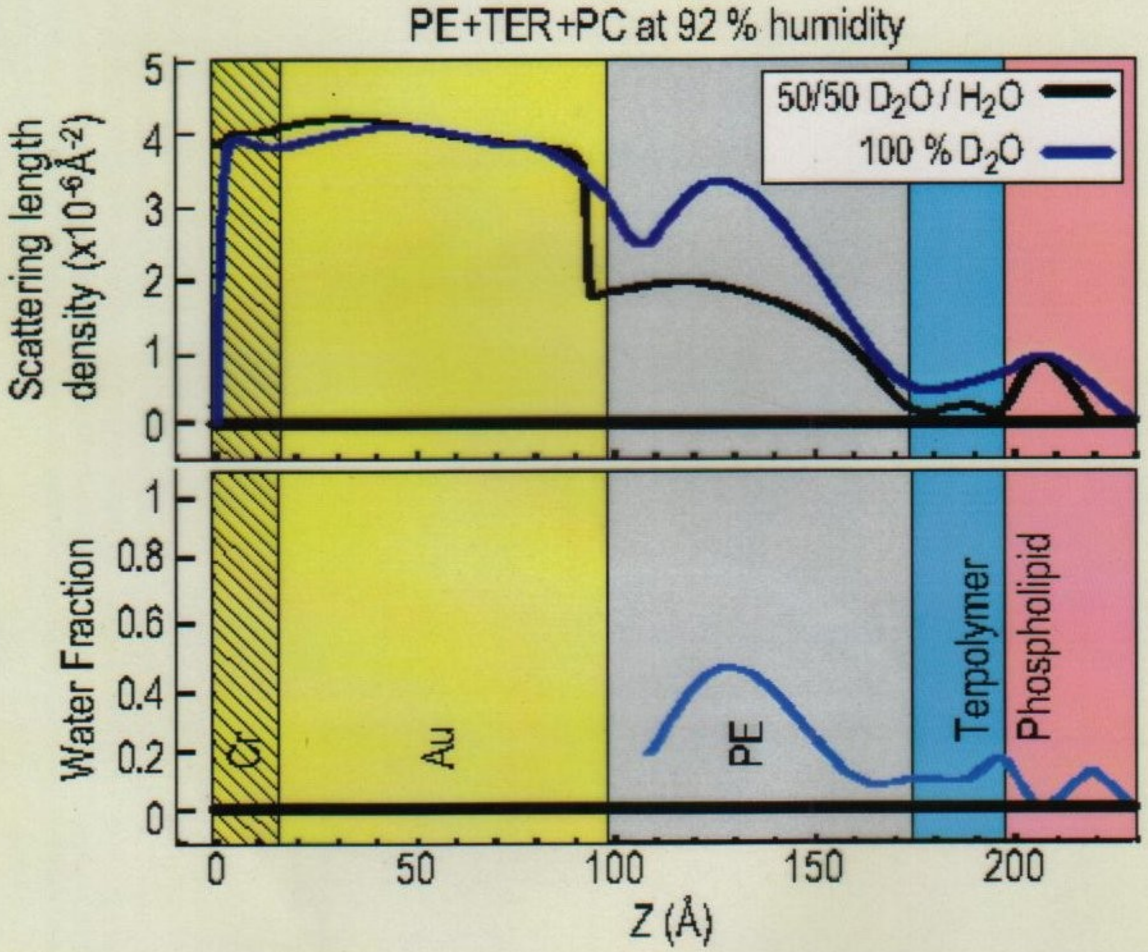

Fig. 3. Scattering length density profiles (top) and water fraction (bottom) for PE+TER+PC under indicated conditions.

Phase Sensitive Neutron Reflectometry on a Water-Cushioned Biomembrane-Mimic

Biomimetic membranes have been developed as models of living cell membranes, and this has applications in the quest for biocompatibility of inorganic materials in biologically active mediums, such as coatings for artificial organs. A membrane consists of a lipid bilayer (two lipid layers) where hydrophobic carbon chains form the inside of the membrane and their polar head groups the interface with the aqueous surrounding medium. A supported membrane-mimic consists of a lipid-like bilayer, typically attached to a single-crystal substrate, with access to water only at the top surface [1, 2]. Here we use neutron reflectometry to study a system in which water has access to both sides of a membrane-mimic attached to such a substrate, thus making the system a closer mimic to a real cell membrane.

The system devised by Liu *et al.* [3] consists of a water-swellable polyelectrolyte that electrostatically binds to the substrate and acts as a "cushion" for the membrane, not unlike the cytoskeletal support found in actual mammalian cell membranes. The lower half of the membrane-mimic is a terpolymer that attaches to the polyelectrolyte. A phospholipid layer forms on top of the terpolymer and the bilayer is finally chemically crosslinked for added stability. The system is shown schematically in Fig. 1.

Neutron reflectivity measurements were performed at the NG-1 vertical stage reflectometer to obtain the compositional profile at every step of the assembling process of the membrane-mimic which consisted of three stages: a) polyelectrolyte multilayer (PE), b) polyelectrolyte multilayer plus terpolymer (PE+TER), and c) polyelectrolyte multilayer plus terpolymer plus phospholipid layer (PE+TER+PC) [4]. The spatial resolution attained was approximately 10 Å, about half the thickness of a membrane bilayer, making it possible to distinguish the two layers of a membrane but not the structure of a single layer.

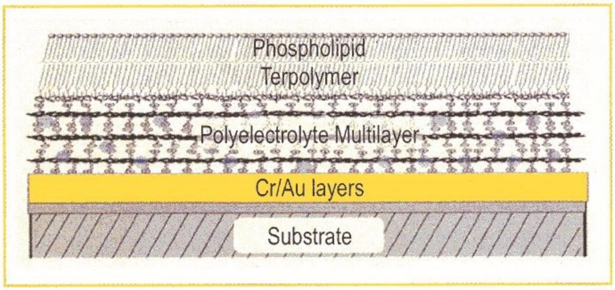

Fig. 1. Schematic diagram of a biomimetic membrane. The phospholipid layer at the top combines with the terpolymer layer to form a membrane-mimic that in turn resides on the water (blue dots) permeable "cushion" polyelectrolyte multilayer. The latter attaches electrostatically to the Au-capped substrate.

A unique compositional profile of the biomimetic film with no a priori knowledge of the sample's composition is obtained by measuring the reflectivity of equivalent samples made onto two substrates [5]. The substrates used were single crystal silicon (Si) and sapphire (Al_2O_3) coated with chromium (Cr) and then a gold (Au) layer to allow the polyelectrolytes to bind to a similar surface on both wafers.

Figure 2 shows the compositional profiles for the PE, PE+TER and PE+TER+PC assemblies in a D_2O atmosphere at 92 % relative humidity. The figure shows that the hydration of the PE layer is almost unaffected by the addition of the terpolymer and the phospholipid layer. Also, upon the addition of the phospholipid layer to the PE+TER assembly, the composite PE+TER+PC assembly shows an increase in thickness of approximately 30 Å, consistent with the formation of a single phospholipid layer at the surface. It is also clear that the addition of a phospholipid layer onto the terpolymer layer rearranges this region

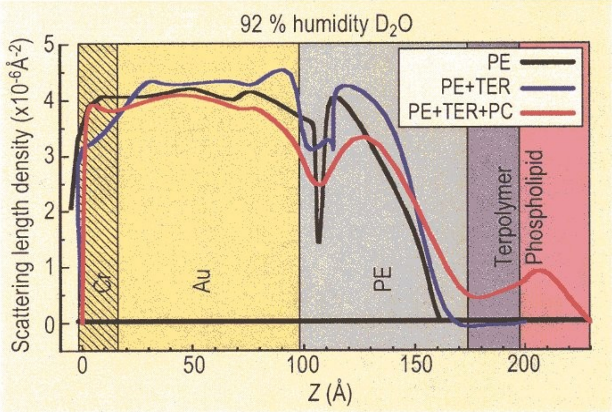

Fig. 2. Compositional profile of biomimetic membrane in a D_2O atmosphere at 92 % relative humidity at various stages of assembly on Au-capped substrate: only polyelectrolyte (PE), polyelectrolyte and terpolymer (PE+TER), polyelectrolyte, terpolymer and phospholipid (PE+TER+PC). The compositional profile is given by the scattering length density, SLD, profile when using neutrons.

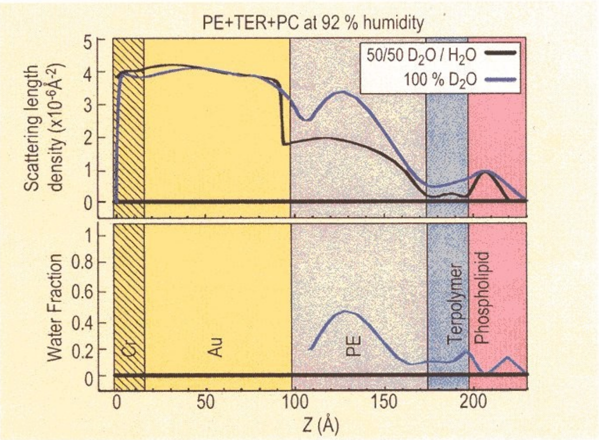

Fig. 3. Scattering length density profiles (top) and water fraction (bottom) for PE+TER+PC under indicated conditions.

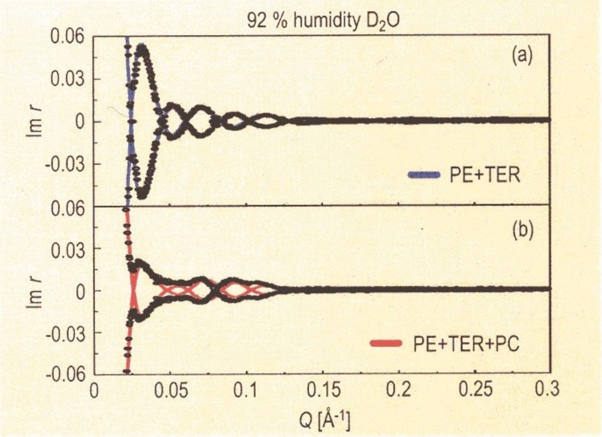

Fig. 4. Imaginary part of the complex reflectivity, Im *r*(*Q*), data (symbols) and calculated curves (lines) obtained from the SLD profiles for the PE+TER and the PE+TER+PC assemblies shown in Fig. 2.

significantly, since the terpolymer layer only becomes apparent after the phospholipid layer is added. It is possible to verify with an independent technique (contact angle) that the terpolymer was in fact deposited because it forms a hydrophobic outer layer. The outer surface becomes hydrophilic once the phospholipid layer is deposited onto the terpolymer layer.

Figure 3 (top) shows the profile for the PE+TER+PC assembly under 92 % relative humidity in 100 % D_2O and in 50/50 D_2O/H_2O. The overall thickness change due to the intake of water, in going from dry (not shown) to 92 % relative humidity, was found to be 20 Å. Figure 3 (bottom) shows the water fraction in the assembly under 92 % relative humidity. This is obtained by assuming that the distribution of each component in the layers is unaffected by having either D_2O or 50/50 D_2O/H_2O. From the figure it can be seen that the polyelectrolyte multilayer has a 40 % water uptake. This is a significant amount of water, which suggests that the polyelectrolyte multilayer can work as a "cushion" for membrane-mimetic systems. The terpolymer and the phospholipid layers contain an average of 10 % water, which is also significant, suggesting that these layers are not tightly packed.

The method of making equivalent samples on two substrates to obtain a unique compositional profile has a built-in congruency test, particularly useful in checking the reproducibility of the samples as well as the quality of the films. The test is to compare the calculated imaginary part of the complex reflectivity from the obtained profile with the corresponding data, as is shown in Fig. 4 for the PE+TER and PE+TER+PC assemblies. From Fig. 4 it is concluded that the PE+TER samples are homogenous and essentially identical while for the PE+TER+PC assembly, the absence of true zeros, as indicated by the calculated curve, is suggestive of a small degree of sample inhomogeneity.

The system from Liu *et al.* has many characteristics desirable in a biomimetic membrane. It is a single membrane-mimic attached to a significantly hydrated soft "cushion" support that allows some membrane proteins to function. Thrombomodulin, a membrane protein relevant to blood-clotting, is being studied in this membrane-mimic environment to further develop biocompatible coatings for artificial organs [6].

References

[1] E. Sackmann, Science **271**, 43 (1996).

[2] A. L. Plant, Langmuir **15**, 5128 (1999).

[3] H. Liu, K. M. Faucher, X. L. Sun, J. Feng, T. L. Johnson, J. M. Orban, R. P. Apkarian, R. A. Dluhy, E. L. Chaikof, Langmuir **18**, 1332 (2002).

[4] U. A. Perez-Salas, K. M. Faucher, C. F. Majkrzak, N. F. Berk, S. Krueger, E. L. Chaikof, Langmuir **19**, 7688 (2003).

[5] C. F. Majkrzak, N. F. Berk, U. A. Perez-Salas Langmuir **19**, 1506 (2003).

[6] J. Feng, P. Y. Tseng, K. M. Faucher, J. M. Orban, X. L. Sun, E. L. Chaikof, Langmuir **18**, 9907 (2002).

U. A. Perez-Salas
NIST Center for Neutron Research
National Institute of Standards and Technology, Gaithersburg, MD 20899-8562

K. M. Faucher
Emory University School of Medicine, Atlanta, GA 30322

C. F. Majkrzak, N. F. Berk, S. Krueger
NIST Center for Neutron Research
National Institute of Standards and Technology
Gaithersburg, MD 20899-8562

E. L. Chaikof
Emory University School of Medicine
Atlanta, GA 30322

Nanoparticle distribution in polymer-based solar cells affects solar cell performance: A neutron reflectivity study

Jonathan Kiel[1], Brian Kirby[2], Charles Majkrzak[2],
Brian Maranville[2], Michael Mackay[3]

Thursday, August 20th, 2009

1) Michigan State University, Department of Chemical Engineering and Materials Science
2) National Institute of Standards and Technology, Center for Neutron Research
3) University of Delaware, Materials Science and Engineering

UNIVERSITY OF DELAWARE

MICHIGAN STATE UNIVERSITY

NIST Center for Neutron Research

Components of organic solar cells

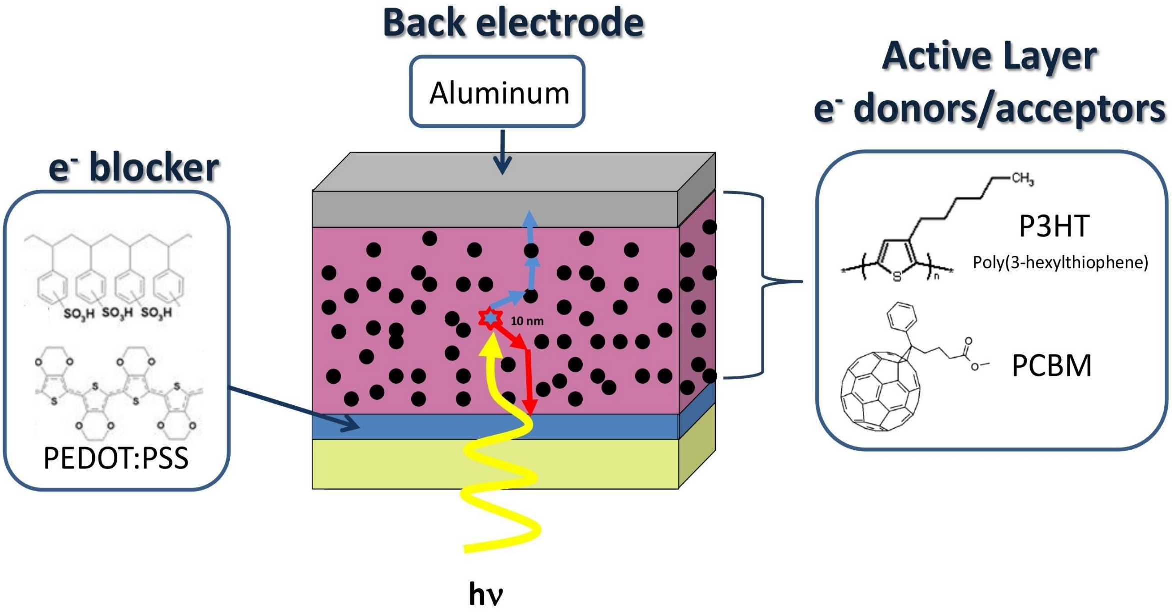

Back electrode

Aluminum

Active Layer

e$^-$ donors/acceptors

P3HT

Poly(3-hexylthiophene)

PCBM

e$^-$ blocker

PEDOT:PSS

hν

- Exciton diffusion length ~10 nm
- PCBM:P3HT morphology very important

What is the morphology of the active layer

Energy Diagram of Organic Solar Cell

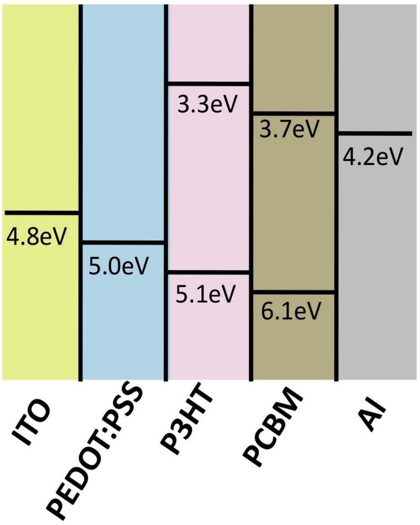

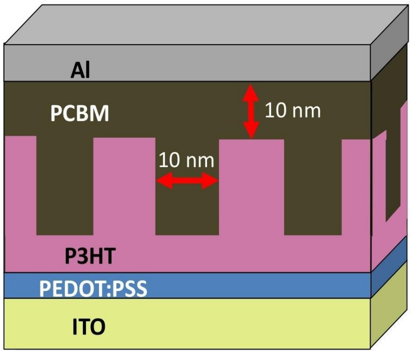

Idealized morphology

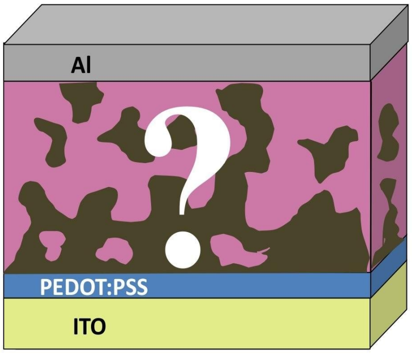

Actual morphology

K. M. Coakley, M. D. McGehee, *Chemical Materials,* **2004**

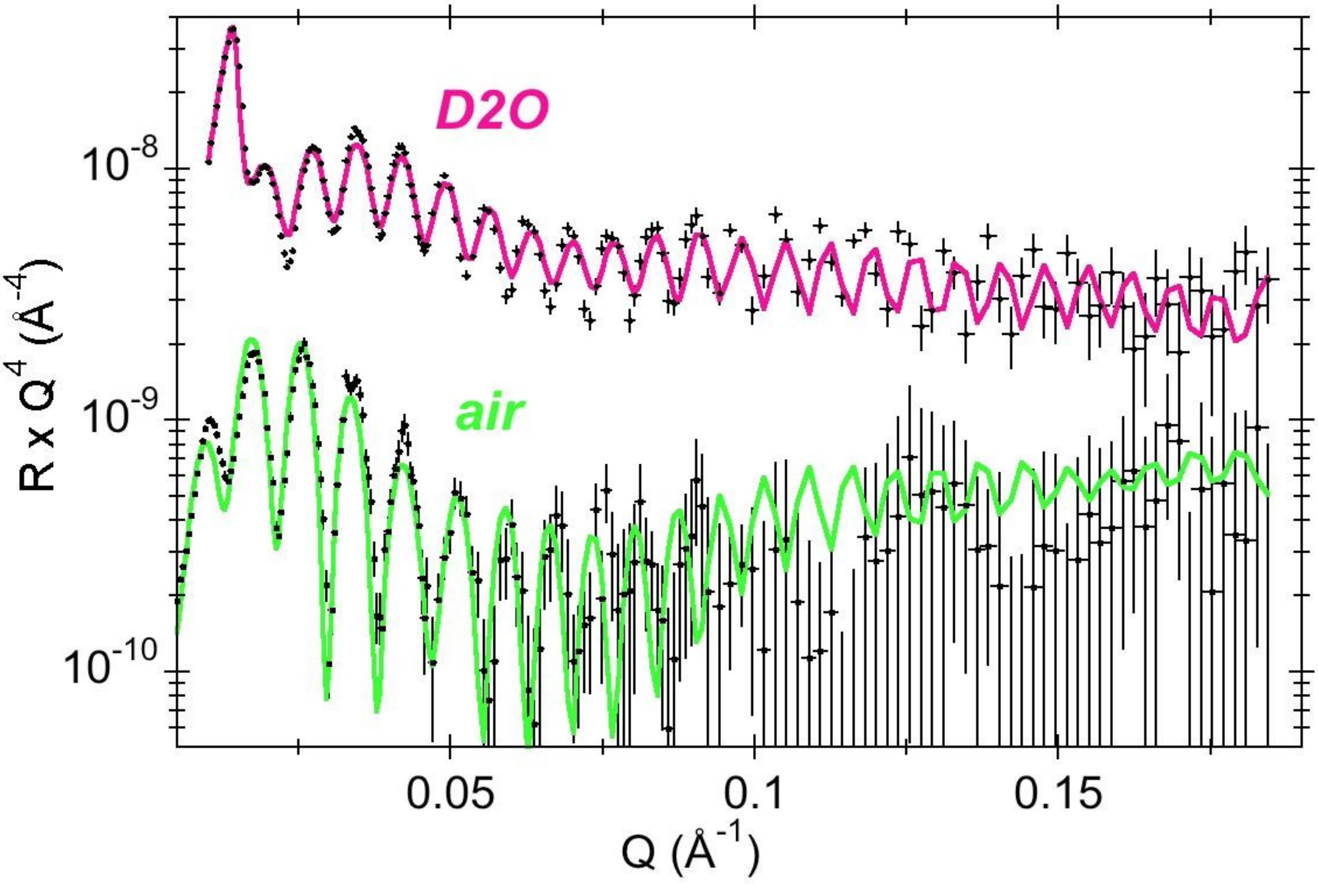
D2O
air
R x Q^4 (Å^{-4})
Q (Å^{-1})
10^{-8}
10^{-9}
10^{-10}
0.05
0.1
0.15

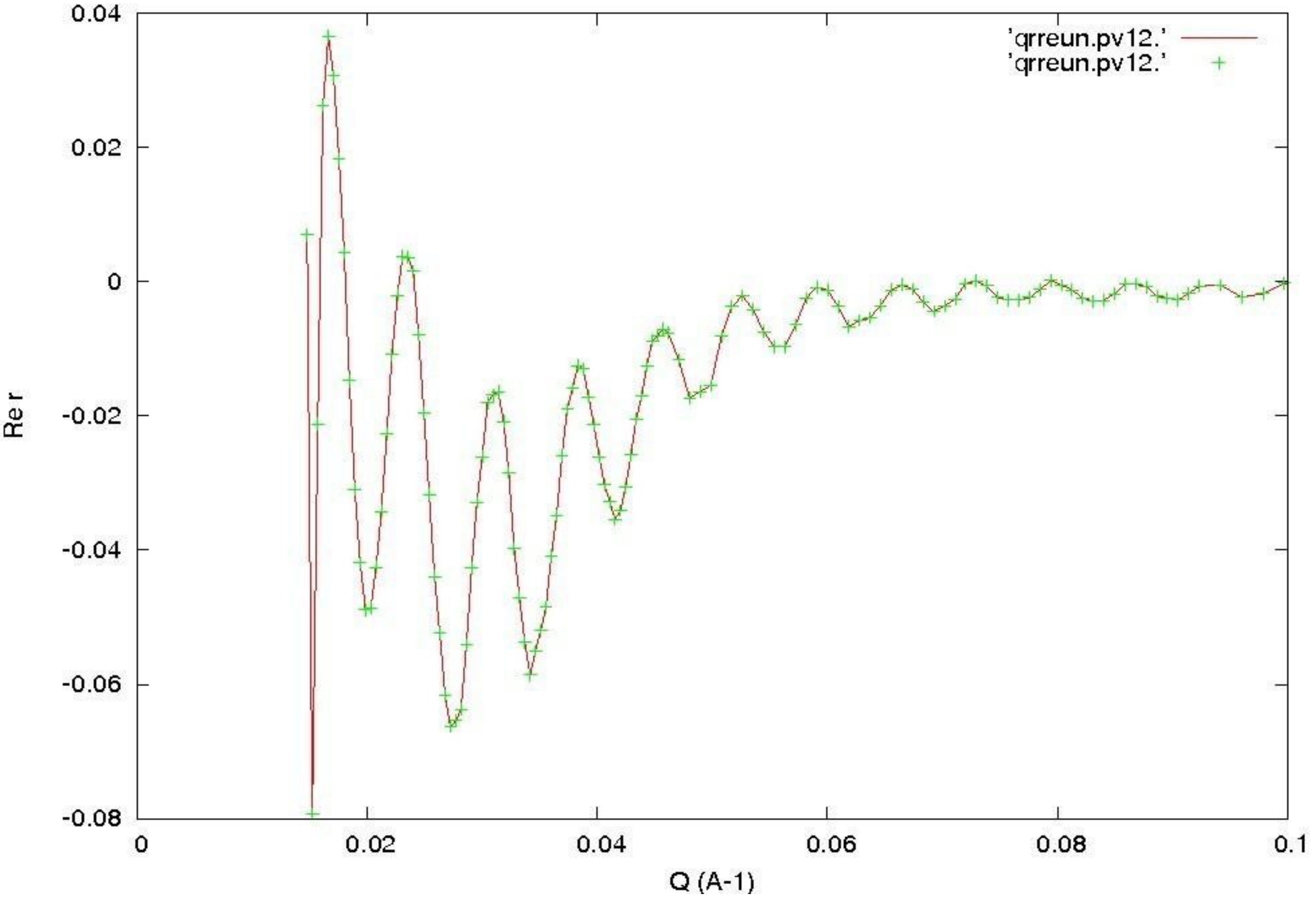
'qrreun.pv12.'
'qrreun.pv12.'
Re r
0.04
0.02
0
-0.02
-0.04
-0.06
-0.08
0
0.02
0.04
0.06
0.08
0.1
Q (A-1)

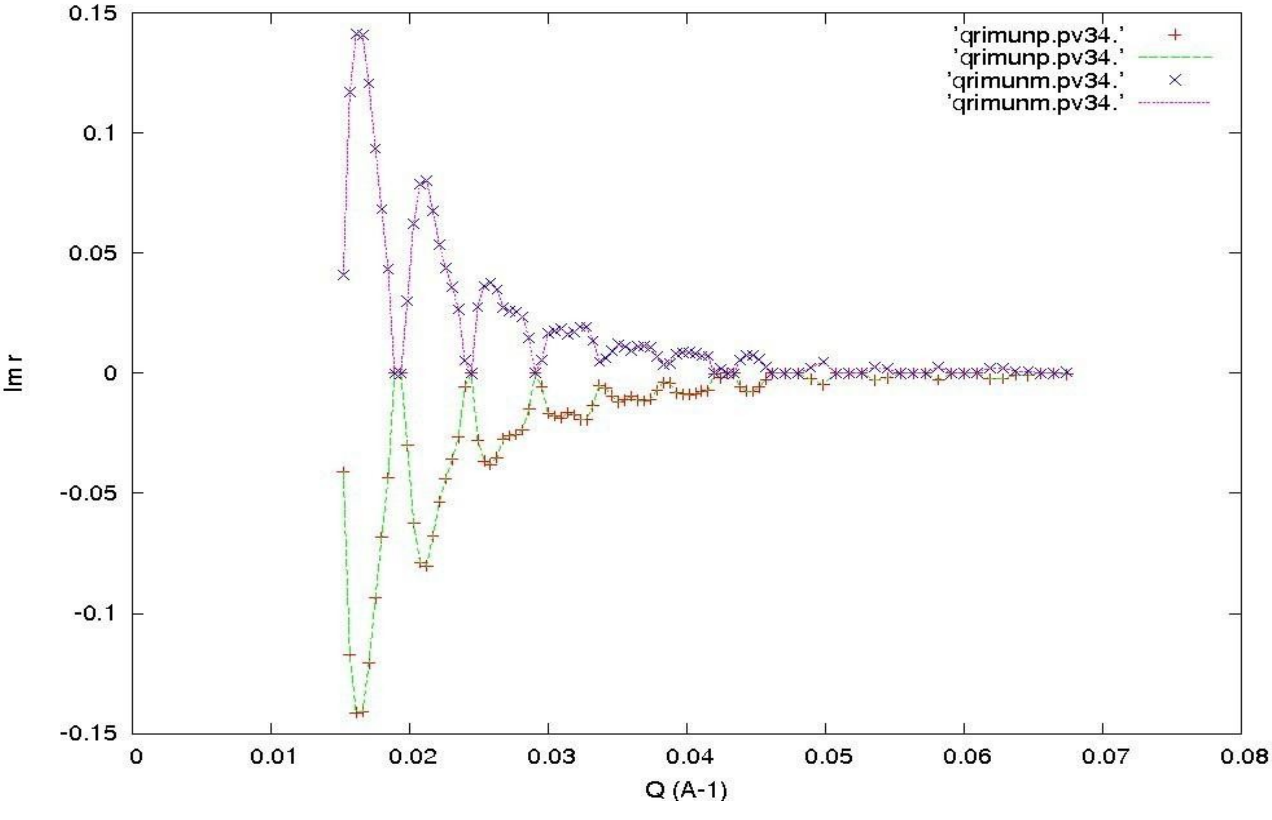
'qrimunp.pv34.'
'qrimunp.pv34.'
'qrimunm.pv34.'
'qrimunm.pv34.'
Im r
0.15
0.1
0.05
0
-0.05
-0.1
-0.15
0
0.01
0.02
0.03
0.04
0.05
0.06
0.07
0.08
Q (A-1)

PCBM Volume % Comparison

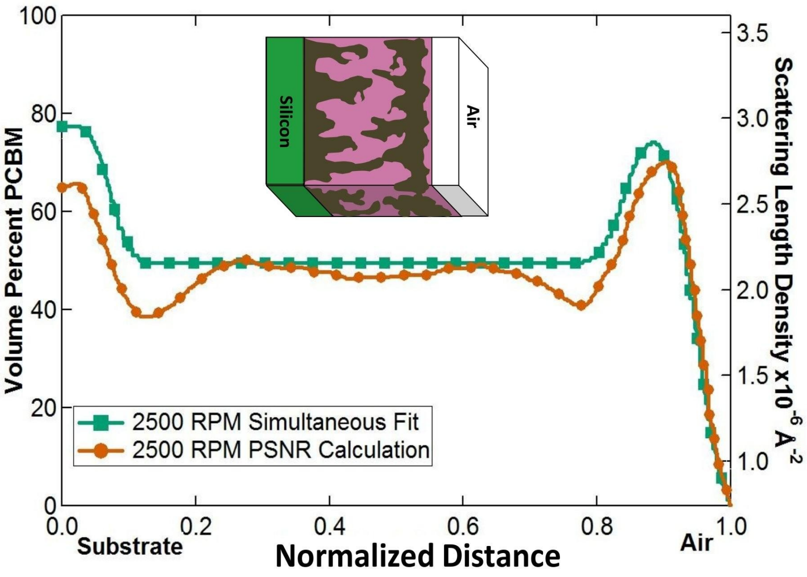

$$\text{Vol\% PCBM} = \frac{\text{SLD}_{\text{measured}} - \text{SLD}_{\text{P3HT}}}{\text{SLD}_{\text{PCBM}} - \text{SLD}_{\text{P3HT}}}$$

- Simultaneous fitting and PSNR calculations show great agreement
- High PCBM concentration at substrate
- High PCBM concentration near air interface

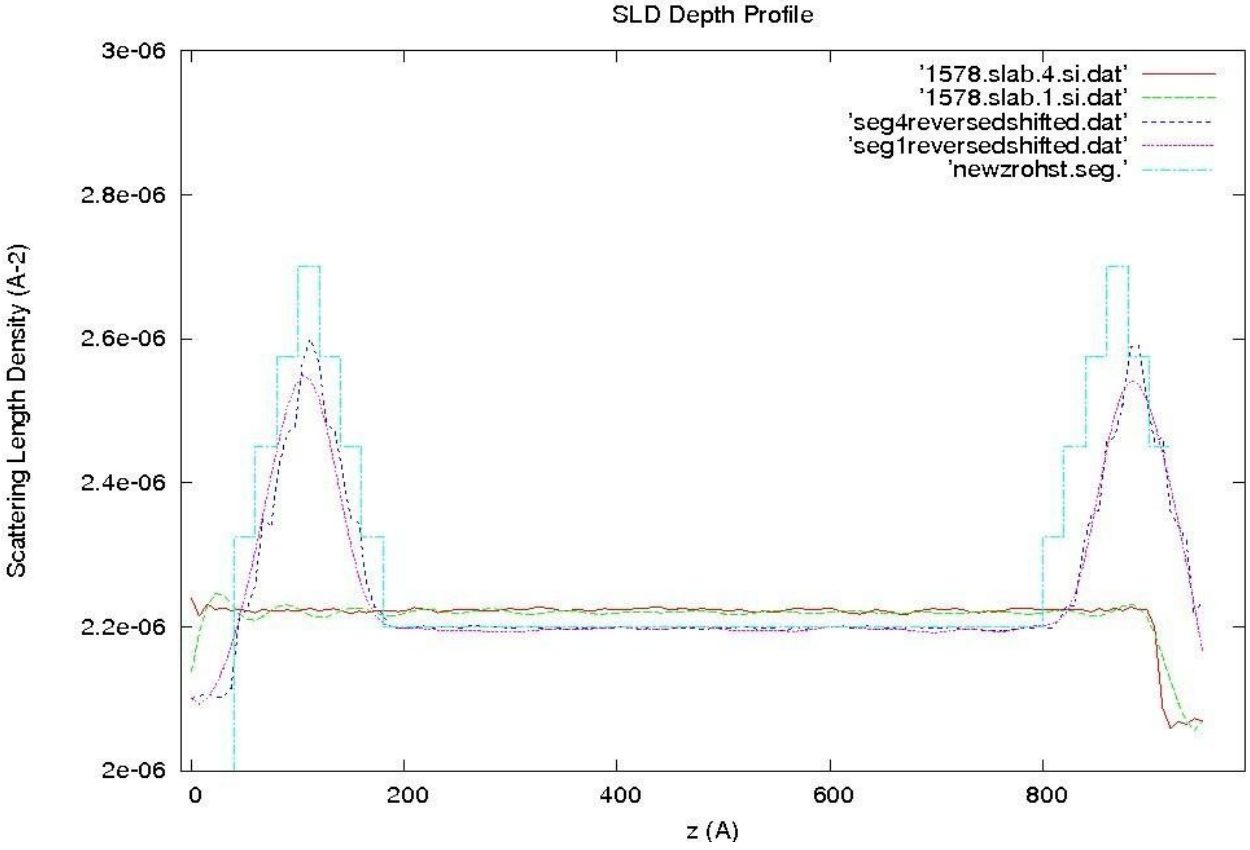
SLD Depth Profile
'1578.slab.4.si.dat'
'1578.slab.1.si.dat'
'seg4reversedshifted.dat'
'seg1reversedshifted.dat'
'newzrohst.seg.'
Scattering Length Density (A-2)
3e-06
2.8e-06
2.6e-06
2.4e-06
2.2e-06
2e-06
0
200
400
600
800
z (A)

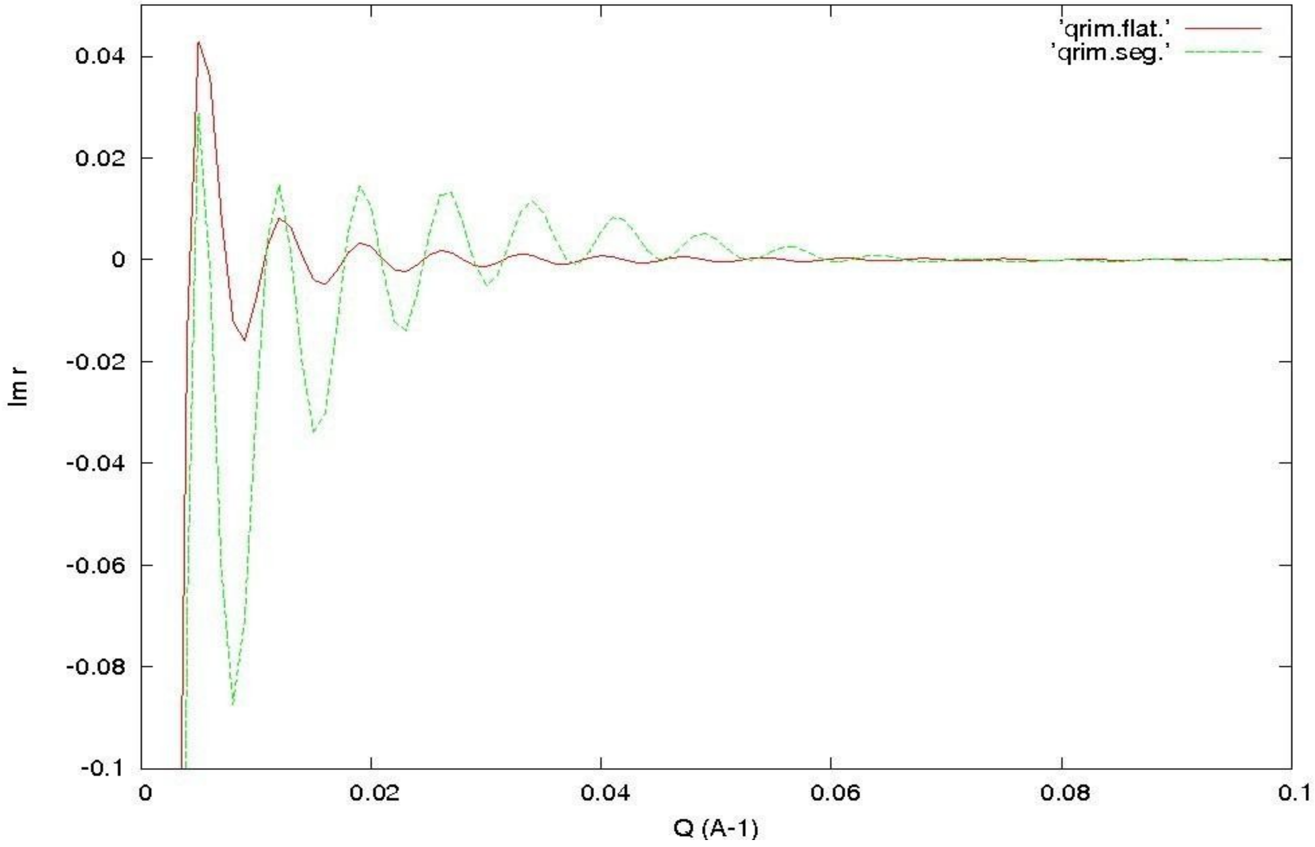
'qrim.flat.'
'qrim.seg.'
Im r
0.04
0.02
0
-0.02
-0.04
-0.06
-0.08
-0.1
0
0.02
0.04
0.06
0.08
0.1
Q (A-1)

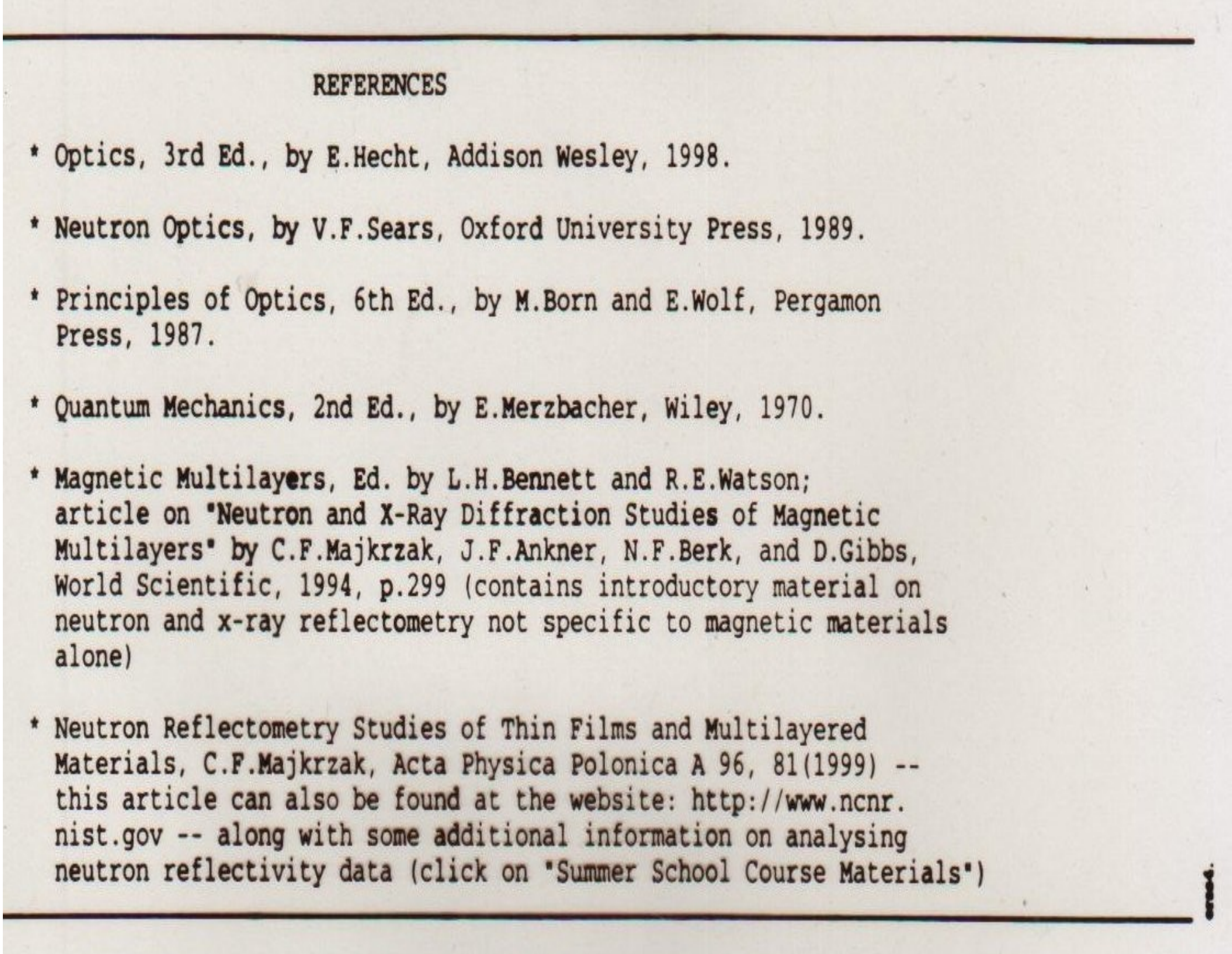

REFERENCES

- Optics, 3rd Ed., by E.Hecht, Addison Wesley, 1998.
- Neutron Optics, by V.F.Sears, Oxford University Press, 1989.
- Principles of Optics, 6th Ed., by M.Born and E.Wolf, Pergamon Press, 1987.
- Quantum Mechanics, 2nd Ed., by E.Merzbacher, Wiley, 1970.
- Magnetic Multilayers, Ed. by L.H.Bennett and R.E.Watson; article on "Neutron and X-Ray Diffraction Studies of Magnetic Multilayers" by C.F.Majkrzak, J.F.Ankner, N.F.Berk, and D.Gibbs, World Scientific, 1994, p.299 (contains introductory material on neutron and x-ray reflectometry not specific to magnetic materials alone)
- Neutron Reflectometry Studies of Thin Films and Multilayered Materials, C.F.Majkrzak, Acta Physica Polonica A 96, 81(1999) -- this article can also be found at the website: http://www.ncnr.nist.gov -- along with some additional information on analysing neutron reflectivity data (click on "Summer School Course Materials")

B.J.Kirby et al., Phase-sensitive specular neutron reflectometry . . ., *Current Opinion in Colloid & Interface Science* **17** (2012) 44-53.

C.F.Majkrzak et al., *J. Appl. Phys.* **110** (2011).

www.ncnr.nist.gov -- look here for information about neutron reflectometry in general as well as in specific studies highlighted in past and current annual reports for the facility.

“Structural Investigations of Membranes in Biology by Neutron Reflectometry”, C.F.Majkrzak, N.F.Berk, S.Krueger, and U.A.Perez-Salas, Chapter 12 in *Neutron Scattering in Biology*, Edited by J.Fitter, T.Gutberlet, and J.Katsaras, (Springer, Berlin, 2006) p.225-263.

“Polarized Neutron Reflectometry”, C.F.Majkrzak, K.V.O'Donovan, and N.F.Berk, Chapter 9 in *Neutron Scattering from Magnetic Materials*, Edited by T.Chatterji, (Elsevier, Amsterdam, 2006) p.397-471.

“Phase-Sensitive Neutron Reflectometry”, C.F.Majkrzak, N.F.Berk, and U.A.Perez-Salas, *Langmuir* **19**, 7796 – 7810 (2003).